Ultrafast Photophysical Processes in Electronically Excited Flavin and β-Carotene

D i s s e r t a t i o n

zur Erlangung des akademischen Grades

d o c t o r r e r u m n a t u r a l i u m

(Dr. rer. nat.)

im Fach Chemie

eingereicht an der

Mathematisch-Naturwissenschaftlichen Fakultät

der Humboldt-Universität zu Berlin

von

Dipl.-Chem. Martin Quick

Präsident der Humboldt-Universität zu Berlin

Prof. Dr. Jan-Hendrik Olbertz

Dekan der Mathematisch-Naturwissenschaftlichen Fakultät

Prof. Dr. Elmar Kulke

Gutachter/innen:

1. Prof. Nikolaus P. Ernsting
2. Prof. Thomas Lenzer
3. Dr. Erik Nibbering

Tag der mündlichen Prüfung: 02.02.2016

Inhaltsverzeichnis

1 Introduction

In this dissertation the spectroscopic study of two prominent bio-molecules is presented in the form of three publications. In the first publication riboflavin is studied in aqueous solution with fs-transient absorption and FLuorescence UP-conversion Spectroscopy (FLUPS). The second and third publication both concern β-carotene as the target-molecule which is measured in hexane with transient absorption and Femtosecond-Stimulated Raman (FSR) spectroscopy. Riboflavin and β-carotene are flagships amongst their types of electronic system. While riboflavin is a rigid condensate of three aromatic rings β-carotene consists of a flexible polyene chain with conjugated double bonds that connect two terminal β-ionone rings. Due to their ubiquitous presence and their essential roles in life-related molecular processes these molecules have been the subject of countless research projects in the past decades. To comprehend the interaction of these target-molecules with their respective natural environment, detailed knowledge from measurements in solution is considered a prerequisite. Odd behavior in solution that might be overlooked could complicate the interpretation in more complex systems. Therefore a complete clarification is necessary, and this why a re-examination of even such well-studied electronic systems in solution is definitely worth a try.

A careful and comprehensive examination requires access to a wide range of broad-band spectroscopic techniques that are adapted for the respective molecular system. The right choice of a method to examine a molecular system depends on the dominating electronic property and open questions that remain to be answered. Neutral riboflavin, for example, is a relatively strong fluorescing chromophore (quantum yield ~ 0.26) with an interesting pH dependent behavior. It exists in three states of protonation in the electronic ground-state with two pK_a values, at 0 and 9.75 [1,2]. However- the quantum yield of the emission does not follow the same trend, when the pH is lowered. Instead, it decreases already around pH 2 which suggests an excited state proton-transfer from the solvent to the chromophore. A weak emission band around 660 nm was attributed to protonated riboflavin in the ground-state [3] but it does not follow its mole-fraction, as will be shown. It immediately suggests itself to monitor the evolution of this NIR band with broad-band absorption and -fluorescence. On the other hand β-carotene only fluoresces in the short living S_2-state (~200 fs) and relaxes very fast to S_1 via internal conversion. However, the Raman activity is high for local modes in the polyene (C-C and C=C stretch). β-carotene has been thoroughly examined with fs-transient absorption and FSR spectroscopies [4-9]. Recent studies suggest the existence of two isomers in the electronic ground-state that are separated by an energy-barrier and which determines the population ratio [10]. Since excess energy from internal conversion is located in S_1, the driving force for a migration of population between these two isomers is provided. This migration should be visible in the transient spectrum. While the transient Raman spectrum is well characterized for frequencies >900 cm^{-1} no results have been published yet for the low-frequency region (80 – 900 cm^{-1}). Riboflavin, then

again, does not show the same significance in the Raman spectrum. However, transient absorption is a universally applicable technique, which in combination with one of these broad-band methods provides a powerful toolbox.

Another point addresses the probability of finding any new results- at all. The general aim of spectroscopic studies is to comprehend the interaction of a chromophore with light in either natural environment (DNA or protein) or for specific mechanical purposes, for example in molecular machines and switches. Therefore, initially, systematic research in solution, as the simplest form of environment, gives information about how the incident light-energy is converted within the molecule. Interaction of the solute with the solvent ensemble, in response, can give clues about the physicochemical potential of the chromophore. For example, in protic solvents protonation, deprotonation and solvation may occur. In nonpolar solvents, however, the (nonpolar) chromophore is most likely to perform structural rearrangements while the surrounding molecules rather act as acceptor for excess energy from the internal conversion process. System-relevant information is obtained from spectroscopic measurements, such as (transient) band-positions, -shapes and time-constants. In case of unresolved questions the systematic variation of the solvent and chemical modifications of the molecule both lead to further clarification. The next (and most likely not last) step is to study the chromophore in its default environment. Again information is gathered from spectroscopic measurements and must be compared with the obtained parameters from the basic studies. Now, differences must be attributed to the non-trivial nature of the complex environment whereby also first conclusions can be drawn considering the results from the measurements in solution. A full understanding of the default system requires systematic research which involves a piecewise substitution of potential ambient acceptor/receptor molecules in the structure-determining binding sites. This is especially the case for proteins in which functional amino-acids in close proximity determine the reaction pathway. Such systematical researches have been challenging tasks to scientific work-groups since time-resolved spectroscopic methods exist.

The quality and quantity of research results increased with the constant development of the measurement systems and reasonable methods for evaluation. For the former two lines have been followed: First, the design and improvement of spectroscopic setups and detection-systems (broadband-techniques, spectral resolution, signal/noise) that allows to measure the chromophores response on the electronic (transient absorption and emission) and on the vibrational level (infra-red and Raman). Second, the time-window on which reactions and dynamics can be observed has been shortened from several hundred nanoseconds to tens of femtoseconds (time-resolution). Hereby, the discovery of a mode-locked laser with titan-ion doped sapphire-crystal as gain medium (Ti:Sa-laser) [11] and the development of self-strarting Kerr-lens mode-locking [12,13] made the femtosecond-regime conveniently and widely accessible. However, despite this technical progress, no further significant improvement is expected for certain spectroscopic techniques at one point. From this follows immediately that no new information can be gathered from the considered

molecule as the, so called, state-of-the-art already revealed all technique-related spectroscopic properties. This point of stagnation is reached even faster with growing authority on the considered research project. Does that mean in turn that further serious investigation of an excessively studied molecular system become inconclusive? Let us therefore exemplarily discuss the technical aspects that must be regarded in a transient absorption (TA) experiment and check at which point this limit of improvement is reached. The optical pump pulse is required to be short (50 fs) and tunable from the ultra-violet to the near-infrared. The latter is achieved by using (noncollinear) optical parametric amplification. To record broadband absorption spectra one may use a super-continuum that can be generated in nonlinear media, such as CaF_2, yielding a time-resolution better than 100 fs. In combination with an appropriate detector system a spectral window of <300 to >1500 nm can be covered, which is relevant for monitoring electronic transitions. The quality of the TA spectra depends on the stability of the probe light whose fluctuations also affect the S/N ratio. These fluctuations in spectra can be suppressed in two ways: by either working with a stable laser output or by using a reference detector that corrects the absorption signal for the probe structure at each shot. The spectral resolution is no crucial factor since electronic bands are broad by their nature. Assuming that the optical elements have the highest quality and a good focusing onto the sample cell is guaranteed, then all requirements for an advanced transient-absorption setup are fulfilled, in principle. To put this TA setup to the test consider β-carotene in the condensed phase as an example for a well characterized molecular system. It has a structurally well resolved stationary absorption spectrum where vibronic bands are separated by ~1500 cm^{-1}, each having a width of ~800 cm^{-1}. The pulse for optical pumping needs to be spectrally narrower than the width of these bands to avoid population transfer into undesired vibronic states. On the other hand the time-resolution decreases when the optical pulse narrows. Usually, the compromise is a pulse duration of ~50 fs which corresponds to 300 cm^{-1} width, when a Gaussian band-shape is assumed. The broad super-continuum probe pulse (covers ~20000 cm^{-1}) leads to 20 fs time-resolution in the experiment. The choice of pump and probe shows that the technical limitations in a transient absorption experiment are mainly determined by the time-bandwidth relation. Thus further improvement of the laser-system, *i.e*. shortening of the laser-output into the atto-second regime, cannot change this spectroscopic technique for the better. The same argument holds for the detection system. Since β-carotene in solution exhibits intense excited state absorption (ESA) to tens of mOD, there is no substantial improvement expected for the S/N ratio even when the sensitivity of the photo-diode is increased.

Nowadays- these technical implementations mentioned above have become standard in laboratories that perform fs time-resolved absorption experiments. However, over time, the continual gathering of information about a molecular system with one technique has always been an interplay with the improvement of this technique. Here such an interplay is exemplarily illustrated for β-carotene in solution which was investigated with transient

absorption spectroscopy (**Fig. 1**). Shown is always the pioneering work in which a TA-related result (green) was published for the first time. In β-carotene the S_1 state cannot be populated directly for symmetry reasons, which is why S_2 becomes the lowest bright state. Internal conversion from S_2 to S_1 proceeds on a very fast time-scale (within 0.5 ps) and could not be resolved at the initial stage of research. Instead the slower $S_1 \rightarrow S_0$ relaxation was observed by Wasielewski in 1986 [14]. $S_y \leftarrow S_1$ ESA was recorded in the region 520 - 570 nm and the life-time of S_1 was determined to 8.4 ps. In 1991 Shreve *et al.* used short pulses for pumping and probing and a cross-correlation of 200 fs was obtained to resolve the earliest kinetics [15]. For technical reasons the S_2 life-time (250 fs in ethanol) was taken from the $S_y \leftarrow S_1$ ESA as it appears on the same time scale as the S_2 state decays. Not until 2001 the intense $S_x \leftarrow S_2$ ESA band could be monitored around 1000 nm by the groups of Zhang [4] and Yoshizawa [5]. The use of an appropriate detection-system made the near-infrared (NIR) region accessible. It was also the time when the Ti:Sa-laser has been established in most of the laboratories that operate on the ultrafast time-scale. Thus internal vibrational redistribution (IVR) in S_1 could be identified as the other ultrafast relaxation kinetic (530 fs in hexane and 620 fs in cyclohexane)

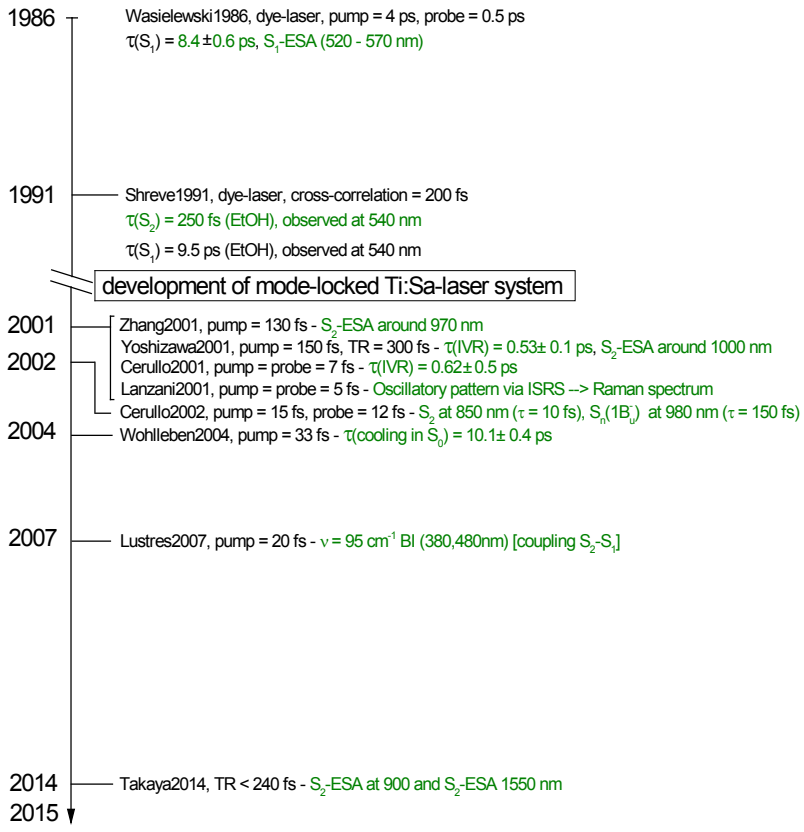

Figure 1: Overview of pioneering work that refer to results from transient absorption measurements on β-carotene.

[5,16]. Yet another relaxation process which acts on a slightly longer time-scale than the decay of S_1 has not been recognized until 2004. Wohlleben *et al*. analyzed their TA data globally and attributed this slower relaxation process (10.1 ps in hexane) to cooling in S_0 [17]. In

principle no temporal resolution in the femtosecond regime is necessary to distinguish kinetics on the picosecond time-scale. The recognition of the slowest kinetic was the result of two given conditions: an improvement of the detection system which led to less noisy data and the application of an appropriate evaluation algorithm. Since the contribution of ground-state cooling to the TA spectra is small, a sufficient S/N ratio is required to provide a reliable separation via global analysis. In studies before 2000 it has been common practice to determine time-constants at single wavelength-traces. As a consequence, kinetics that proceed with similar time-constants could not be resolved and kept unrecognized. Recently the spectral window was extended to 1550 nm by Takaya *et al.* whereby the $S_2 \leftarrow S_1$ transition could be observed [18]. Thus the exact value for the energy term of the S_1 state was obtained experimentally for the first time. Less clearly appears the existence of an additional dark electronic state S_n with B_u^- symmetry which is controversially discussed. Cerullo *et al.* used pump- and probe-pulses with 15 and 12 fs duration and ascribed an ultrafast decaying broad feature around 850 nm (τ = 10 fs) to the actual S_2 state [19]. The subsequent rise of another broad band around 980 nm was consequently attributed to the $S_m \leftarrow S_n$ transition. However Lustres *et al.* considered this finding to be a coherent artifact originating from a simultaneous interaction with pump and probe [20]. Beside this traditional gathering of electronic bands and time-constants there has also been a focus on oscillations that are superimposed with the time-traces. These originate from oscillating wave-packets that are created impulsively (either in ground- or excited state) with an ultra-short pump pulse of few femtoseconds and which modulate the transient electronic signal. A Raman-spectrum is created when these traces are converted into the frequency domain via Fourier-transform. In this way Raman active modes from S_0 and S_1 were obtained for β-carotene by Lanzani *et al.* [21]. To monitor these modulations time-dependently on a full wavelength-range the TA scheme was modified by one or more additional femtosecond pulses. Dependent on the number of pulses these new techniques are called pump-impulsive-vibrational-spectroscopy (pump-push-probe) or pump-degenerate-four-wave-mixing (pump-pump/Stokes-probe) and have been recently applied to β-carotene [22,23]. However these modified pulse-sequences deviate from the original TA scheme (pump-probe) and shall not be considered in this outline. Instead, the conclusions will be summarized in the following. (i) An appropriate time-resolution is essential to resolve fast kinetics, in principle, but both a sufficient S/N ratio and an appropriate analyzing method are crucial for a reliable recognition. (ii) The wide use of the advanced Ti:Sa laser-system leads to a comparatively quick and therefore comprehensive research of a chromophore. It should be therefore rather unlikely to reveal fundamentally new results on a molecule as time goes by. For β-carotene this limit was reached apparently in 2004 with the detection of ground-state cooling. In all succeeding reports no new information about electronic transitions and kinetics were published and only the existing results were reproduced. One reason might be the rising focus on vibrational spectroscopic techniques to which transient absorption itself rather acts as a concomitant tool by confirming time-constants and establishing resonance conditions.

At this point one should take up the question again if a re-examination of an extensively studied molecular system can still yield results that contribute to a fundamental understanding. As outlined above most of the applied spectroscopic techniques are well established. If not substantially, a mere improvement is rather unlikely to reveal any new information. The focus must also be set on the evaluation process and how to estimate the quality of the results. In doing so one should not be steered by the existing picture of the examined electronic system, even though it is supposed to be well established. With the examples: riboflavin and β-carotene it will be shown that even for such intensively studied molecules fundamentally new results can be found by the right choice of established spectroscopic techniques on the highest level and a systematical evaluation procedure.

2 Nonlinear Spectroscopy (this follows large refs. 1 and 2, see citations within)

2.1 Theoretical Background

2.1.1 The Density Matrix

The time evolution of a quantum mechanical system with its wave-function Ψ(x,t) can be described by the *Schrödinger equation*,

$$\frac{d}{dt}|\psi\rangle = -\frac{i}{\hbar}\mathcal{H}|\psi\rangle$$
(2.1)

where $\mathcal{H}$ is the quantum-mechanical Hamiltonian. The expectation value of an observable O is given by

$$\langle \mathrm{O}\rangle = \langle\psi|\mathrm{O}|\psi\rangle.$$
(2.2)

In the same way the probability *p*(a) that the system is in a specific state $|a\rangle$ is

$$p(a) = \langle a|\psi\rangle\langle\psi|a\rangle.$$
(2.3)

Here, the density operator

$$\rho = |\psi\rangle\langle\psi|$$
(2.4)

is introduced. In the matrix representation, the diagonal elements $\rho_{aa} = \langle a|\psi\rangle\langle\psi|a\rangle$ give the probability for the system to be in state $|a\rangle$. The expectation value $\langle \mathrm{O}\rangle$ depends linearly on the density matrix via

$$\langle \mathrm{O} \rangle = Tr(\mathrm{O}\rho).$$
(2.5)

The trace operation Tr(…) corresponds to $\Sigma_i = \langle i| \dots |i\rangle$. The equation of motion can also be derived for the density operator, the *Quantum Liouville Equation*:

$$\frac{d}{dt}\rho = -\frac{i}{\hbar}[\mathcal{H}, \rho] = -\frac{i}{\hbar}(\mathcal{H}\rho - \rho\mathcal{H}).$$
(2.6)

Equations (2.1) and (2.6) are formally isomorph. The Hamiltonian in (2.6) acts on both sides of the density operator.

2.1.2 Description of Mixed Systems

A quantum system can be represented by a mixture of pure states $|\psi_1\rangle$, $|\psi_2\rangle$, …, $|\psi_n\rangle$, that are populated with the probabilities $P(1)$, $P(2)$, …, $P(n)$. The expectation value of an observable O is then obtained from

$$\langle \mathrm{O} \rangle = \sum_m P(m)\, \langle \psi_m | \mathrm{O} | \psi_m \rangle = \sum_m P(m)\, Tr(\mathrm{O}\rho_m).$$
(2.7)

Therefore the density operator ρ of a mixture can be described as the weighted statistical average over the individual density operators ρ_m,

$$\rho = \sum_m P(m)\, \rho_m$$
(2.8)

The diagonal elements $\rho_{aa} = \sum_m P(m)\, p_m(a)$ are the probabilities that the pure state $|a\rangle$ is contained in the statistical mixture described by ρ and are also termed the *population* of $|i\rangle$.

2.1.3 Time Evolution of a System

To solve the equations in (2.1) and (2.6), one seeks expressions for the time-dependent wavefunction $\psi(t)$ and density operator $\rho(t)$. The differential form of the *Schrödinger equation*:

$$\frac{d}{dt}|\psi\rangle = -\frac{i}{\hbar}\mathcal{H}|\psi\rangle$$
(2.1)

suggests that a linear operator $\mathcal{U}(t, t_0)$ exists, which allows to propagate the system in time and transforms the state vector $|\psi(t_0)\rangle$ at a time t_0 to the state vector $\psi(t)\rangle$ at later time t,

$$|\psi(t)\rangle = \mathcal{U}(t, t_0)|\psi(t_0)\rangle.$$
(2.9)

This operator is called the *time evolution operator*. When the Hamiltonian is time-independent, then equation (2.9) is solved by

$$\mathcal{U}_0(t, t_0) = e^{-\frac{i}{\hbar}\mathcal{H}\cdot(t-t_0)}.$$
(2.10)

In spectroscopy, the free evolution of the chromophore is perturbed by an incoming light field. This interaction is usually weak enough that perturbation theory is valid. The full Hamiltonian $\mathcal{H}(t)$may then be divided into a time-independent part $\mathcal{H}_0$and a time-dependent part $\mathcal{V}(t)$,

$$\mathcal{H}(t) = \mathcal{H}_0(t) + \mathcal{V}(t).$$
(2.11)

The interaction Hamiltonian $\mathcal{V}(t)$is commonly described in the *dipole approximation,*

$$\mathcal{V}(t) = -\mu E(t),$$

where μ is the dipole operator and E is the electric field.

The treatment of the time-dependent wavefunctions is facilitated by a transformation to the interaction picture:

$$|\psi_I\rangle \equiv \mathcal{U}_0^{\dagger}(t, t_0)|\psi\rangle$$
(2.12)

Here $\mathcal{U}_0^{\dagger}(t, t_0)$is the Hermitian conjugate of the time evolution operator for the conservative system. The density matrix in the interaction picture is defined as

$$\rho_I = \mathcal{U}_0^{\dagger}(t, t_0)\rho\mathcal{U}(t, t_0)$$
(2.13)

Because the expectation value of an observable O should not be affected by this transformation the same alternative definition of the operator Ocan be accomplished,

$$\mathrm{O}_I = \mathcal{U}_0^{\dagger}(t, t_0)\mathrm{O}\mathcal{U}(t, t_0).$$
(2.14)

In the interaction picture, the Schrödinger equation simplifies to

$$\frac{d}{dt}\left|\psi_I\right\rangle = -\frac{i}{\hbar}\mathcal{V}_I|\psi_I\rangle$$
(2.15)

In a similar way the Quantum Liouville equation can be written as

$$\frac{d}{dt}\rho_I = -\frac{i}{\hbar}[\mathcal{V}_I, \rho].$$
(2.16)

These equations of motion do not depend any more on the full Hamiltonian $\mathcal{H}$, but only on the weak perturbation $\mathcal{V}_I$. Therefore, expansion to a series and suitable truncation becomes feasible. Time integration over (2.16) gives

$$\rho_I(t) = \rho_I(0) - \frac{i}{\hbar}\int_0^t d\tau\,[\mathcal{V}_I(\tau), \rho(\tau)].$$
(2.17)

Upon iterative insertion of the density matrix one obtains

$$\rho_I(t) = \rho_I^{(0)}(t) + \sum_{n=1}^{\infty}\left(-\frac{i}{\hbar}\right)^n \int_0^t d\tau_n \int_0^t d\tau_{n-1} \dots \int_0^t d\tau_2 \times \left[\mathcal{V}_I(\tau_n), [\mathcal{V}_I(\tau_{n-1}), \dots [\mathcal{V}_I(\tau_1), \rho_I(-\infty)] \dots]\right],$$
(2.18)

where $\rho(-\infty)$is the equilibrium density matrix before the interaction with the light field. The density operator may be transferred back to the Schrödinger picture. By further changing the integration variables from time points τ_i to time spans t_i with $\tau_i = t_i - t_{i-1}$, equation (2.22) can be written as

$$\rho(t) = \rho^{(0)}(t) + \sum_{n=1}^{\infty}\left(-\frac{i}{\hbar}\right)^n \int_0^t \int_0^t \dots \int_0^t dt_n\, dt_{n-1} \dots dt_1 \times \mathcal{U}_0(t, t_o)\left[\mathcal{V}_I(t_n), [\mathcal{V}_I(t_{n-1}), \dots [\mathcal{V}_I(t_1), \rho(-\infty)] \dots]\right]\mathcal{U}_0^{\dagger}(t, t_0)$$
(2.19)

2.1.4 The Induced Polarization

The incoming electric fields induce a time-dependent polarization $P(t)$, which is to first order the expectation value of the dipole operator,

$$P(t) = Tr\big(\mu\rho(t)\big).$$
(2.20)

Equation (2.23) suggests that the polarization may be expanded into a series,

$$P(t) = P^{(1)} + P^{(2)} + \cdots$$
(2.21)

The nth order polarization can then be expressed by

$$P^{(n)}(t) = \int_0^\infty \int_0^\infty \dots \int_0^\infty dt_n\, dt_{n-1} \dots dt_1$$

$$\times R^{(n)}(t_n, t_{n-1}, \dots t_1) E^{(n)}(t_n, t_{n-1}, \dots t_1)$$

(2.22)

or alternatively in the frequency domain,

$$P^{(n)}(\omega) = \int_0^\infty \int_0^\infty \dots \int_0^\infty dt_n\, dt_{n-1} \dots dt_1$$

$$\times R^{(n)}(t_n, t_{n-1}, \dots t_1) FT\left(E^{(n)}(t_n, t_{n-1}, \dots t_1)\right).$$

(2.23)

Here the interaction Hamiltonian $\mathcal{V}_I(t) = -\mu_I(t)E(t)$ was inserted and the time ordered product of electric fields was collected in the term $E^{(n)}(t_n, t_{n-1}, \dots t_1)$.

$$E^{(n)}(t_n, t_{n-1}, \dots t_1) = E^{(n)}(t - t_n) E^{(n)}(t - t_n - t_{n-1}) \dots E^{(n)}(t - t_n - t_{n-1} - \cdots t_1)$$

(2.24)

The action of the dipole operators $\mu_I(t_i)$ on the equilibrium density matrix in contained in the nth response function $R^{(n)}(t_n, t_{n-1}, \dots t_1)$,

$$R^{(n)}(t_n, t_{n-1}, \dots t_1) =$$

$$\left(\frac{i}{\hbar}\right)^n Tr\big(\mu_I(t)\big[\mu_I(t_n), [\mu_I(t_{n-1}), \dots [\mu_I(t_1), \rho(-\infty)] \dots]\big]\big)$$

(2.25)

Evaluation of the nested commutators in the last equation produces 2^n terms, each corresponding to a different interaction pathway. As an example, consider the third-order response function $R^{(3)}(t_3, t_2, t_1)$. It may be written as the sum of eight dipole correlation functions $R^{(3)}_{[k]}$, which are pairwise complex conjugate to each other,

$$R^{(3)}(t_3, t_2, t_1) = \sum_{[k]=1}^{8} R^{(3)}_{[k]},$$

(2.26)

where

$$R^{(3)}_1(t_3, t_2, t_1) = -\frac{i}{\hbar^3} \sum_{a,b,c,d} p(a)\, \mu_{ab}\mu_{bc}\mu_{cd}\mu_{da} I_{dc}(t_3) I_{db}(t_2) I_{da}(t_1),$$

(2.26a)

$$R^{(3)}_2(t_3, t_2, t_1) = -\frac{i}{\hbar^3} \sum_{a,b,c,d} p(a)\, \mu_{ab}\mu_{bc}\mu_{cd}\mu_{da} I_{dc}(t_3) I_{db}(t_2) I_{ab}(t_1)$$

(2.26b)

$$R^{(3)}_3(t_3, t_2, t_1) = -\frac{i}{\hbar^3} \sum_{a,b,c,d} p(a)\, \mu_{ab}\mu_{bc}\mu_{cd}\mu_{da} I_{dc}(t_3) I_{ac}(t_2) I_{ab}(t_1)$$

(2.26c)

$$R_4^{(3)}(t_3,t_2,t_1) = -\frac{i}{\hbar^3}\sum_{a,b,c,d} p(a)\,\mu_{ab}\mu_{bc}\mu_{cd}\mu_{da} I_{ba}(t_3) I_{ca}(t_2) I_{da}(t_1)$$
(2.26d)

$$R_5^{(3)}(t_3,t_2,t_1) = -\frac{i}{\hbar^3}\sum_{a,b,c,d} p(a)\,\mu_{ab}\mu_{bc}\mu_{cd}\mu_{da} cb(t_3) I_{db}(t_2) I_{ab}(t_1)$$
(2.26e)

$$R_6^{(3)}(t_3,t_2,t_1) = -\frac{i}{\hbar^3}\sum_{a,b,c,d} p(a)\,\mu_{ab}\mu_{bc}\mu_{cd}\mu_{da} I_{cb}(t_3) I_{db}(t_2) I_{da}(t_1)$$
(2.26f)

$$R_7^{(3)}(t_3,t_2,t_1) = -\frac{i}{\hbar^3}\sum_{a,b,c,d} p(a)\,\mu_{ab}\mu_{bc}\mu_{cd}\mu_{da} I_{cb}(t_3) I_{ca}(t_2) I_{da}(t_1)$$
(2.26g)

$$R_8^{(3)}(t_3,t_2,t_1) = -\frac{i}{\hbar^3}\sum_{a,b,c,d} p(a)\,\mu_{ab}\mu_{bc}\mu_{cd}\mu_{da} I_{ad}(t_3) I_{ac}(t_2) I_{ab}(t_1)$$
(2.26h)

The auxiliary function $I_{ij}(t)$ describes the evolution of the system upon dipole interaction. In the formalism developed so far, a system prepared in the superposition state $|i\rangle\langle j|$ evolves according to

$$I_{ij}(t) = exp\left[-i\omega_{ij}t\right]$$
(2.27)

Here ω_{ij} is the transition frequency between states $|i\rangle$ and $|j\rangle$.

2.1.5 Relaxation

Relaxation effects are included here by the dephasing rate Γ_{ij} and the auxiliary function can be expressed in terms of the complex frequency $\widetilde{\omega}_{ij} = \omega_{ij} - \Gamma_{ij}$:

$$I_{ij}(t) = exp\left[-i\widetilde{\omega}_{ij}t\right]$$
(2.28)

In the *Bloch* approximation, the dephasing rate Γ_{ij} may be written as

$$\Gamma_{ij} = \frac{1}{2}\left(\gamma_i + \gamma_j\right) + \tilde{\Gamma}_{ij}.$$
(2.29)

The terms γ_i and γ_j refer to the inverse life-times of states $|i\rangle$ and $|j\rangle$. $\tilde{\Gamma}_{ij}$ is the pure dephasing which is the result of interactions between the oscillating ensemble with the environment. The band-shape of the damped oscillation $I_{ij}(t)$ is obtained via Fourier transform.

$$\int_{-\infty}^{\infty} dt\, I_{ij}(t) e^{i\omega t} = \left(\frac{\pi}{\Gamma_{ij}}\right) L\left(\omega - \widetilde{\omega}_{ij}\right),$$

(2.30)

$$L\left(\omega - \widetilde{\omega}_{ij}\right) = i\Gamma_{ij}/\pi\left(\omega - \widetilde{\omega}_{ij}\right).$$

The function $L\left(\omega - \widetilde{\omega}_{ij}\right)$ is a complex Lorentzian and can be divided into a real and imaginary part

$$Re\left(L\left(\omega - \widetilde{\omega}_{ij}\right)\right) = \frac{\Gamma_{ij}/\pi}{\left(\omega - \widetilde{\omega}_{ij}\right)^2 + \Gamma_{ij}}$$

(2.31a)

$$Im\left(L\left(\omega - \widetilde{\omega}_{ij}\right)\right) = \frac{\left(\omega - \widetilde{\omega}_{ij}\right)\Gamma_{ij}/\pi}{\left(\omega - \widetilde{\omega}_{ij}\Gamma_{ij}\right)^2 + {\Gamma_{ij}}^2}$$

(2.31b)

The width of these Lorentzians are determined by the dephasing time of the oscillation $I_{ij}(t)$. Electronic coherence that is created between two states $|i\rangle$ and $|j\rangle$ dephases on a much shorter time scale (5 – 10 fs) than coherence between vibrational states (1 – 2 ps). The reason is that the electron shell of a chromophore is largely exposed to the fluctuating electric field of the solvent molecules.

2.1.6 Propagation of the Electric Field through a Medium

The polarization $P(r,t)$ is connected to the electric field $E(r,t)$ by the Maxwell wave equation:

$$\left(\nabla^2 - \frac{1}{c^2}\frac{\partial^2}{\partial t^2}\right) E(r,t) = \frac{1}{\epsilon_0 c^2}\frac{\partial^2}{\partial t^2} P(r,t)$$

(2.32)

Solutions for $P(r,t)$ and $E(r,t)$ to this differential equation is provided by oscillation functions in complex form,

$$E(r,t) = \tilde{E}(r,t) exp(-i\omega t + ikr) + cc. = \mathcal{E}(r,t) + \mathcal{E}^*(r,t)$$

(2.33a)

$$P(r,t) = \tilde{P}(r,t) exp(-i\omega t + ikr) + cc. = \mathcal{P}(r,t) + \mathcal{P}^*(r,t)$$

(2.33b)

Where the complex amplitudes carry a phase factor ϕ,

$$\tilde{E}(r,t) = E_0(r,t) e^{i\phi},$$

(2.34a)

$$\tilde{P}(r,t) = P_0(r,t) e^{i\phi}.$$

(2.34b)

The notation of the electric field terms is not uniform in the literature. To describe the complex amplitudes some authors introduce an additional factor of 1/2, which then has to be taken into account in the subsequent equations. Here the following conventions are made: the complex electric field amplitudes are denoted by $\tilde{E}$ and $\tilde{E}^*$; their absolute value is E_0 and it is assumed that $E_0(r,t)$ has its maximum at t = 0. The electric field is written in equation (2.33a) as the sum of two complex conjugate terms, each describing an oscillation in the complex plane. These complex field terms are represented by the caligraphic letters E and E_. The same notation is used for the polarization. The Fourier transform operation $FT(\dots)$ interconverts expressions between time and frequency, and also between coordinate and momentum space. The actual space is indicates by the arguments t/ω and r/k.

2.2 Linear Spectroscopy

In linear absorption an incoming electric field $E(r,t)$ induces electronic coherence between the ground state $|g\rangle$ and excited electronic state $|e\rangle$. The corresponding polarization is given by the convolution of the electric field with the first-order response function $R^{(1)}(t_1)$,

$$P^{(1)}(r,t) = \int_0^\infty dt_1 R^{(1)}(r,t_1) E^{(1)}(r,t-t_1). \\ = \sum_{[k]} \int_0^\infty dt_1 R_{[k]}^{(1)}(r,t_1) E(r,t-t_1)$$

(2.35)

where

$$R_1^{(1)}(t_1) = \frac{i}{\hbar} p(g) \left|\mu_{eg}\right|^2 I_{eg}(t_1),$$

(2.36a)

$$R_2^{(1)}(t_1) = -\frac{i}{\hbar} p(g) \left|\mu_{eg}\right|^2 I_{ge}(t_1).$$

(2.36b)

The term $p(g)$ denotes the ground-state population. Both auxiliary functions $I_{eg}(t_1)$ and $I_{ge}(t_1)$ are complex conjugated. The electric field $E^{(1)}(r,t-t_1)$ is equal to the probe field,

$$E^{(1)}(r,t-t_1) = \tilde{E}(t-t_1) exp[-i\Omega(t-t_1) + rt] + cc.$$

(2.37)

The pathways $R_{[k]}^{(n)}$ that contribute to the n[th] order signal can be illustrated by energy ladder diagrams (**Fig.2.1**). Assume a two level system with a ground state g and an excited state e. The incoming field with the frequency ω_{eg} acts at $t-t_1$ on the system and creates electronic coherence between both states. This interaction is depicted with vertical arrows. Full arrows correspond to interaction of the dipole operator on the bra-side, and dashed

arrows correspond to interaction on the ket-side. The evolution of the coherence proceeds temporally from left to right with $I_{eg}(t_1) = exp\left[-i\tilde{\omega}_{eg}t\right]$ and $I_{ge}(t_1) = exp\left[-i\tilde{\omega}_{ge}t\right]$, respectively. The last arrow is needed to evaluate the signal polarization at t_1 with a last dipole transition.

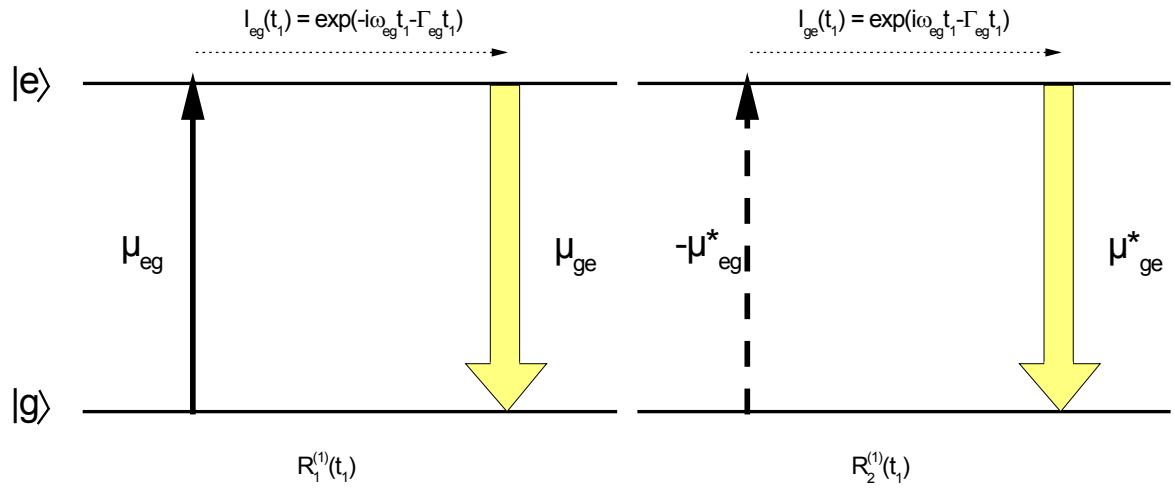

Figure 2.1: Energy ladder diagram of a two level system when pathways from a first-order response function are assumed. Vertical arrows denote interaction of the dipole operator on the ket-side (dashed) and bra-side (full). The created electronic coherence evolves from left to right with $I_{eg}(t_1)$ and $I_{ge}(t_1)$, respectively. The last interaction refers to the signal read-out of the polarization.

The time window for the inherent Fourier transform is only a few femtoseconds. As a consequence the signals in absorption spectra amount to several thousand wavenumbers.

2.3 Transient Absorption

In a transient absorption experiment an optical pump pulse transfers population from the electronic ground-state into the Franck-Condon region of the excited state. With delay time t_d a second pulse, the white light, probes the transitions to higher states. The signal is recorded in the direction of the probe pulse. Transient absorption is a 3rd order spectroscopy and the polarization $P^{(3)}$ must be determined for this experiment.

$$P^{(3)}(t) = \int_0^\infty \int_0^\infty \int_0^\infty d_3 dt_2 dt_1 \times R^{(3)}(t_3, t_2, t_1) E^{(3)}(t_3, t_2, t_1) \quad (2.38)$$

The total electric field consists of the pump-field $E_1(r, t + t_d)$ and probe-field $E_2(r, t)$,

$$E(r,t) = E_1(r, t + t_d) + E_2(r,t).$$
(2.39)

For the effective coherent field product only those terms are taken into account where the resulting k-vector points into the same direction as the incoming probe-light. Those are:

$$E_{SA}^{(3)}(t, t_3, t_2, t_1) = E_2(t - t_3)E_1^*(t - t_3 - t_2 + t_d)E_1(t - t_3 - t_2 - t_1 + t_d)$$
(2.40a)

$$E_{SB}^{(3)}(t, t_3, t_2, t_1) = E_2(t - t_3)E_1(t - t_3 - t_2 + t_d)E_1^*(t - t_3 - t_2 - t_1 + t_d)$$
(2.40b)

$$E_{CA}^{(3)}(t, t_3, t_2, t_1) = E_1(t - t_3 + t_d)E_2(t - t_3 - t_2)E_1^*(t - t_3 - t_2 - t_1 + t_d)$$
(2.40c)

$$E_{CB}^{(3)}(t, t_3, t_2, t_1) = E_1(t - t_3 + t_d)E_1^*(t - t_3 - t_2 + t_d)E_2(t - t_3 - t_2 - t_1)$$
(2.40d)

$$E_{DA}^{(3)}(t, t_3, t_2, t_1) = E_1^*(t - t_3 + t_d)E_2(t - t_3 - t_2)E_1(t - t_3 - t_2 - t_1 + t_d)$$
(2.40e)

$$E_{DB}^{(3)}(t, t_3, t_2, t_1) = E_1^*(t - t_3 + t_d)E_1(t - t_3 - t_2 + t_d)E_2(t - t_3 - t_2 - t_1)$$
(2.40f)

Basically three fields contribute to the signal: a sequential part (subscript S), a coherent part (C) and a double coherent part (D). The subscripts A and B denote the substitution of the first and second interaction with one another. For the sequential part the first two interactions are performed with the pump-field and the probe follows after a delay time t_d. Obviously, signal generation according to this scheme starts not before both, pump and probe overlap temporally. While $E_S^{(3)}$ corresponds to the absorption of one photon, $E_D^{(3)}$ refers to the term *Two-photon absorption*. However, the latter contribution is not considered here. The coherent contribution starts with two subsequent interactions with pump and probe. Because the first interaction induces electronic coherence between two electronic states which lives for only a few femtoseconds, this contribution occurs when both pulses overlap in time. In this section, we only focus on the sequential contribution. The relevant response-function to the third-order effective field is $R^{(3)}(t_3, t_2, t_1)$ with

$$R_{[k]}^{(3)}(t_3, t_2, t_1) = -\frac{i}{\hbar^3} p(g) \hat{\mu}_{[k]} exp\left[-i\tilde{\omega}_{mn} t_3 - i\tilde{\omega}_{kl} t_2 - i\tilde{\omega}_{pq} t_1\right].$$
(2.41)

Within $\hat{\mu}_{[k]}$ lays the product of the dipole matrix elements, $\mu_{fe}\mu_{ef}\mu_{cd}\mu_{ab}$ that correspond to all involved transition dipole-moments in the pathway [k]. Exemplarily shown is the 3rd-order interaction sequence of the general form

$$|g\rangle\langle g| \xrightarrow{\mu_{ab}} |m\rangle\langle n| \xrightarrow{\mu_{cd}} |k\rangle\langle l| \xrightarrow{\mu_{ef}} |p\rangle\langle q|. \quad (2.42)$$

The unperturbed electronic system is initially in the ground state. After the first interaction with the coherent field the system is prepared into the state $|m\rangle\langle n|$ via the dipole-operator, acting with μ_{ab}. Subsequent interaction changes the system either on the bra- or ket-side to the final state $|p\rangle\langle q|$ from where polarization is evaluated. Several pathways [k] exist for a three state model in which only the sequential part to the signal is considered. These contributions are illustrated in **Fig.2.2**.

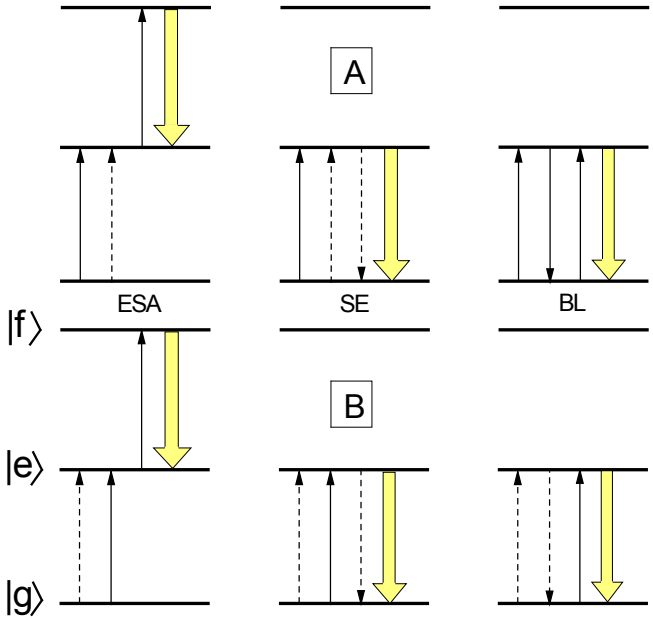

Figure 2.2: Energy ladder diagram of a three level system with ground-state g and excited states e and f when pathways from a third-order response function are assumed. Here only those diagrams are shown that contribute to the sequential interaction scheme: Transient absorption (left), stimulated emission (middle) and bleach (right). The differentiation between A and B take into account that the first two interactions can be swapped.

The contributions to the TA signal can be classified into excited state absorption (ESA), stimulated emission (SE) and bleach (BL). For ESA and SE two interactions with the pump-field change the state of the system from $|g\rangle\langle g|$ to $|e\rangle\langle e|$ and population is transferred to the excited state e. The third interaction proceeds after a time delay t_d when the probe-light arrives. Here electronic coherence is either created with a higher state f (ESA) or with the ground-state (SE). Evaluation of the polarization is symbolized with the fourth arrow. For bleach signal generation the first two interactions take place on each the bra- and ket-side and no change for the system is achieved. A third interaction creates coherence between g and e that correspond to ground-state absorption. Population in the excited-state will relax back to the electronic ground-state because it is energetically unfavorable. This process takes place statistically which manifests in a life-time of the respective state.

2.4 Femtosecond Stimulated Raman spectroscopy (this follows the supporting information in ref. 3)

2.4.1 The Electric Field and Basic Calculation of the Transient Raman Spectrum

The femtosecond stimulated Raman signal is treated within the fifth-order perturbation formalism. A useful approximation is the assumption that the interaction with the actinic pump and the scattering events, induced by the Raman and probe pulses, are well separated in time with a time delay t_d. The actinic pump prepares the system with population in a specific excited state $p(a)$. The Raman and probe pulses induce the optical changes in the third-order of the incoming electric fields. In the previous section a unified description of sequential and coherent contributions to optical transients in the third-order was outlined. The sequential contribution generates the background and is not considered here. We focus on the coherent contribution which arises from the simultaneous Raman and probe pulses, $\Delta A^{(3)}(\omega_2, 0)$, and generates the background-free Raman signal. The quantity of interest is the transient spectrum $\Delta A^{(5)}(\omega_2, t_d)$ induced by the actinic pump and measured at delay t_d by the coinciding Raman and probe pulses as function of probe frequency ω_2; it can be written as

$$\Delta A^{(5)}(\omega_2, t_d) = 2\omega_2 \sum_a p(a, t_d) \Delta A^{(3)}(\omega_2, 0) \quad (2.43)$$

$$\Delta A^{(3)}(\omega_2, 0) = Im\left(P^{(3)}(\omega_2)/E_2(\omega_2)\right) \quad (2.44)$$

Note that the absence of actinic excitation $p(a, t_d)$ corresponds to the time-independent population in the ground state, and the ground state Raman signal is defined by (2.44).

The induced polarization $P^{(3)}(\omega_2)$ which is taken in the probe direction $\mathbf{k_2} = \mathbf{k_1} - \mathbf{k_1} + \mathbf{k_2}$, and which causes the transient signal $\Delta A^{(3)}(\omega_2, 0)$, is captured though the nonlinear response $R^{(3)}_{[k]}(t_3, t_2, t_1)$ and the Fourier transform of the effective coherent field product $E^{(3)}(t_3, t_2, t_1)$, see (2.23).

$$P^{(3)}(\omega_2) = \int_0^\infty \int_0^\infty \int_0^\infty d_3 dt_2 dt_1 \times R^{(3)}(t_3, t_2, t_1) FT\left(E^{(3)}(t_3, t_2, t_1)\right) \quad (2.45)$$

This time, the effective coherent field product is constructed from the sum over Raman-$E_1(r, t)$ and probe-field $E_2(r, t)$ that are not separated by a delay time t_d,

$$E(r, t) = E_1(r, t) + E_2(r, t) \quad (2.46)$$

Only the coherent contribution is considered here:

$$E_{CA}^{(3)}(t,t_3,t_2,t_1) = E_1(t-t_3)E_2(t-t_3-t_2)E_1^*(t-t_3-t_2-t_1)$$
(2.47a)

$$E_{CB}^{(3)}(t,t_3,t_2,t_1) = E_1(t-t_3)E_1^*(t-t_3-t_2)E_2(t-t_3-t_2-t_1)$$
(2.47b)

The order of interaction is determined to Raman-probe-Raman and probe-Raman-Raman. To calculate $\Delta A^{(3)}(\omega_2,0)$ we seek concrete expressions for all contributing terms. The electric field of the Raman- and probe field are

$$E_{1,2}(t) = \tilde{E}_{1,2}(t)exp(-i\Omega_{1,2}t)$$
(2.48)

where $\Omega_{1,2}$ and $\tilde{E}_{1,2}(t)$ are the central frequency and temporal envelope of Raman/probe pulses, respectively. Exact forms for $FT\left(E^{(3)}(t_3,t_2,t_1)\right)$ with transform-limited and linearly chirped Gaussian envelopes are presented in refs. [4,5,6,7,8,9] and the reader is referred to these papers for details. Here a useful form is presented for the calculation of background-free Raman signal with two-sided exponential decay pulse envelope [10], i.e, $\tilde{E}_{1,2}(t) = exp(-\gamma_{1,2}|t|)$ with pulse width $\gamma_{1,2}$. This form is prefered over a Gaussian, since it allows one to find a simple analytic expression. When the probe is a much shorter than Raman pulse, $\gamma_1 \ll \gamma_2$, the result is obtained as

$$FT\left(E^{(3)}(t_3,t_2,t_1)\right) = I_1(t_3,t_2,t_1) + I_2(t_3,t_2,t_1)$$
(2.49)

$$I_1(t_3,t_2,t_1) = exp(i\omega_2 t_3 + i(\omega_2 - \Omega_1 + i\gamma_1)t_2 - i(\Omega_1 - i\gamma_1)t_1)$$
(2.49a)

$$I_2(t_3,t_2,t_1) = exp(i\omega_2 t_3 + i(\omega_2 - \Omega_1 + i\gamma_1)t_2 + i(\omega_2 + 2i\gamma_1)t_1)$$
(2.49b)

The response-function for the third-order interaction that is used here, differs slightly from (2.41) for simplicities in the calculations,

$$R_{[k]}^{(3)}(t_3,t_2,t_1) = -i\hat{\mu}_{[k]}exp\left[-i\tilde{\omega}_{mn}t_3 - i\tilde{\omega}_{kl}t_2 - i\tilde{\omega}_{pq}t_1\right].$$
(2.50)

Then the third-order polarization spectrum $P^{(3)}(\omega_2)$ is written as the sum over all possible pathways $[\mathrm{k}]$:

$$P^{(3)}(\omega_2) = \sum_{[k]} \int_0^\infty \int_0^\infty \int_0^\infty d_3 dt_2 dt_1$$

$$\times R^{(3)}_{[k]}(t_3, t_2, t_1) \times \left(I_1(t_3, t_2, t_1) + I_2(t_3, t_2, t_1)\right)$$

(2.51)

After substitution of $I_{1,2}(t_3, t_2, t_1)$ and $R^{(3)}_{[k]}(t_3, t_2, t_1)$ into (2.50), the integration is carried out analytically and the induced signal is expressed by auxiliary functions $F_{1,2}(mn, kl, pq)$. An analytical expression is given for $\Delta A^{(3)}(\omega_2, 0)$ by

$$\Delta A^{(3)}(\omega_2, 0) = \sum_{[k]} \left(\hat{\mu}_1 F_1(mn, kl, pq) + \hat{\mu}_1 F_2(mn, kl, pq)\right)$$

(2.52)

$$F_{1,2}(mn, kl, pq) = Im\left\{f_{mn} \times g_{kl} \times h^{(1),(2)}_{pq}\right\}$$

(2.53)

$$f_{mn} = 1/(\omega_2 - \tilde{\omega}_{mn}), \qquad g_{kl} = i/(\omega_2 - \Omega_1 - \tilde{\omega}_{kl} + i\gamma_1)$$

(2.54)

$$h^{(1)}_{pq} = -/\left(\Omega_1 + \tilde{\omega}_{pq} - i\gamma_1\right) \qquad h^{(2)}_{pq} = i/\left(\omega_2 - \tilde{\omega}_{pq} + i\gamma_1\right)$$

(2.55)

Taking the imaginary part in (2.53), the Raman signal in the $\tau_1 \to \infty$ limit can be presented as

$$F_1(mn, kl, pq) = \frac{a_1 x^2 + b_1 x + c_1}{[(x+\delta_{mn})^2 + \Gamma^2_{el}][(x+\nu)^2 + \Gamma^2_{vib}]\left[\delta^{(1)2}_{pq} + \Gamma^2_{el}\right]}$$

(2.56)

$$F_2(mn, kl, pq) = \frac{a_2 x^2 + b_2 x + c_2}{[(x+\delta_{mn})^2 + \Gamma^2_{el}][(x+\nu)^2 + \Gamma^2_{vib}]\left[\left(x+\delta^{(1)2}_{pq}\right)^2 + \Gamma^2_{el}\right]}$$

(2.57)

$$a_1 = \Gamma_{el},\ b_1 = \Gamma_{el}\left(\delta_{mn} + \nu - \delta^{(1)}_{pq}\right) - \Gamma_{vib}\delta^{(1)}_{pq},$$

(2.58a)

$$c_1 = -\Gamma^2_{el}\Gamma_{vib} + \Gamma_{el}\,\nu\left(\delta_{mn} - \delta^{(1)}_{pq}\right) - \Gamma_{vib}\delta_{mn}\delta^{(1)}_{pq}$$

(2.58b)

$$a_2 = 2\Gamma_{el} + \Gamma_{vib},\ b_2 = \Gamma_{el}\left(\delta_{mn} + 2\nu + \delta^{(1)}_{pq}\right) + \Gamma_{vib}\left(\delta_{mn} + \delta^{(2)}_{pq}\right),$$

(2.58c)

$$c_2 = -\Gamma_{el}^2\Gamma_{vib} + \Gamma_{el}\,\nu\left(\delta_{mn} + \delta_{pq}^{(2)}\right) + \Gamma_{vib}\delta_{mn}\delta_{pq}^{(2)}$$

(2.58d)

where $x = \omega_2 - \Omega_1$ is the probe-Raman detuning, ν is vibrational frequency, and we used $\delta_{pq}^{(1),(2)} = \Omega_1 \pm \omega_{pq}$, $\delta_{mn} = \Omega_1 - \omega_{mn}$and $\Gamma_{el} = \Gamma_{mn} = \Gamma_{pq}$, $\Gamma_{vib} = \Gamma_{kl}$.

The overall transient signal is the sum of all pathways [k] where all vibrational manifolds in ground $g(\nu_1, \nu_2, \dots)$ and excited states $e(\nu_1, \nu_2, \dots)$, $f(\nu_1, \nu_2, \dots)$ are included. As regards the influence of environment, remember that this was already taken into account by the empirical population and pure dephasing times. The corresponding decay rates discussed so far are the result of fast perturbations by solvents. The remaining influence on the chromophore is considered here in the limit of an infinitely long bath correlation time, *i.e.* for a frozen solvent. This static inhomogeneous broadening may be incorporated[1] by convolution the homogeneous response functions, Eq. (A13), with a static (Gaussian) distribution of transition frequencies.

2.4.2 Calculations of Raman Diagrams

Here we present the rules to calculate the Raman diagrams presented in Fig. 2. The induced polarization $P^{(3)}(\omega_2)$ which causes the transient signal $\Delta A^{(3)}(\omega_2, 0)$, is the sum over possible vibronic pathways [k] (2.53). We focus on the Raman pathways which are presented in **Figs. 2.3** and **2.4** as energy ladder diagrams. For simplicity consider response function R_3 (diagram 1 in **Fig. 2.4**) and R_1 (diagram 3a in **Fig. 2.4**) in **Fig. 2.3**. The system is prepared in the S_0 state labeled as 1.

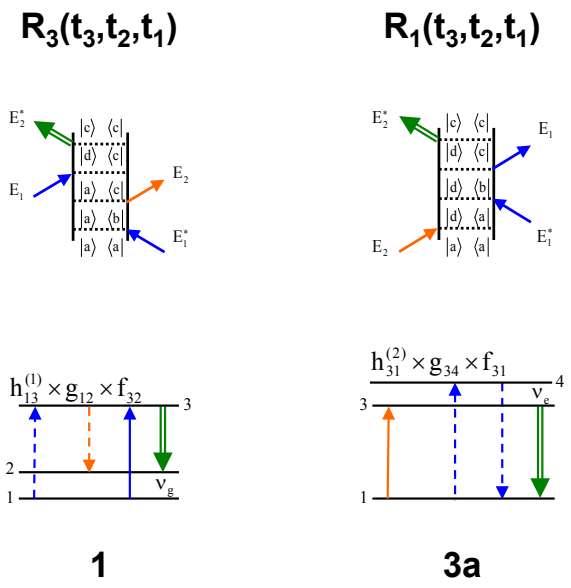

Figure 2.3: Double-side Feyman [2] and ladder diagrams for femtosecond stimulated Raman scattering of a model system with three electronic states. The system is prepared in the S_0 state labeled as 1. Double-sided Feynman diagrams are named according to refs. 2,8,11 , the ladder diagrams are labelled according to Fig.2.3. The subscripts (1) and (2) denote the interaction order (see Eqs. 2.47a-2.47b). Dashed arrows represent bra-side and full arrows ket-side interaction. The electronic states are dressed with modes ν_g and ν_e

The first interaction alters the "bra" q-index ($h_{13}^{(1)}$, $F_1(mn,kl,pq) = F_1(mn,kl,13)$), or the "ket" p-index ($h_{31}^{(2)}$, $F_1(mn,kl,pq) = F_1(mn,kl,31)$),) for diagrams R_3 and R_1, respectively. We introduce the detuning of the Raman frequency from the electronic transition induced by this interaction

$$\delta_{pq}^{(1)} = \Omega_1 + \omega_{pq},\ \delta_{pq}^{(2)} = \Omega_1 - \omega_{pq}$$
(2.59)

Analogously the next interaction changes index k or l ing_{kl}, i.e. $F_1(mn,kl,pq) = F_1(mn,12,13)$ and $F_1(mn,kl,pq) = F_1(mn,34,31)$. The vibrational coherence generated after these interactions is indicated by factors g_{12} and g_{34} and corresponds to the complex frequency

$$\tilde{\omega}_{kl} = \omega_{kl} - i\Gamma_{kl} = -\nu - i\Gamma_{vib}$$
(2.60)

The last interaction changes the m-index for R_3 and n-index for R_1, i.e., $F_1(mn,kl,pq) = F_1(32,12,13)$ and $F_1(mn,kl,pq) = F_1(31,34,31)$. The corresponding electronic detuning from the Raman frequency is given as

$$\delta_{mn} = \Omega_1 - \omega_{mn}$$
(2.61)

Let us recapitulate the equations 2.56 – 2.58. Then, by some rearrangements the contributions from R_3/R_1 diagrams is captured through

$$\Delta A_1 = F_1(32,12,13) = Im\left\{f_{32} \times g_{12} \times h_{13}^{(1)}\right\} = A_0 \times \Phi(\nu_g) \times L(\Gamma_{vib}, \nu_g)$$
(2.62)

$$\Delta A_{3b} = F_2(31,34,31) = Im\left\{f_{31} \times g_{34} \times h_{31}^{(1)}\right\} = A_0 \times \Phi(\nu_e) \times L(\Gamma_{vib}, \nu_e)$$
(2.63)

Here we have introduced the normalization factor $A_0 = \frac{1}{{\Gamma_{el}}^2 \Gamma_{vib}}$ and the auxiliary functions can be evaluated as

$$L(\Gamma_{vib}, \nu_g) \approx \frac{{\Gamma_{el}}^2}{{\delta_{eg}}^2 + {\Gamma_{el}}^2} \times \frac{{\Gamma_{vib}}^2}{(x+\nu_g)^2 + {\Gamma_{vib}}^2} \times \frac{{\Gamma_{el}}^2}{{\delta_{eg}}^2 + {\Gamma_{el}}^2}$$
(2.64)

$$L(\Gamma_{vib}, \nu_e) \approx \frac{{\Gamma_{el}}^2}{{\delta_{eg}}^2 + {\Gamma_{el}}^2} \times \frac{{\Gamma_{vib}}^2}{(x+\nu_e)^2 + {\Gamma_{vib}}^2} \times \frac{{\Gamma_{el}}^2}{{\delta_{eg}}^2 + {\Gamma_{el}}^2}$$
(2.65)

$$\Phi(\nu_g) \approx \frac{{\delta_{eg}}^2 + {\Gamma_{el}}^2}{{\Gamma_{el}}^2}$$
(2.66)

$$\Phi(\nu_e) \approx \frac{(\delta_{eg} - \nu_e)^2 - {\Gamma_{el}}^2}{{\Gamma_{el}}^2} + \frac{2(\delta_{eg} - \nu_e)(\Gamma_{el} + \Gamma_{vib})}{{\Gamma_{el}}^2 \Gamma_{vib}}(x + \nu_e)$$
(2.67)

Here we introduce detuning of the Raman frequency from the electronic transition $|g\rangle \rightarrow |e\rangle$, *i.e.* $\delta_{eg} = \Omega_1 - \omega_{eg}$.

Then, by some rearrangements the contributions from R_3 diagram is captured through

$$\frac{\Delta A_1}{4A_0} \approx -\frac{{\Gamma_{el}}^2}{{\Gamma_{el}}^2 + {\delta_1}^2} \frac{{\Gamma_{vib}}^2}{(\nu+\nu_g)^2 + {\Gamma_{vib}}^2}$$
(2.68)

The contributions from diagrams 3a and 3b in **Fig. 2.4** together with the contributions from excited state $|e\rangle$ (diagrams 2a and 2b, see **Fig. 2.4**) are obtained in a similar manner

$$\frac{\Delta A_{3a}+\Delta A_{3b}}{4A_0} \approx -\left(1-\frac{(\delta_{eg}-\nu_e+\nu_g/2)(\nu+\nu_g)}{\Gamma_{el}\Gamma_{vib}}\right)\left(\frac{{\Gamma_{el}}^2}{{\Gamma_{el}}^2+{\delta_{eg}}^2}\right)^2 \frac{{\Gamma_{vib}}^2}{(\nu+\nu_e)^2+{\Gamma_{vib}}^2}$$

(2.69)

$$\frac{\Delta A_{2a}+\Delta A_{2b}}{4A_0} \approx \left(1-\frac{\delta_{fe}(\nu+\nu_g)}{\Gamma_{el}\Gamma_{vib}}\right)\frac{{\Gamma_{el}}^2}{{\Gamma_{el}}^2+{\delta_{eg}}^2}\frac{{\Gamma_{el}}^2}{{\Gamma_{el}}^2+{\delta_{fe}}^2}\frac{{\Gamma_{vib}}^2}{(\nu+\nu_e)^2+{\Gamma_{vib}}^2}$$

(2.70)

Here we used the detuning of the Raman frequency from the electronic transition $|e\rangle \rightarrow |f\rangle$, *i.e.* $\delta_{fe} = \Omega_1 - \omega_{fe}$

Collecting all S_0 diagrams in **Fig. 2.4** we obtain the S_0 Raman (for simplicity we consider here that $\delta_{ge} = \delta_{fe} = \delta$) signal as

$$\frac{\Delta A}{4A_0} \approx \frac{{\Gamma_{el}}^2}{{\Gamma_{el}}^2+\delta^2}\frac{{\Gamma_{vib}}^2}{{(\nu+\nu_g)}^2+{\Gamma_{vib}}^2}+\frac{(\nu_e-\nu_g/2)(\nu+\nu_g)}{\Gamma_{el}\Gamma_{vib}}\left(\frac{{\Gamma_{el}}^2}{{\Gamma_{el}}^2+\delta^2}\right)^2\frac{{\Gamma_{vib}}^2}{(\nu+\nu_e)^2+{\Gamma_{vib}}^2}$$

(2.71)

The contributions from diagrams 4-8 in **Fig. 2.5** are obtained in the similar manner.

2.4.3 Double-Sided Feynman Diagrams and Energy Ladder Diagrams, and the Transient Raman Signal on the Stokes- and anti-Stokes side

We consider the electronic ground state $|g\rangle$, the first excited state $|e\rangle$, and a higher electronic state $|f\rangle$. To treat vibrational activity we dress each electronic state with modes ν_g(1100 cm^{-1}), ν_e (900 cm^{-1}) and ν_f (700 cm^{-1}). The (dimensionless) mode displacements between $|g\rangle$ and $|e\rangle$ are $\sqrt{2}$. For simplicity, the same displacements are assumed between modes in $|e\rangle$ and $|f\rangle$ and transition dipole momets are $\mu_{eg} = \mu_{fe} = 1$. The detuning of the Raman frequency is equal for $|g\rangle \rightarrow |e\rangle$ and $|e\rangle \rightarrow |f\rangle$ electronic transitions, i.e. $\delta_{ge} = \delta_{fe} = \delta$. Dephasing times contain the electronic $(\Gamma_{el} = 1/5fs)$ and vibrational $(\Gamma_{el} = 1/5ps)$ dephasing times. Simulations of transient Raman signals for the model system with three electronic levels are shown in **Figs. 2.4-2.5**. The probe frequency is assumed to be smaller than the Raman frequency and the wavenumber range that is shown appears with negative sign, denoting the Stokes-region ($\nu_{probe} - \nu_{Raman} < 0$). On the other hand Raman spectra from the anti-Stokes side are calculated for a probe-frequency that is higher than the Raman frequency (see **Figs. 2.6-2.7**). The corresponding spectral window appears with positive wavenumber on the abscissa.

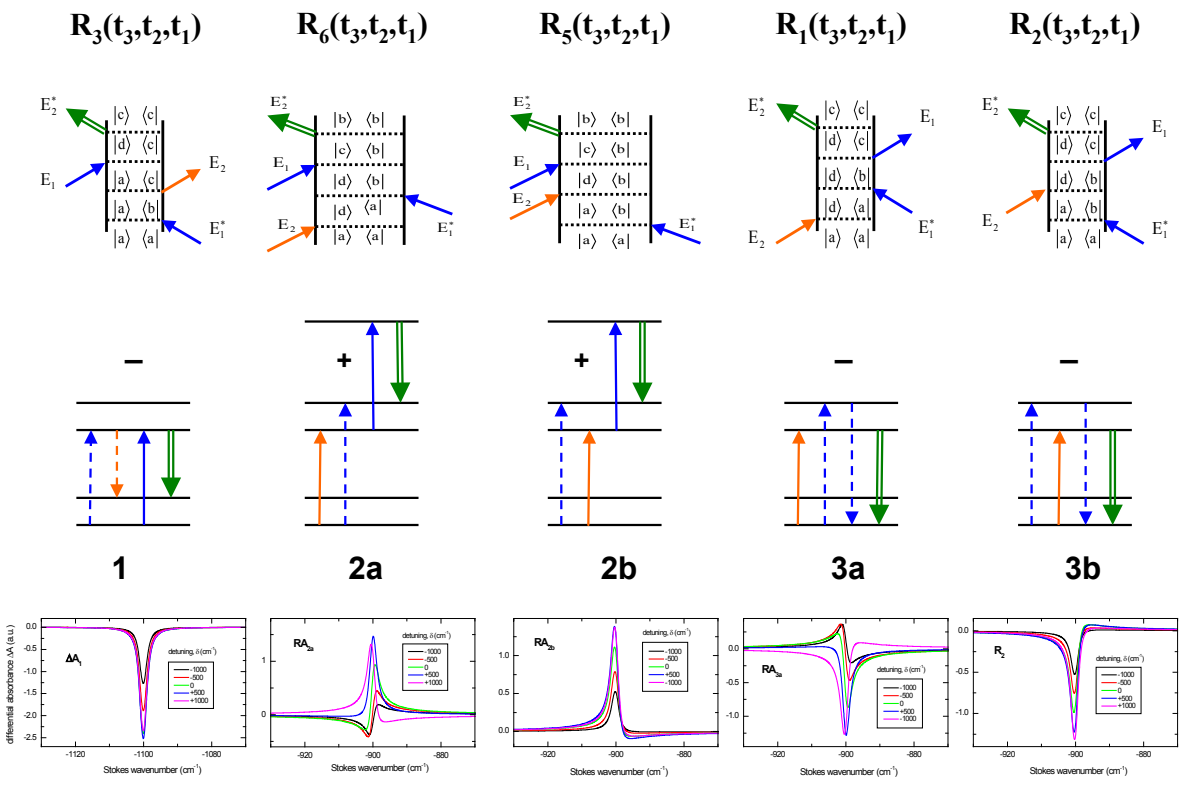

Figure 2.4: Double-sided Feynman [2] and energy ladder diagrams representing the main pathways for stimulated Raman scattering (starting in S_0, without actinic excitation) of a model system with three electronic level. Double-side Feynman diagrams are named according to refs. [2,8,11].

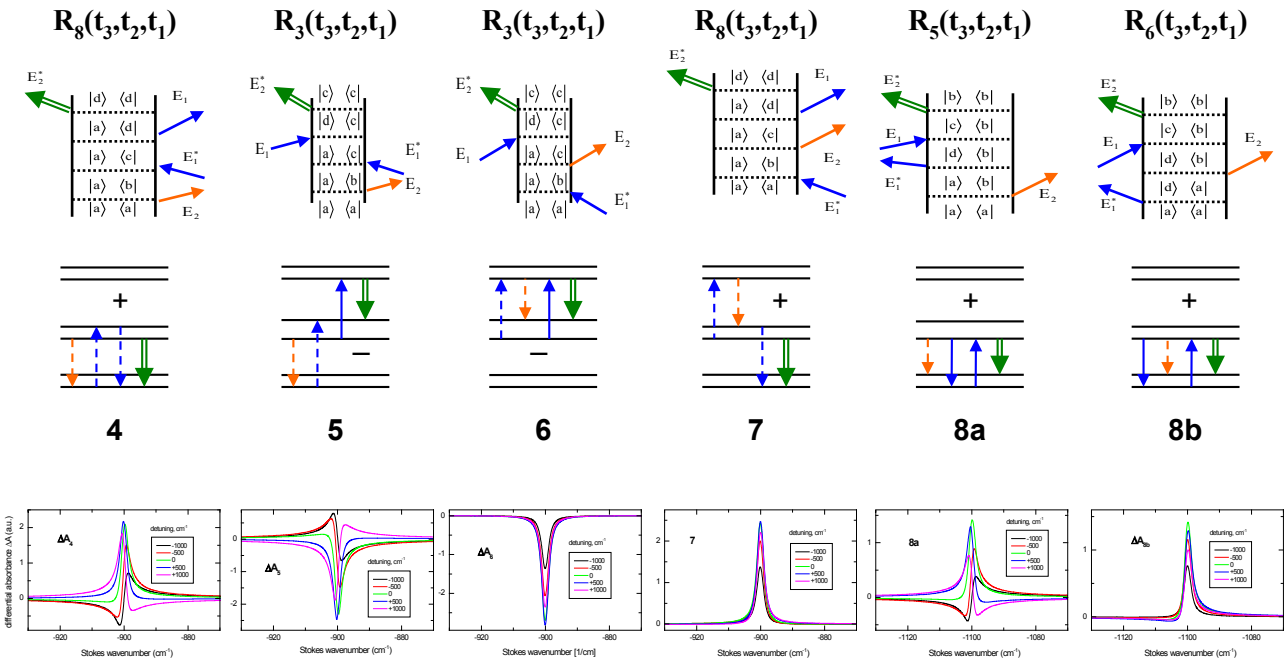

Figure 2.5: Double-sided Feynman [2] and energy ladder diagrams representing the main pathways for stimulated Raman scattering (starting in S_1, with actinic excitation) of a model system with three electronic level. Double-side Feyman diagrams are named according to Ref. 2,8,11-14.

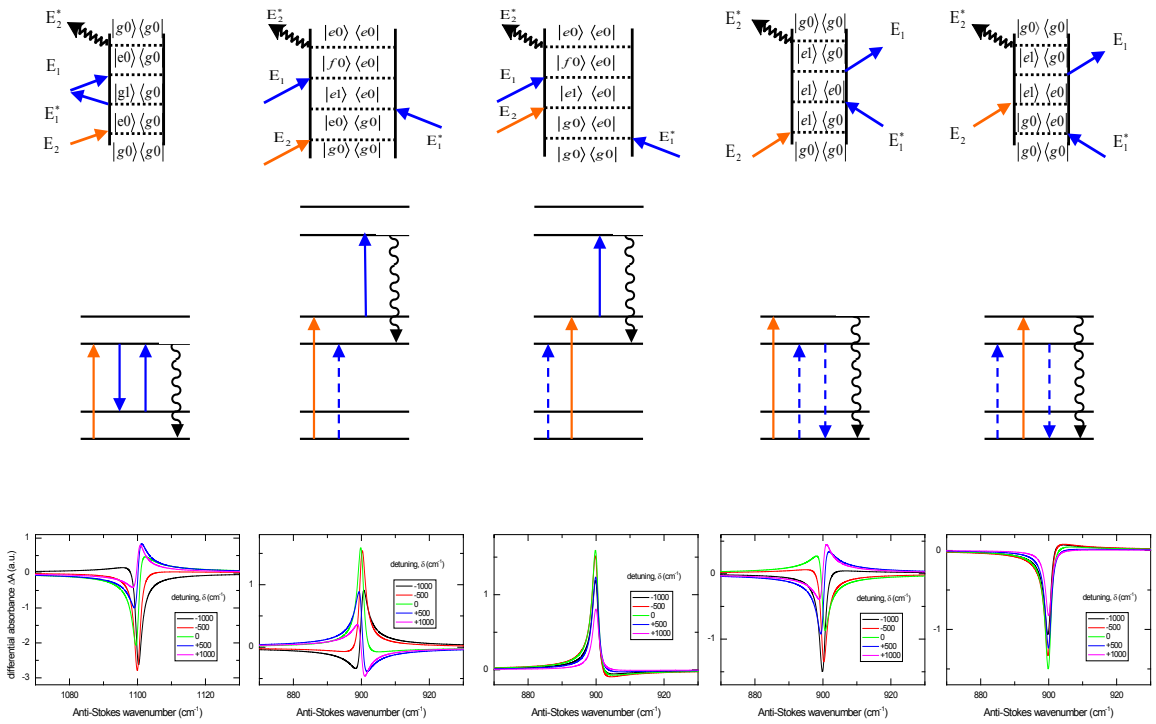

Figure 2.6. Double-sided Feynman and energy ladder diagrams representing the main pathways for *vertical* stimulated Raman scattering. A model system with three electronic levels is assumed and signal (*wavy arrow*) is evaluated on the anti-Stokes side. Without actinic excitation, the initial population resides in S_0. *Red* – interaction with anti-Stokes probe field, *blue* – with Raman pump field.

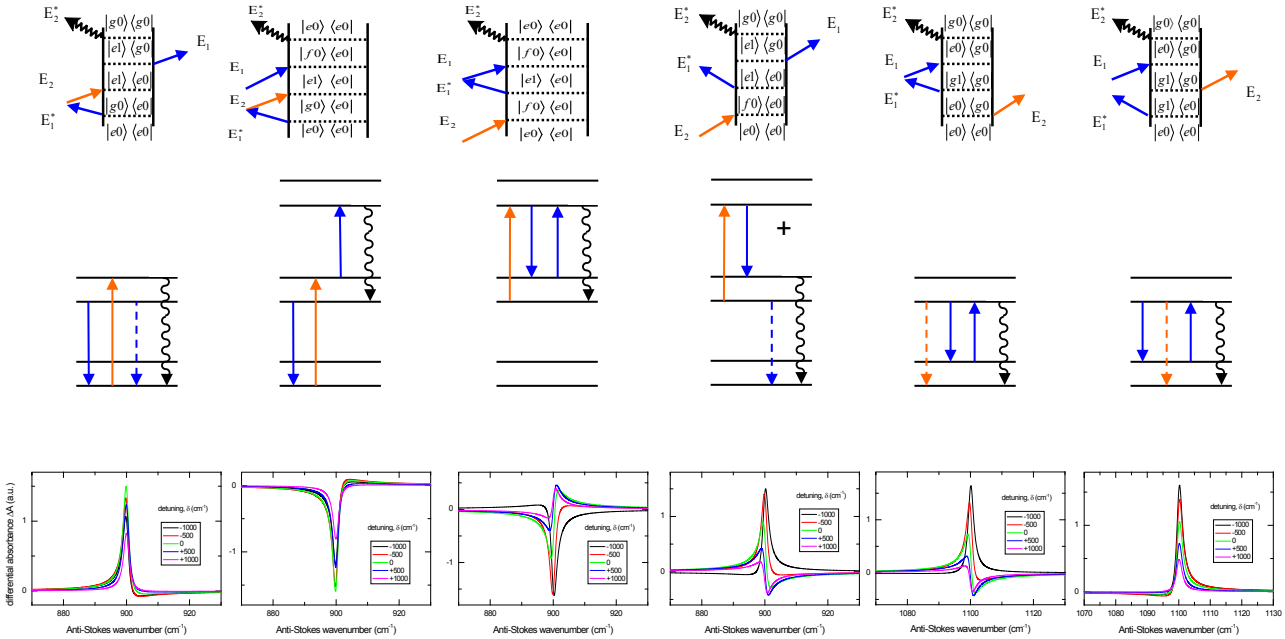

Figure 2.7. Double-sided Feynman and energy ladder diagrams representing the main pathways for *transient* stimulated Raman scattering. By preceding actinic excitation, the initial population is placed into S_2 for the subsequent four-wave mixing process.

2.5 Stern-Vollmer equation [15]

Molecules that exist in the excited state can return to the ground-state either by radiative or non-radiative processes. The fluorescence life-time is defined through

$$\tau_{F,0} = \frac{k_r}{k_r + k_{nr}}.$$

(2.72)

when additional relaxation processes (quenching) concur with the radiative life-time then the (2.72) must be modified

$$\tau_F = \frac{k_r}{k_r + k_{nr} + k_q[Q]},$$

(2.73)

Where [Q] is the quencher concentration and k_q is the rate constant for quenching. The quotient

$$\frac{\tau_{F,0}}{\tau_F} = \frac{k_r + k_{nr} + k_q[Q]}{k_r + k_{nr}} = 1 + \frac{k_q[Q]}{k_r + k_{nr}} = 1 + \tau_{F,0} k_q[Q]$$

(2.74)

is further modified to

$$\frac{1}{\tau_F} = \frac{1}{\tau_{F,0}} + k_q[Q].$$

(2.75)

By plotting the measured inverse fluorescence-lifetime against the given quencher concentration the rate constant k_q can be obtained from the slope.

3 Experimental Section

3.1 Linear Absorption and Fluorescence

UV-vis absorption spectra were measured on a Varian Cary 300. Fluorescence spectra were recorded on a Spex Fluorolog-2 spectrofluorimeter. These spectra are multiplied with a function to correct the data for the varying photometric sensitivity. Emitted fluorescence light was collected under a 90° angle; dispersed and scanned by a rotating grating.

3.2 Generation of Ultrashort Laser Pulses

3.2.1 Titan-Sapphire based laser systems

To produce ultrashort laser pulses a broad band gain medium is required. The Ti:Sa crystal emits in a range from 670 to 1070 nm that corresponds to 5 fs in the best case. A pulse-train of short laser pulses is achieved via mode-locking by which means a fixed phase-relation is established between as many modes as possible. In most Ti:Sa lasers mode-locking is achieved with the Kerr-effect (passive mode-locking). Before mode-locking the light acts as a standing wave and the laser is in the continuous wave (cw) mode, which is the favored one at this stage. Because intense light experiences self-focusing in the Kerr-medium (the Ti:Sa crystal) the amplification of short light-pulses via the pump beam becomes preferred. A push of the spring-loaded mount of one mirror leads to a strong dispersive perturbation for cw oscillation and 'opens' the channel for the pulse mode.

3.2.2 Nonlinear Light Conversion

To create a tunable laser output from the near infra-red fundamental non-linear interaction with appropriate media can be used. The induced polarization in an optical medium does not longer depend linearly on a strong electric field. The polarization can be expanded in series [1],

$$P(t) = \chi^{(1)}E(t) + \chi^{(2)}E^2(t) + \chi^{(3)}E^3(t) + \cdots$$
$$\equiv P^{(1)}(t) + P^{(2)}(t) + P^{(3)}(t) + \cdots \quad (3.1)$$

Here, only the second-order polarization is considered. When an electric field of $E(t) = E_1 e^{-i\omega_1 t} + E_2 e^{-i\omega_2 t} + cc.$ enters the nonlinear medium then the polarization is

$$P^{(2)}(t) = \chi^{(2)}[E_1^2 e^{-2i\omega_1 t} + E_2^2 e^{-2i\omega_2 t} + 2E_1E_2e^{-i(\omega_1+\omega_2)t}$$
$$2E_1E_2e^{-i(\omega_1-\omega_2)t} + cc.] + 2\chi^{(2)}[E_1E_1^* + E_2E_2^*]. \quad (3.2)$$

By using the notation

$$P^{(2)}(t) = \sum_n P(\omega_n) e^{-i\omega_n t}$$
(3.3)

one can list the various frequency components:

$$P(2\omega_1) = \chi^{(2)} E_1^2 \quad \text{(SHG)}$$

$$P(2\omega_2) = \chi^{(2)} E_2^2 \quad \text{(SHG)}$$

$$P(\omega_1 + \omega_2) = 2\chi^{(2)} E_1 E_2 \quad \text{(SFG)}$$

$$P(\omega_1 - \omega_2) = 2\chi^{(2)} E_1 E_2^* \quad \text{(DFG)}$$

$$P(0)=2\chi^{(2)}[E_1 E_1^* + E_2 E_2^*] \quad \text{(OR)}$$
(3.4)

The first and second term refer to the second-harmonic generation (SHG) which leads to a contribution at frequency 2ω. When the two input waves are different then sum-frequency generation can occur (SFG). The decay of an incident photon with frequency $\omega_1$into ω_2 and $\omega_1 - \omega_2$ corresponds to difference-frequency generation (DFG). With the presence of a seed pulse at ω_2 the generation of a photon at $\omega_3 = \omega_1 - \omega_2$ is stimulated, which in turn stimulates the creation of $\omega_2 = \omega_1 - \omega_3$, and so on. In this way the seed pulse is amplified in an optical parametric process. In these cases the nonlinear medium is a BBO (beta-Barium-Borat) crystal, which is birefringent. The sum of the k-vectors of the incoming electric fields must match the k-vector of the generated pulse (phase-matching). Otherwise the optical process becomes less efficient. Therefore the mismatch $\Delta k = k_{out} - k_{in,1} - k_{in,2}$ should be zero.

3.3 Spectroscopic techniques for transient measurements

Two setups are used. One is driven by a titanium:sapphire laser system which delivers 30 fs fundamental pulses around 800 nm (Femtolasers sPro, 500 – 1000 hz). Pulses for continuum generation (20 µJ) are usually taken from the frequency-doubled beam. Pump pulses (0.6 µJ) are conveniently generated at 400 or 267 nm, and other pump wavelength are reached by parametric optical amplification (Light Conversion Topas). The other setup is driven by 150 fs fundamental pulses at 776 nm (Clark-MXR CPA 2001, 920 hz). In this case, 30 fs probe pulses are generated at 520 nm in a two-stage noncollinear optical parametric amplifier (Jobin Yvon NOPA).

3.3.1 Fluorescence Up-conversion

The up-conversion experiment was already described in the references [2-4]. Briefly, the fundamental pulses from a Ti:Sapphire laser (800 nm, 40 fs, 500 µJ, 500 Hz) are split in a 6:1 ratio. The major portion drives a travelling-wave optical parametric amplifier (LIGHTCONVERSION) which delivers 1340 nm pulses (60 µJ) in horizontal polarization for

optical gating. The pulse front is tilted by 20 with a combination of a glass (currently, Schott SF66) prism and a lens, in order to achieve the highest possible time resolution. The minor portion of the fundamental light is used to generate its second (third) harmonic for optical pumping in the up-conversion experiment. The pump pulses (1–2 µJ) are focused onto the sample cell (0.4 mm internal path length) to a spot of 50 lm diameter. The generated fluorescence is collected with an off-axis Schwarzschild objective (not shown) and refocused to an intermediate waist which has 600 µm diameter. The waist is placed onto the refracting edge of a small calcite prism which has 32 apex angle (only about 1.5 mm of material is maximally traversed by the fluorescent light). The full angle which is

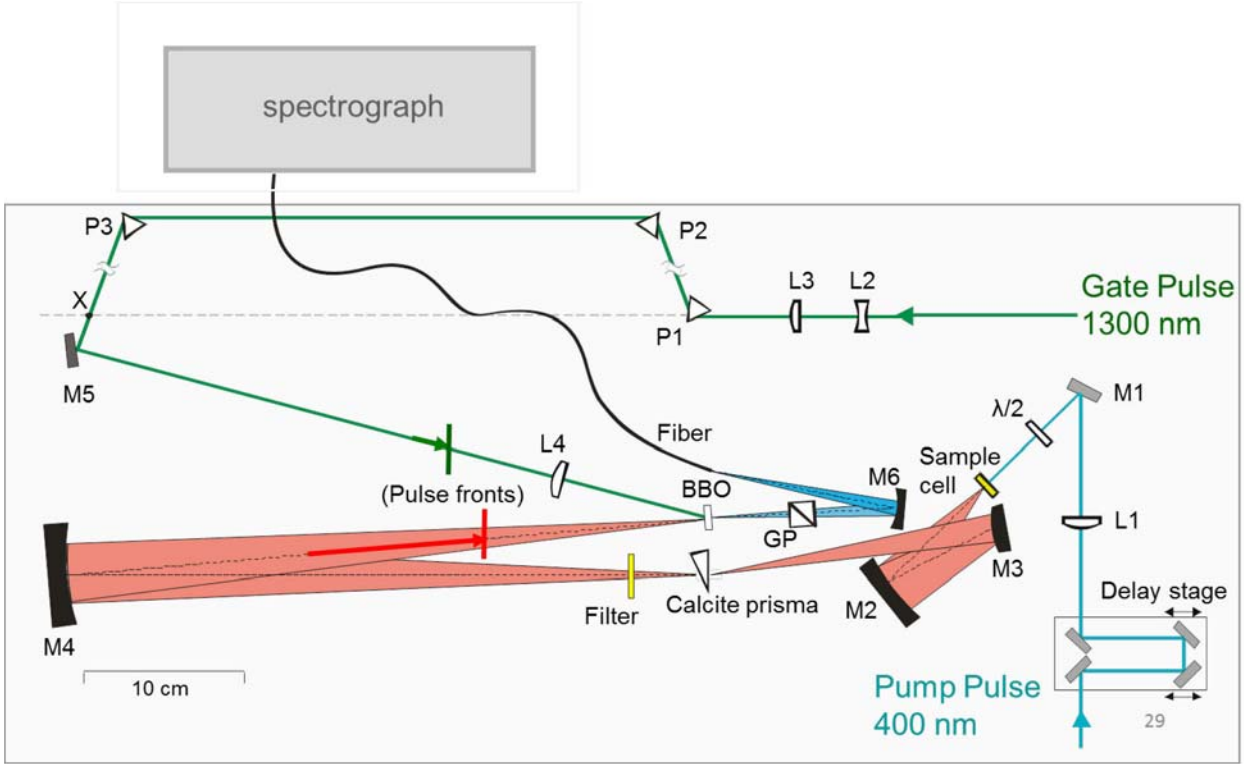

Figure 3.1: Schematic view of the up- and down-conversion setup.

subtended by the cone of fluorescence entering the prism amounts to ~4°. The optical axis of the calcite material is chosen in the vertical direction, and therefore two fluorescence cones leave the prism. They have deviation angles from the original direction of about 15 and 20 at vertical and horizontal polarization, respectively. The second cone of light is blocked, and only the first cone is refocused 1:1 onto the nonlinear optical crystal, in a near-confocal arrangement, by mirror M4. For sum-frequency generation the BBO crystals have cut angle θ_c = 46°, and the angle between gate and central rays of fluorescence is a $\alpha \approx$ 22.5°.

A former variant of the up-conversion setup used potassium dihydrogen phosphate (KDP) as nonlinear medium. In a fixed geometry with optimized external angles the wave-vector mismatch between the incoming beam (fluorescence and gate) and the up-converted light is close to zero over the spectral region 400 – 800 nm for one cut angle of a KDP crystal. The

broad-band operation with a BBO crystal was hindered due to the larger dispersion. However, the introduction of a calcite prism in combination with the collection optics allows efficient up-conversion in the same region. Here, both ends of the fluorescence cone confine an angle of ~5° in which the fluorescence beam is allowed to vary such that the phase mismatch is minimized for each spectral segment between 400 and 800 nm (**Fig. 3.2**).

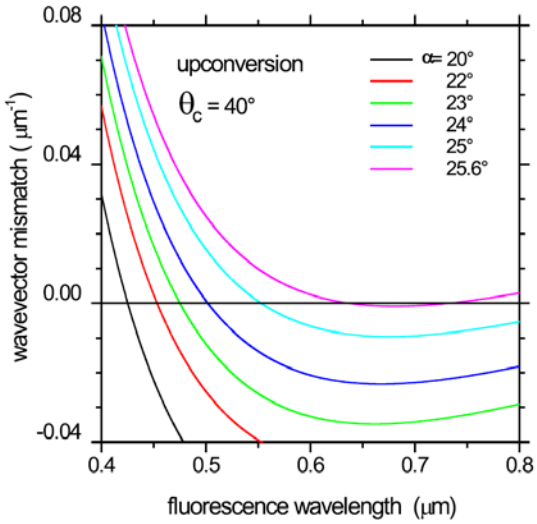

Figure 3.2: Wave-vector mismatch of the up-conversion of fluorescence light (400 – 800 nm) when the relative angle to the gate beam is varied between 20° and 25.6°.

3.3.2 Transient Absorption and Femtosecond Stimulated Raman spectroscopy

3.3.2.1 Single-Shot Spectral Referencing

The spectroscopic scheme for a transient absorption (TA) experiment consists of a pump- and a probe-pulse whose relative arrival into the sample cell is controlled by a delay-stage. A spectrum at delay time t_d is calculated from two subsequent shots where the pump-pulse is blocked in every second. When this scheme is expanded by a narrowband picosecond pulse (Raman pulse) with no delay to the probe a Femtosecond stimulated Raman experiment can be performed. Here, every second Raman pulse is chopped out and the difference is seen as Raman signals in the calculated spectrum. For practical reason the optical pulses for both types of experiment are generated differently but the detection system is kept the same for both [5,6].

The probe-light is divided in half by a beam-splitter (**Fig. 3.4**). One portion is focused into a sample cell where it probes the optical transitions. The corresponding signal is detected when the probe light is dispersed in the signal spectrograph and the corresponding signal-spectrum is recorded. The other part is directly dispersed in the reference spectrograph and the recorded reference-spectrum is used to correct the signal for structural fluctuations in the probe-light. This event is done with every second pump-pulse blocked by a chopper.

Altogether four spectra are recorded for a fixed position of the delay-stage that serve for the calculation of a transient spectrum at delay time t_d (**Fig. 3.5**).

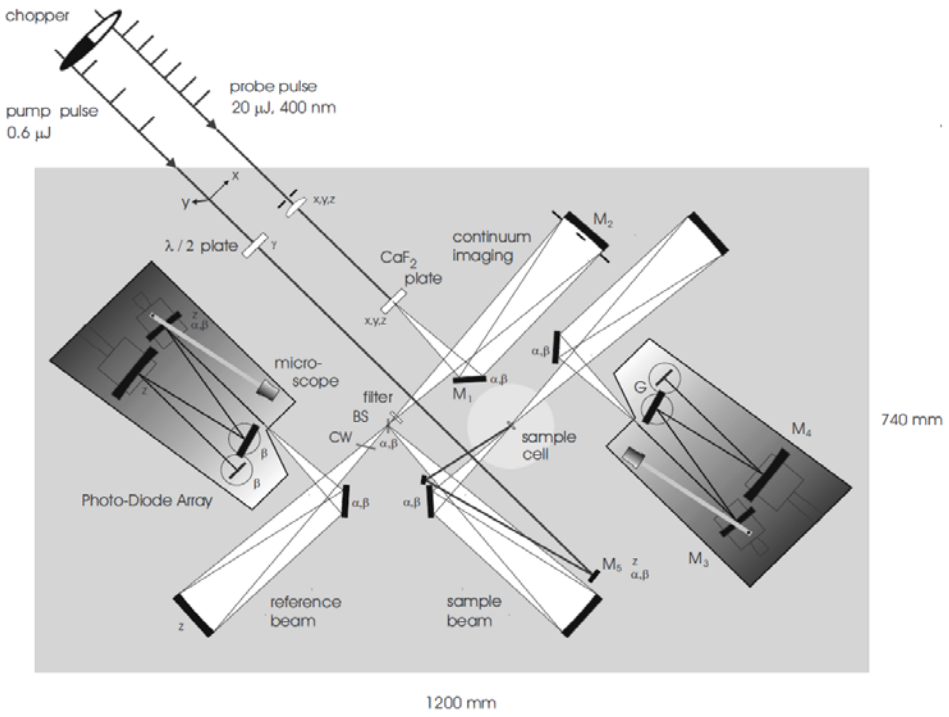

Fig. 3.4: Experimental array of a signal- and reference-spectrograph for single-shot referencing in transient absorption. A beam splitter (BS, 40% transmission, 40% reflection) divides the super-continuum equally after filtering. One portion enters the sample cell and contributes to the signal generation; absorption/emission features are visible on the probe-light in the signal spectrograph. The other part is directly dispersed in the reference spectrograph. For each laser shot (with and without pump) a spectrum is calculated from both.

The spectra on the left refer to the unaltered white-light continua that were directly recorded on the reference detector; one with the pump pulse being blocked and one with a pump pulse passing through, respectively. The spectra on the right result from an interaction of the probe-light with the sample, again with the pump being off and on, respectively. The final spectrum for one delay time t_d is calculated to

$$\Delta A_{TA} = \frac{log\left(I_{pu+pr}^{sig}/I_{pu+pr}^{ref}\right)}{log\left(I_{pr}^{sig}/I_{pr}^{ref}\right)} \quad (3.4)$$

$$\Delta A_{FSR} = \frac{log\left(I_{pu+Ra+pr}^{sig}/I_{pu+Ra+pr}^{ref}\right)}{log\left(I_{pu+pr}^{sig}/I_{pu+pr}^{ref}\right)}. \quad (3.5)$$

The notation I^{sig} and I^{ref} refer to the recorded spectrum on the signal and reference detector.

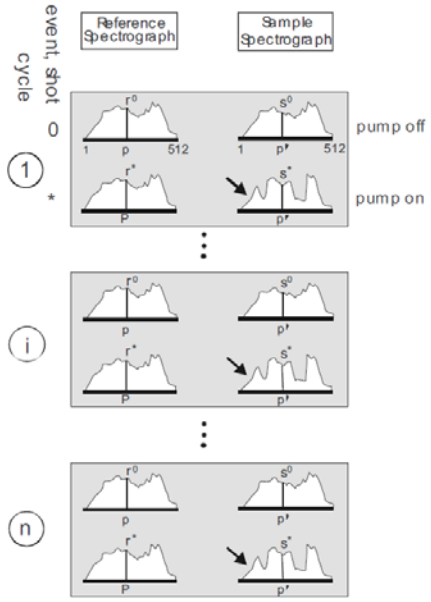

Fig. 3.5: Acquisition sequence and corresponding data package for a fixed delay position. *p*1=*p*2 pixel considered in the reference and sample spectrograph, *r*, *s* corresponding readout. During a sequence the CaF2 plate (in TA) is not moved.

Depending on the pulse that is being chopped the recorded signal either refer to TA (pump pulse is chopped) or FSR (Raman pulse is chopped). To estimate the advantage of a reference spectrograph one may introduce the correlation γ

$$\gamma = \frac{\sum r_i s_i - n\bar{r}\bar{s}}{(n-1)\sigma_r \sigma_s} \quad (3.6)$$

$$\sigma_r = \sqrt{\sum (r_i - \bar{r})^2/(n-1)} \quad (3.7)$$

$$\sigma_s = \sqrt{\sum (s_i - \bar{s})^2/(n-1)}. \quad (3.8)$$

The terms r_i and s_i refer to the photodiode value of the reference and signal spectrograph at one fixed pixel position from one laser shot (event). Altogether n=500 events were taken for the evaluation in the case of an absent pump pulse [6]. Therefore the values for s and r should strongly correlate yielding a straight line (called q) when both are plotted against each other. As seen from the black dots in **Fig. 3.6** the values correlate strongly and result in γ = 0.992. When r_i and s_i result from two subsequent events the correlation drops to 0.5 because the natural fluctuation of the probe light is not taken into account (seen as grey points in **Fig. 3.6**).

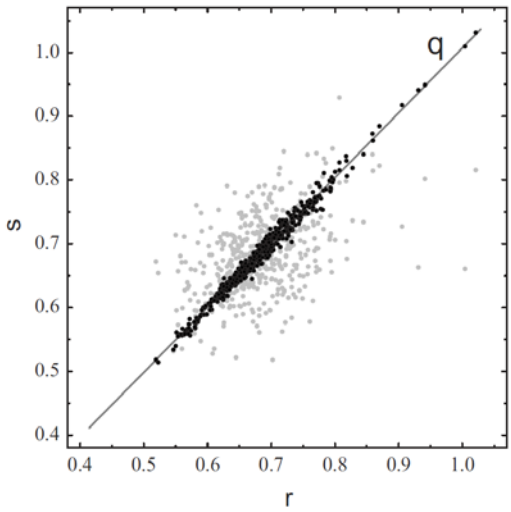

Fig. 3.6: Acquisition sequence and corresponding data package for a fixed delay position. *p*1=*p*2 pixel considered in the reference and sample spectrograph, *r*, *s* corresponding readout. During a sequence the CaF2 plate (in TA) is not moved.

3.3.2.2 Generation of the narrowband Raman pulse

The necessity of a narrow Raman pulse is reasonable from the calculated Raman line-shapes, for example from the ground-state Raman signal in (2.64)

$$L\left(\Gamma_{vib}, \nu_g\right) \approx \frac{{\Gamma_{el}}^2}{{\delta_{eg}}^2+{\Gamma_{el}}^2} \times \frac{{\Gamma_{vib}}^2}{\left(x+\nu_g\right)^2+{\Gamma_{vib}}^2} \times \frac{{\Gamma_{el}}^2}{{\delta_{eg}}^2+{\Gamma_{el}}^2}. \quad (2.64)$$

The signal shape is calculated from a product of three Lorentzian functions. The first and third term originate from the induced electronic coherence with a life-time of $1/\Gamma_{el}$ It contributes with broad and nearly flat Lorentzian functions. Vibrational coherence that is induced lives with Γ_{vib} ~ 1 ps^{-1} which provides a comparably large time window for the inherent Fourier transform of the vibrational modulations. To use the full window which causes signal-widths close to the Fourier limit Raman pulses with picosecond duration are needed. Such long pulse durations are provided by a narrow band-width (~10 cm^{-1}). The generation of such pulses is outlined in detail in ref. 6. The fundamental (776 nm) is split so that one part is used to create the Raman seed. The second part is frequency doubled in a BBO crystal and used for early stage amplification via non-collinear OPA (NOPA). The third fraction produces a chirp-free picosecond pump pulse by non-collinear SH generation of counter-chirped fundamental beams [7-9]. The Raman seed is spectrally filtered from a continuum that is generated by focusing the fundamental onto a sapphire-plate. After two NOPA stages the amplified Raman seed is filtered again to have picosecond duration. Further amplification is only efficient when the pump-pulse that is used in the following NOPA-stages has also picosecond duration. The scheme for the generation of such pump-pulse is shown in **Fig. 3.7**.

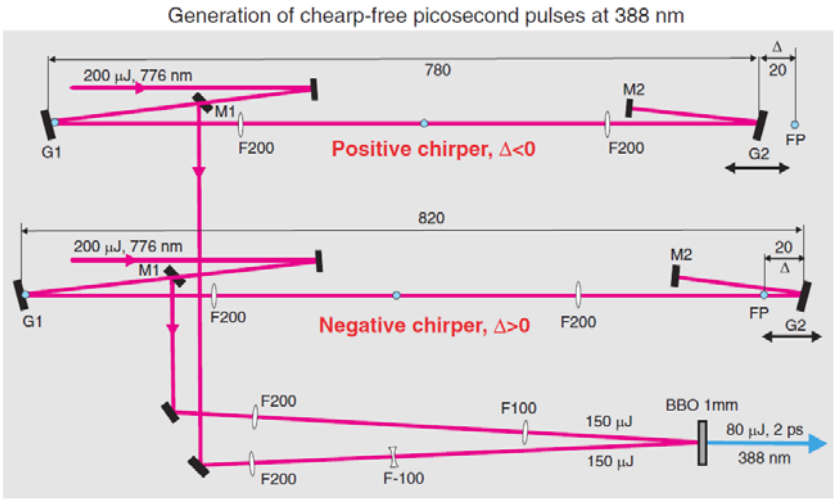

Fig. 3.7: (Color online) Generation of chirp-free picosecond SH [7]. Fundamental pulses (200 μJ) are chirped positively (top) or negatively in a classical 4F-scheme [8,9] consisting of gratings G1, G2, lenses F200, of back mirror M2 and output mirror M1. Grating G2 is shifted by Δ = ±20 mm from the focal point (FP, marked light). The two counter-chirped beams are mixed in BBO to result in chirp-free 1.4 ps pulses.

Two equal amounts of the fundamental pulse enter the 4F-scheme. After hitting grating 1 (G1) the light is focused either before or after the second grating (G2). In this way the path to the BBO crystal is larger either for the high-frequency part (negative chirp) or for the low-frequency part (positive chirp). The magnitude of the chirp is determined by the distance between focal point (FP) and G2. If a longer Raman pump is required then the distance is increased. The conversion efficiency for the SH generation amounts ~30 % which is determined by the phase-matching conditions. In two further NOPA stages the Raman seed is amplified with the picosecond pump pulse to finally yield 1.5 ps duration.

3.4 Data processing

Data processing is mainly performed with MATLAB, version 7.9.0529 (R2009b) and Wolfram Mathematica 4, version 4.0.0.0. The final data matrix that undergoes the evaluation procedure is an average over several measured spectra. Small shifts in time originate from hysteresis effects due to the back- and forward driving delay-stage and are corrected by hand. Spikes from background-radiation are removed manually. A constant signal from pump scattering is eliminated by the subtraction of an averaged spectrum from negative delay time.

3.4.1 Time-correction

The arrangements for transient absorption and femtosecond stimulated Raman spectroscopy both work with positively chirped continuum-pulses for probing [10]. As a result

the measured spectra must be corrected for that chirp. Therefore the TA spectra of the pure solvent are measured independently. In most experiments the pump wavelength is pre-resonant with the electronic transition of the solvent, so that there is only the coherent response of pump and probe within the cross-correlation time. **Fig. 3.8** shows a contour plot of the data matrix that contains transient absorption of the solvent (acetonitrile). The correction function (red) is obtained by evaluating the solvent signal in the time-domain. The coherent response can be well fitted by the cross-correlation function and their derivatives [10]. In doing so for one obtains the time-zero delay for all probe-wavelengths.

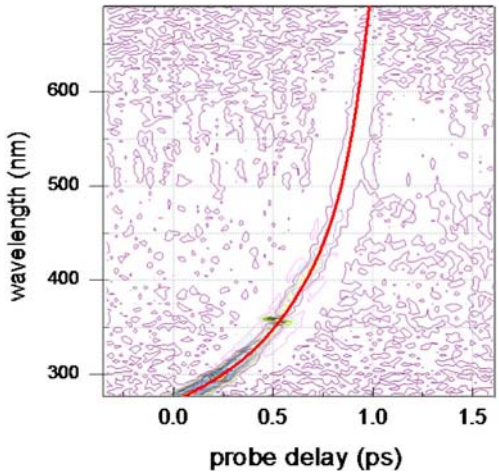

Fig. 3.8: A contour plot of the data matrix from the solvent is shown with the plotted correction-function (red).

The correction-function compensates the data for the chirp and the spectrum is building up for all frequencies at the same time (**Fig. 3.9**).

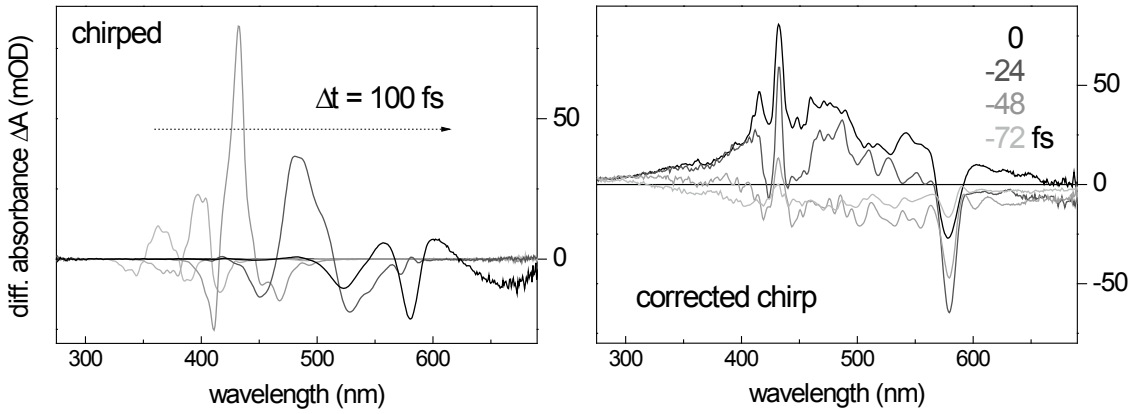

Fig. 3.9: The delayed interaction between pump and chirped super-continuum in TA causes a build-up of the spectrum from the high-frequency side to the low-frequency side. This can be followed with the immediate response from the stimulated Raman signal of the solvent in the cross-correlation region. After time-correction the coherent signal from the solvent rises (and decays) at all frequencies simultaneously.

3.4.2 Time-functions

Since most relaxation processes are statistical in the sense that the velocity of an evolution depends linearly from the population number at the initial point, exponential time-functions are commonly used for description

$$A(\lambda, t) = \sum_i f_i(k_i, \tau_0, t_0, t) A_i(\lambda) exp\big(-k_i(t - t_0)\big).$$
(3.9)

Before evolution is started, for example in the excited state, the molecules must be excited with a pump pulse. The finite duration of the assumed Gaussian shaped pulse is considered in the factor f_i.

$$f_i = exp[-k_i(t - t_0)] exp[(k_i\tau_0/2)^2] Erfc\left[-\frac{(t-t_0)}{\tau_0} + k_i\tau_0/2\right]/2\,.$$
(2.10)

A fit with n exponential time-functions yield n spectra $A_i(\lambda)$ that display the entire spectral characteristic that evolves with the rate constant k_i. These spectra are termed Decay Associated Spectra (DAS).
Another kind is the non-exponential time-function. The general form is

$$A_{ne}(\lambda, t) = f_i A_{nE,i}(\lambda) exp\big(-\{k_i(t - t_0)\}^{\beta}\big).$$
(3.11)

The exponent β stretches $(0 < \beta < 1)$ or compresses $(1 < \beta < 2)$ the exponential evolution. Such behavior occurs when the configuration of the potential energy surface is time-dependent.

3.4.3 Band Integrals

The evolution of a transient spectrum can be divided into two contributions; the migration of population from a higher state to a lower electronic state via internal conversion or the emission of a photon and the migration of population within an electronic state via vibrational relaxation. The former contribution shows up as a rise or decay of transient bands in the spectrum. Relaxation within an electronic state leads to a shift of the respective transient band because the transition frequency depends on the vibronic level that is populated. An example for both types of relaxation is shown for C_9-ethyl-β-carotene in **Fig. 3.10**. The population of S_1 via internal conversion is accompanied by the rise of the $S_y \leftarrow S_1$ ESA band with ~200 fs time-constant (panel a). The subsequent redistribution of excess energy in S_1 among all modes is seen as up-shift of this ESA band (panel b).

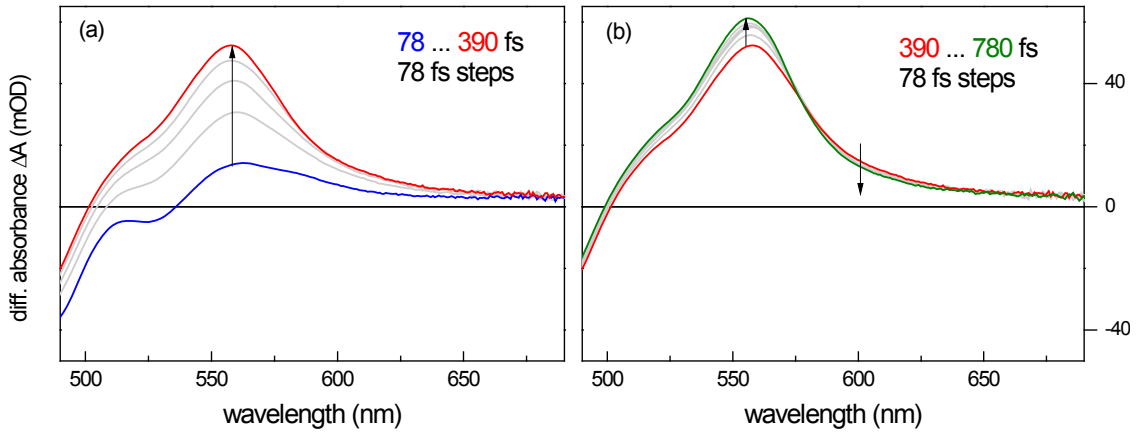

Fig. 3.10: Typical evolution of transient bands using the example of C_9-ethyl-β-carotene. (a) The $S_y \leftarrow S_1$ ESA band shows up as S_1 is populated with τ~200 fs via internal conversion from S_2. (b) Blue-shift of the $S_y \leftarrow S_1$ ESA band via internal vibrational redistribution with ~350 fs.

The relaxation scheme for this molecule regarding only migration between electronic states can be expressed as $S_2 \rightarrow S_1 \rightarrow S_0$. As apparent from **Fig. 3.11**, left panel, two time-constants are not enough to fit the time-traces because the vibrational relaxation contributes with one additional fast rise and decay on the high- (555 nm) and low-frequency side (600 nm) of the ESA band. To compensate for that shift and extract the pure relaxation between electronic states it is advantageous to perform a band integral over the corresponding ESA band

$$BI(t;\lambda_1,\lambda_2) = \int_{\lambda_1}^{\lambda_2} \Delta A(t,\lambda)\lambda^{-1} d\lambda \quad (3.12)$$

which is basically a summation over all transition probabilities starting from any vibronic level of the lower electronic state to a higher electronic state. By the integration in (3.12) the loss of intensity on the low-frequency side is compensated by the gain of intensity of the high-frequency side (see **Fig. 3.10**, panel b) and only the population and depopulation of the electronic state, respectively, remains (**Fig. 3.11**, right panel). A fit with two time-constants now lead to a flat residual.

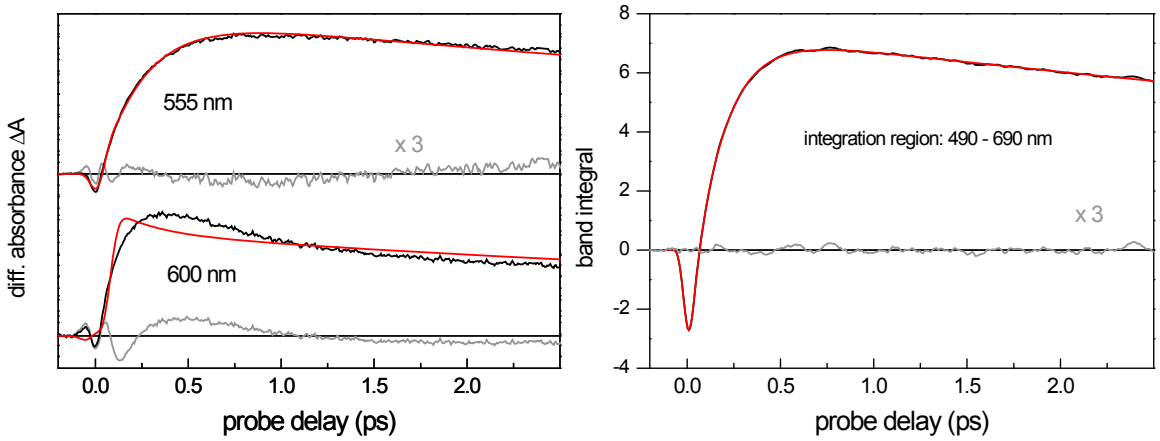

Fig. 3.11: left panels: Representative time-traces (black) of the spectral evolution of C_9-ethyl-β-carotene and fits (red). The residuals (grey) are shown with three times magnification for 555 nm. Right panel: By integrating the spectral area according to (3.12) the spectral shift is canceled from the evolution and only relaxation between states remain.

3.4.4 Correction for the electronic Background (follows in parts supporting information in ref. 11)

When a transient Raman spectrum is measured with a Raman pump that is resonant with an excited state transition then the spectra contain both, the Raman signals and a broad electronic background. These features originate from a coherent and a sequential contribution when Raman-pump and –probe simultaneously interact with the electronic system in third order (**Fig. 3.10**). Initially, the actinic pump pulse transfers population into S_1 (blue arrows). The coherent contribution corresponds to the third-order polarization which is outlined in section **2.4**, (**Fig. 3.10**, left). The Raman-pulse can also act as actinic pump that transfers population into S_n (green arrows) in which electronic coherence with a higher state S_m is immediately created by the probe-pulse (red arrow). By the read-out arrow (thick yellow arrow) a broad TA spectrum is recorded (**Fig. 3.12**, right).

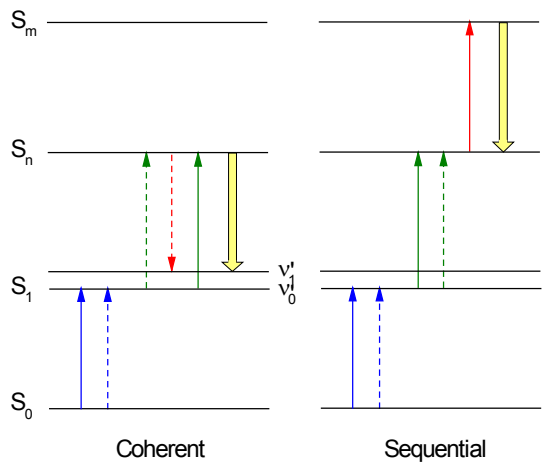

Fig. 3.12: Energy ladder diagrams for the coherent and sequential contribution of the measured FSR spectrum.

To obtain the desired Raman signals appropriate methods must be found to model the broad background. Principally, one can use interpolation-functions that are defined section-wise. Here, splining-points are set at spectral positions where no Raman signal is present. Between these points proceed third-order polynomials, of which two adjacent ones share one splining-point at which both hold the same second and third derivative. One example is given in **Fig. 3.13**.

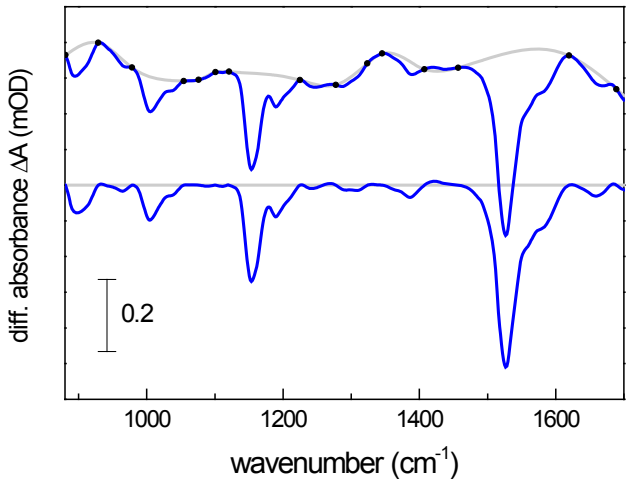

Fig. 3.13: Above: FSR spectrum (blue line) with electronic background. A splining-function (grey line) is determined by setting splining-points (black dots). Below: FSR spectrum is corrected, by which means all Raman signals have been subtracted from the electronic background.

With a Raman-excitation that is resonant with the $S_1 \leftarrow S_0$ transition then excited-state modes can be probed even when population is still in the electronic ground-state (see **Fig. 2.4**, 2a,b and 3a,b). As outlined in section **2.4** the width of these signals depend on the dephasing time between vibrational states that, again, depends on the life-time of the electronic state and the pure dephasing time (2.29). In case of β-carotene the vibrational

dephasing time of ~1 ps exceeds the life-time of the involved excited-state ~200 fs and the Raman signal appears broadened. Methods to reliably separate broad vibrational bands from the electronic background are illustrated in **Fig. 3.14**.

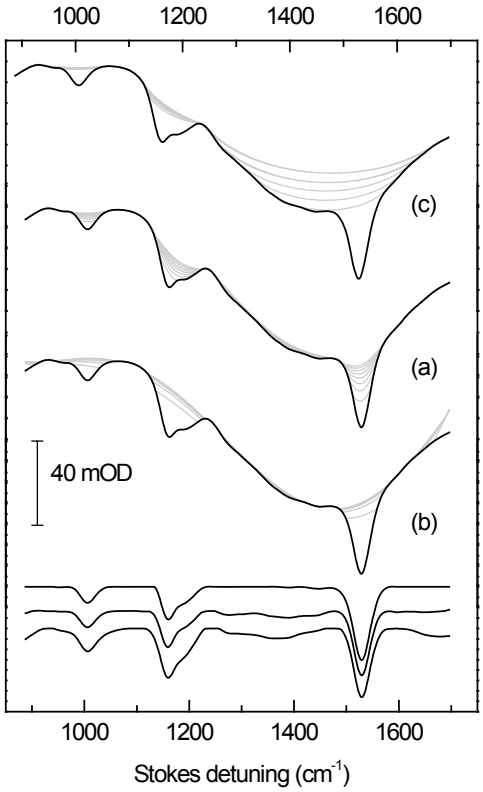

Fig. 3.14: In order to extract broad Raman signals from the electronic background, three techniques were implemented. **(a)** - Repeated *application* of a broad filter removes sharper features from the spectrum, whereas the slowly varying background is hardly affected. **(b)** – as in (a), but with interpolating polynomial instead. **(c)** - Scanning circle of decreasing radius until (by inspection) the background is reached. The resulting Raman spectra after subtraction of the electronic background are shown in the lower section.

For each spectral fragment $S \equiv \Delta A(\nu)$ recorded by vertical FSR, the electronic absorption background $B(\nu)$ to the Raman signal was estimated by several methods. **Fig. 3.14a** demonstrates the repeated application of a broad filter as described in the paper. The intermediate $\bar{S}(\nu)$ may also be constructed by an interpolating polynomial of low order, or by the average of such interpolations with different orders. Corresponding iterations are shown in **Fig. 3.14b**. In another method, features with different curvature (like signal and background) are distinguished by the use of a circle having pixel radius *r*, **Fig. 3.14c**. Basically a circle "rolls" along the broad electronic background of spectrum S and ignores narrow Raman signals. The technical implementation of the path is ensured by subtraction of the smallest vertical distance between circle and spectrum. Consider one spectral position ν_i

whose background-value shall be determined. While the circle passes by, multiple vertical distances to ν_i are recorded of whom only the smallest value/distance counts. The final background is then constructed from all valid values.

3.4.5 Singular Value Decomposition

When a spectrum is repeatedly measured by varying a physical quantity (let us use the pH value as example), one observes a systematic dependency. This observation can be attributed to the transformation from one species to another accompanied by spectral changes. By knowing the species-associated spectra (SAS) and the dependency from the pH value it should be possible to create a matrix that distinguishes from the original data only by random noise. The mathematical procedure behind, is the concept of singular value decomposition (SVD)

$$M = USV^T$$
(3.13)

The matrix M contains the original data and is split into the matrices U, S and V^T; the superscript T refers to transposition. U and V have no physical meaning but they reflect basis-spectra (U) and how their amplitudes depend on a varying pH value (V^T). The symmetric matrix S contains the singular values which are arranged in descending order, thus giving the weighting for each basis-spectrum. Only the first j values which are comparably larger than the remaining ones are significant. In this way only the first j rows and columns are kept in U and V^T, respectively. Furthermore the new matrix S_c (c for cut) can be divided into two matrices by applying a square root and multiplying it to U_c and V_c^T from the right and from the left, respectively, to form new matrices U_{cN} and $V_c^T{}_N$

$$M_C = \left(U_c\sqrt{S_C}\right)\left(\sqrt{S_C}V_c^T\right) = U_{cN}V_{cN}^T.$$
(3.14)

As already mentioned the matrix M (or M_C) can be basically reconstructed from two matrices that contain the SAS and the pH dependency of their respective intensity (called EVO)

$$M_C = U_{cN}V_{cN}^T \approx SAS \times EVO.$$
(3.15)

The matrix EVO is constructed from the pH dependent mole-fraction in the form

$$f_a = \frac{10^{-2pH}}{10^{-2pH}+10^{-2pH-pK_1}+10^{-pK_1-pK_2}}$$
(3.16a)

$$f_b = \frac{10^{-pH-pK_1}}{10^{-2pH}+10^{-2pH-pK_1}+10^{-pK_1-pK_2}}$$
(3.16b)

$$f_c = \frac{10^{-pK_1-pK_2}}{10^{-2pH}+10^{-2pH-pK_1}+10^{-pK_1-pK_2}},$$
(3.16c)

where two pK_a values are assumed to describe the protonation equilibria between three species. A matrix F_{OPT} can be found that satisfies the equation

$$V_{cN}^{T} = F_{OPT} EVO$$
(2.17)

in the sense of least square deviation which also yields the optimum pK_a-values. By multiplying F_{OPT} with U_{cN} from the right one obtains the corresponding SAS.

3.5 Experimantal Details

The experimental details that refer to the performed measurements in publication 2 and 3 are mentioned here. The related information for the first publication is available within the main text.

Sample preparation. β-carotene (Fluka) was used as received. For each measurement solutions in *n*-hexane were freshly prepared and then continuously bubbled with argon.

Transient absorption measurements. The TA setup with applications has been described elsewhere [5,10]. It provides spectral coverage 275 – 690 nm and 650 – 1050 nm with a 0.1 ps instrumental response and timing precision of 0.02 ps over the full probe range. A solution of 0.09 mM of β-carotene, or 0.12 mM of et- and iPr-β-carotene, respectively, was flown through a sample cell of 0.4 mm internal thickness. Transient absorption spectra $\Delta A(\lambda, t)$ of β-carotene were recorded upon 498 nm excitation. For the et-β-carotene and iPr-β-carotene excitation was performed with pulses centered at 490 nm. 10 – 20 pump-probe scans were averaged to improve the signal-to-noise ratio. All TA spectra were recorded at the magic angle between pump- and probe polarizations.

Femtosecond stimulated Raman experiments. The transient Raman setup was similar to that for TA measurements [6]. The picosecond narrow Raman pump (0.05 μJ, 920 Hz) was tuned to λ_R = 540, 573 and 621 nm. In case of λ_R = 776 nm the Raman pump was filtered from the fundamental amplifier-output. The polychromator dispersion was adjusted to cover a 1000 cm^{-1} probe range. Stokes and anti-Stokes Raman signal was recorded by chopping the Raman beam, with actinic excitation at λ_{ac} = 490 nm. In this registration scheme, signals at negative pump-probe delays correspond to ground-state Raman contributions from both solute and solvent. For positive delays these contributions are eliminated by subtracting the (averaged) signal from negative delays. 24 pump-probe scans were averaged to improve the signal-to-noise ratio.

Sample preparation. β-carotene (Fluka) was used as received. Its concentration in n-hexane was ~0.16 mM (near saturation) so that the peak absorbance was ≈1 in a 0.4 mm flow cell. For each measurement solutions were freshly prepared and then continuously bubbled with argon.

Femtosecond stimulated Raman experiments. The Raman pump (0.2 μJ, 920 Hz, 10 cm^{-1} fwhm) was tuned in the wavelength range λ_R = 480–580 nm. The actinic (λ_{ac} = 490 nm, 30 fs, 1 μJ), probe (30 fs, 1000 cm^{-1} wide, chirped), and Raman beams were focused on a flow sample cell in the boxcar geometry. The spot size was about 100 μm for the actinic and probe beams and 30 μm for the Raman beam. The polychromator dispersion was adjusted to cover a 1000 cm^{-1} probe range. In measurements with/without actinic excitation, the signal was recorded by chopping the Raman pump with the actinic excitation being open/blocked. In this registration scheme, signals at negative pump-probe delays correspond to ground-state Raman and solvent contributions. For positive delays, these contributions are eliminated by subtracting a representative spectrum obtained at negative delays. 50–100 pump-probe scans were averaged to achieve a sufficient signal-to-noise ratio. Note that Raman gain is drawn in our figures as a decrease of optical density, similar to stimulated emission.

—*J. Phys. Chem. B* — [1]

Fluorescence following Excited-State Protonation of Riboflavin at N(5)

Martin Quick, Alexander Weigel,[#] Nikolaus P. Ernsting[*]

Department of Chemistry, Humboldt-Universität zu Berlin,

Brook-Taylor-Str. 2, D-12489 Berlin, Germany

ABSTRACT

Excited-state protonation of riboflavin in the oxidized form is studied in water. In the -1 < pH < 2 range, neutral and N(1)-protonated riboflavin coexist in the electronic ground state. Transient absorption shows that the protonated form converts to the ground state in <40 fs after optical excitation. Broadband fluorescence upconversion is therefore used to monitor solvation and protonation of the neutral species in the excited singlet state exclusively. A weak fluorescence band around 660 nm is assigned to the product of protonation at N(5). Its radiative rate and quantum yield relative to neutral riboflavin are estimated. Protonation rates agree with proton diffusion times for H^+ concentrations below 5 M but increase at higher acidities, where the average proton distance is below the diameter of the riboflavin molecule.

KEYWORDS Fluorescence Upconversion Spectroscopy, FLUPS, Solvation, Excited-State Proton Transfer, ESPT.

[1] Reprinted ("Adapted" or "in part") with permission from Quick, M.; Weigel A.; Ernsting, N.P. Fluorescence following Excited-State Protonation of Riboflavin at N(5). *J. Phys. Chem. B*, **2013**, *117*, 5441-5447.
[#] current address: Department of Chemistry, University of Oxford, Great Britain
[2*] Phone (+49) 30 2093 5551, Fax (+49) 30 2093 5553, E-mail: nernst@chemie.hu-berlin.de

1. INTRODUCTION

Riboflavin is the precursor of flavin adenine dinucleotide (FAD), the carrier of high-energy electrons in respiratory metabolisms.[1] It is also the cofactor in redox-active flavoproteins [2-4] and in blue-light activated photoreceptors such as phototropines, cryptochromes, and photolyases. [5-9] In a rigid protein binding pocket, aspects of flavin (photo-) chemistry are optimized for the biological function. In solution, on the other hand, all redox/protonation species in the electronic ground and excited states can be accessed in principle. Extensive research has thus been focused on the electronic structure of the chromophore and its dependence on substitution [10-15], H-bonding and solvation, [16-19] and conformation, [20, 21] all of which play a role in a flavoprotein.

We examine riboflavin in the oxidized form which in aqueous solution is the most stable one. In the electronic ground state S_0, three different protonation states are found (**Fig. 1):** the neutral form RF, the protonated form RFH^+, and the deprotonated form RF^-.[10, 22] Their mole fractions as a function of pH are given in **Fig. 2a**, and the optical absorption spectra of the species are compared in **Fig. 2b**. Neutral RF is characterized by an absorption band around 450 nm, which corresponds to the $S_1 \leftarrow S_0$ transition, of $\pi\pi^*$ character with an $n\pi^*$ admixture depending on the environment.[18] In the ground state it is the only observed species between pH 2 and 9. At higher pH, anionic RF^- is formed with a pK_a value of 10.1 as the N(3)-H bond is deprotonated. In strongly acidic solutions, cationic RFH^+ forms with pKa = -0.1 and can be monitored by an intense absorption band at 390 nm. By comparing spectral

changes with quantum-chemical predictions, it was concluded that protonation occurs at N(1) in the electronic ground state. [23]

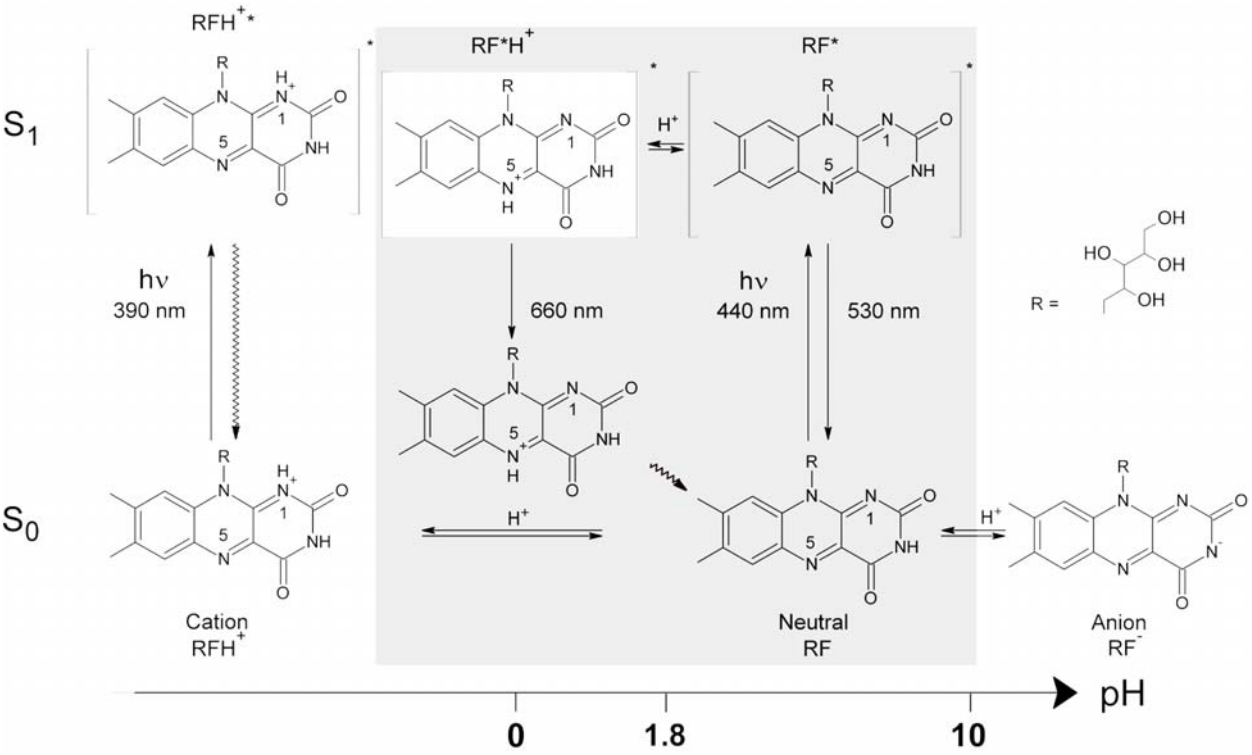

Fig.1. Protonation reactions of oxidized riboflavin (RF) in the electronic ground- and excited singlet states in aqueous solution. In this work the marked pH range is examined and the N(5) protonated form in the S_1 state (white box) is identified experimentally.

After optical excitation of neutral riboflavin, the resulting RF* can return to the ground state via fluorescence around 530 nm and also by non-radiative processes. In contrast to absorption, fluorescence reports on the mole fractions of different species in the excited state. Relative fluorescence quantum yields ϕ/ϕ_{max} of the RF* band are represented as empty circles in **Fig. 2a**. In the pH range 4–8, the yield is maximal. Towards higher pH it decreases exactly like the mole fraction of RF in the ground state, but in the other direction, as the pH dips below 4, the fluorescence yield decreases even though the mole fraction of RF in the ground state remains unchanged

initially. This effect shows that the basicity is higher in the excited state ($pK_a^* = 1.8$). In water below pH 2, proton transfer from the solution becomes the preferred reaction pathway when photoexciting neutral riboflavin.

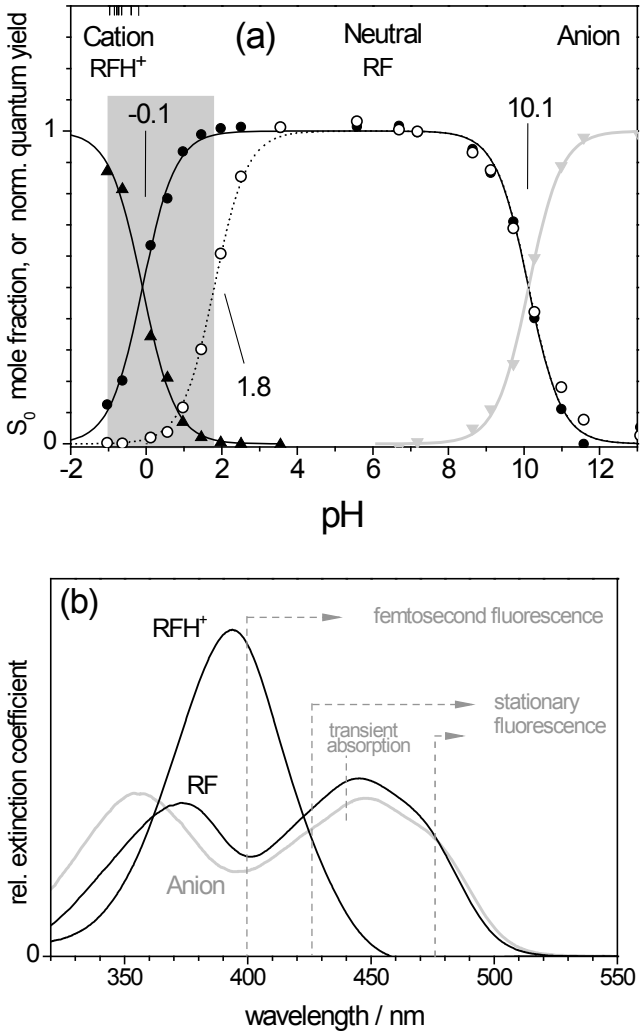

Fig. 2 (**a**) Mole fractions of cationic, neutral, and anionic RF as function of pH, from absorption in the electronic ground state (full circles and triangles). The relative fluorescence quantum yield of neutral RF is also shown (empty circles, from excitation at 428 nm). pK_A values are obtained from fits (lines). In the remainder we focus on the pH range -1 to +2 (gray band).

(**b**) Ground-state absorption spectra of the three species and excitation wavelengths (dashed lines).

Excited-state proton transfer (ESPT) from water to flavin has been the subject of many publications (see 22, 24, 25 and references therein). In the literature, it is often taken for granted that protonation in the excited singlet state occurs at N(5), different from the ground state. [24, 25] The argument is based on a computational study which was performed decades ago[26] and confirmed by advanced calculations only recently.[27, 28] Even though, to the best of our knowledge there is no direct experimental evidence for the hypothesis. The reaction results in a species whose chemical structure and optical properties are currently not known.

A quantitative examination of the protonation kinetics in the excited state was limited to pH 1 where the decay of RF* occurs on the 100 ps time scale.[22, 24, 25] Here we concentrate on the range until pH -1, which is marked by a gray band in **Fig. 2a**. In this range all population changes due to protonation are found, in S_0 as well as in S_1. The ESPT process is accelerated into the pico- and femtosecond regime so that fluorescence upconversion and pump-probe absorption measurements are required to resolve the protonation kinetics. Using a broadband scheme, we are able to gate entire fluorescence spectra with 180 fs time resolution. In this way, not only the decay of RF* is monitored as its 530 nm emission band disappears, but also spectral shifts and other changes on a 10 ps time scale are charted with unprecedented accuracy. Such transient fluorescence methods are more conclusive than transient absorption, which suffers from spectral congestion.

An intermediate emission band at 660 nm is found and confirmed by stationary measurements. Actually, this band was already noted in stationary work by Li and Glusac.[24] These authors attributed it to riboflavin which is protonated in the

electronic ground state at N(1) and then excited. Here we show instead that the precursor is excited neutral riboflavin. The conclusion is reached from two observations: (i) the pH dependence of the emission intensity compared with the known population fractions in **Fig. 2a**, and (ii) the spectral evolution of the emission shape and intensity.

Assignment of the carrier for the 660 nm emission becomes possible with the help of a model compound, also from Glusac and coworkers.[29] In this way the identity with excited flavin that has been protonated at N(5) is established. Solvation and protonation of the originally created RF* are distinguished by broadband femtosecond fluorescence measurements. Radiative properties are obtained, and protonation rates are related to the proton diffusion constant.

2 RESULTS

2.1 Stationary Absorption and Fluorescence.

Stationary absorption spectra for pH -1 to +13 (not shown) were analyzed with singular-value decomposition (SVD). Using model functions for the pH–dependent mole fractions, we find the three species-associated spectra which were already shown in **Fig. 2b**. Comparison with the pure spectra in ref. 22 shows good agreement, and the pK_a values -0.1 ± 0.3 and 10.1 ± 0.5 (resulting in the solid lines in the figure) are consistent with the published ones.[30, 31]

Stationary fluorescence from excitation of the RF/RFH^+ mixture is analyzed in **Fig. 3**. With $\lambda_{exc} = 475$ nm the "neutral" RF* fluorescence is favored; the corresponding band (dashed line in the upper panel) is known from the measurement at pH 7. As was already mentioned, with decreasing pH the neutral fluorescence disappears. At the same time a new emission band (labeled X in the figure) appears around 660 nm, which is very weak. By pH -0.2 it has become stronger than the neutral fluorescence, as can be seen in **Fig. 4b** below. The new component is best found by global analysis of a set of fluorescence spectra which were recorded at various pH. Relative contributions are compared in **Fig. 3b**. As the solution is made more acidic, the deep-red emission at first increases as the "neutral" band decreases. From a fit to our measurements we obtain the corresponding $pK_a^* = 1.8 \pm 0.2$ consistent with previous reports (dashed line), but then the relative population of RF, needed for excitation, decreases due to protonation in the electronic ground state with pK_a=-0.1. Multiplication of the two population functions gives the gray interpolation curve that peaks at pH~0.95.

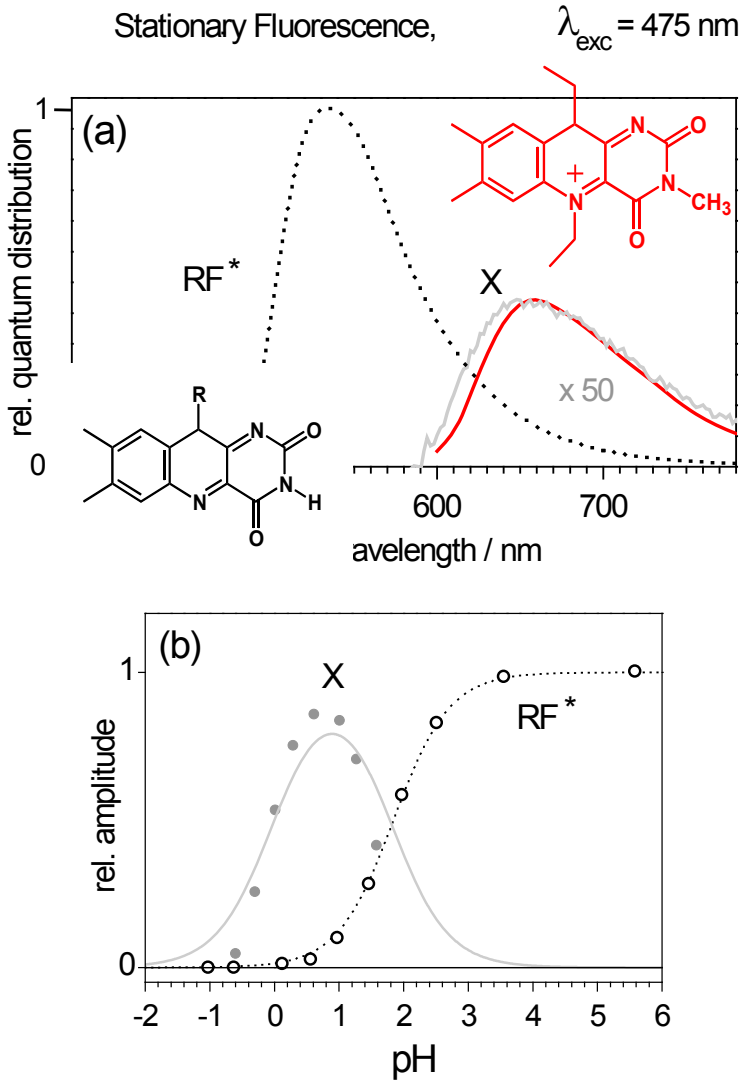

Fig. 3 (**a**) Fluorescence upon excitation at 475 nm is dominated by emission from neutral RF* (dashed line). A very weak component X (solid gray) appears at high acidity around 660 nm. Shown are the 1st and 2nd principal components from a global analysis of the emission spectra $F(\lambda, pH)$. The fluorescence spectrum of 3-methyl lumiflavin which has been ethylated at N(5) (marked red) has been taken from ref. 29.

(**b**) Relative contributions of the two components as function of pH. Lines are the result of fits (see text). The same result, but at lower S/N, is obtained with excitation at the 428 nm isosbestic point or at 403 nm.

The same fluorescence spectra and their dependence on pH are observed if the excitation wavelength is changed to $\lambda_{exc} = 403$ nm, close to the maximum of the RFH absorption band, or to 428 nm, the isosbestic point for absorption. As shown in the Supporting Information, the emission spectrum is independent of the excitation

wavelength. Only the total fluorescence yield is reduced and as a consequence, the two bands in **Fig. 3b** and the corresponding amplitude curves have lower signal/noise. This already suggests that fluorescence selectively probes neutral riboflavin, independent of eventually co-excited RFH^+. Confirmation comes from the transient view, as will be discussed.

2.2 Transient Fluorescence and Absorption.

Transient fluorescence spectra were obtained for aqueous solutions of sulfuric acid at pH=-0.20, -0.40, -0.65, -0.73, -0.78, -0.88 and -0.97 (see the Experimental Section for pH measurements). The excitation had to be performed at 403 nm for technical reasons, on the blue side of the lowest RF absorption band, as shown in **Fig. 2b**. It is resonant with the strong absorption of the protonated species, and this circumstance will be considered carefully later. In **Fig. 2a**, where the relative populations are plotted as a function of pH, the current pH values are marked at the top border.

At pH ~ 0 the neutral and N(1)-protonated forms of riboflavin coexist in the electronic ground state S_0, and fluorescence quenching evidences protonation in the excited state. **Fig. 4** shows the fluorescence behavior at pH = -0.20 where $[RF] \approx [RFH^+]$. By 0.4 ps pump-gate delay the intense Raman signal from the aqueous solvent has decayed enough so that the entire fluorescence spectrum is revealed (blue line in panel **a**). This first spectrum shows a band which peaks at ~ 515 nm. Then, until 4 ps the intensity decreases while the band shifts to 528 nm (green line), that is, near the maximum of stationary RF* fluorescence in neutral water (535

nm). Subsequently the amplitude decays, and simultaneously, within 100 ps, a weak new band rises. This new fluorescence (red line) has a broad maximum around 660 nm and disappears within a nanosecond. Multiexponential global fitting of the evolution in **Fig. 4a** yields time constants $\tau_1 = 0.9$ ps, $\tau_2 = 65.1$ ps, and $\tau_3 \approx 260$ ps. Time integration over the entire evolution gives the stationary fluorescence spectrum which is shown in **Fig. 4b** as a black line. For comparison we also provide an emission spectrum of riboflavin at pH -0.2, as recorded with a conventional fluorometer (gray line) with excitation of RF at 475 nm. Different shapes for $\lambda > 660$ nm can be attributed to systematic errors in the photometric correction of the upconversion experiment.

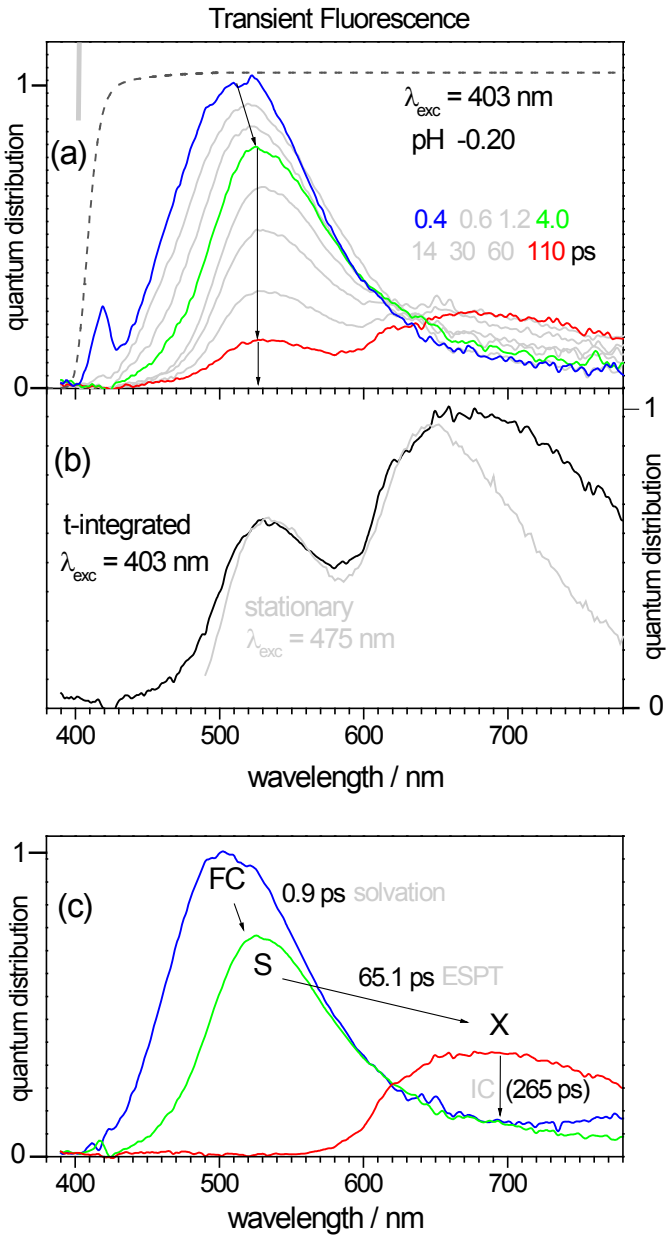

Fig. 4 (**a**) Broadband transient fluorescence spectra in sulfuric acid at pH -0.20. The initial emission can be assigned to neutral RF* even though RFH^+ absorbs most of the exciting 403 nm light (see text). The magic angle spectra were calculated from measurements with parallel and perpendicular polarization. The temporal resolution was 180 fs (fwhm) and the spectral evolution is indicated by arrows. The observation window, due to transmission of a cutoff filter, is indicated by a dashed line.

(**b**) The time-integrated spectrum (black line) shows a dominant deep-red component. It is similar to the stationary fluorescence at pH -0.20 when RF is excited preferentially (gray). Co-excitation of RFH^+ at 403 nm has no effect on stationary or transient fluorescence spectra, apart from lowering their intensity.

(**c**) Species-associated spectra for a (virtual) sequence of states. In the global analysis, the time constant τ_3=265 ps was constrained to the value from transient absorption.

Transient absorption spectra for nearly the same pH are shown in **Fig. 5**. In this kind of experiment, femtosecond optical pumping was tuned to 442 nm, where neutral RF absorbs preferentially ($\varepsilon_{RF} / \varepsilon_{RFH+} \approx 4.5$). Consider the earliest spectrum shown, at 0.4 ps (blue line in panel **a**). The bleach (BL) of RF is recognized as $\Delta OD(\lambda) < 0$ around 440 nm. The negative-going region around 570 nm belongs to stimulated emission (SE) from RF*. The SE spectrum of RF* is obtained independently from the stationary emission in **Fig. 3a** and found to have its peak at 548 nm. The discrepancy is explained by excited-state absorption (ESA), which has a band in between BL and SE, causing the local maximum of $\Delta OD(\lambda)$ at 500 nm. Strong induced absorption in the UV, with maximum at 354 nm, has similarly been assigned to ESA.[18]

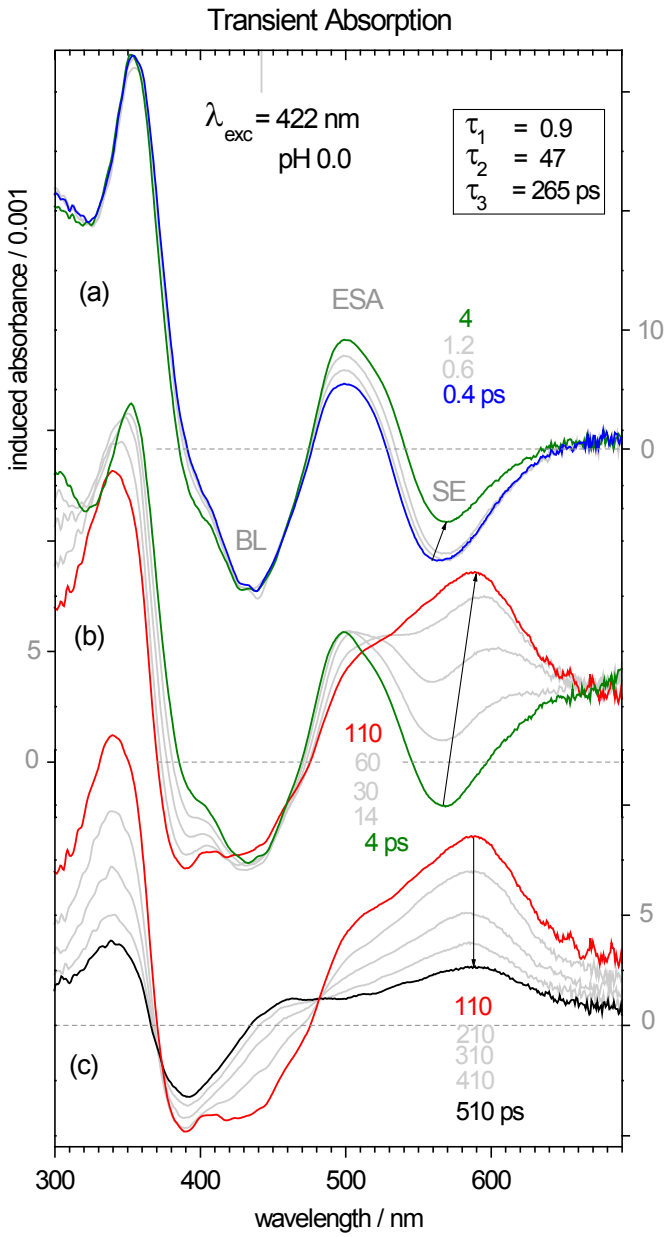

Fig. 5 Transient absorption of riboflavin in perchloric acid at pH 0. Optical pumping at 442 nm creates mainly RF*. Spectra were recorded with 60 fs time resolution under magic angle conditions (**b,c**) or with parallel pump-probe polarization (**a**). The evolution is indicated by arrows and time constants from a global analysis are indicated.

The absorption dynamics at pH 0 is clearly three-exponential; the time-constants constants are obtained similar to those from the fluorescence experiment: $\tau_1 = 0.9$ ps, $\tau_2 = 47$ ps, $\tau_3 = 265$ ps, and a constant term which remains at long delay

time. τ_1 represents an initial decrease of stimulated emission together with a small red-shift (panel **a**). The most notable feature is the 47 ps decay of stimulated emission of excited neutral riboflavin and the parallel rise of ESA in its place (panel **b**). The process has already been assigned to ESPT. Note that the bleach stays almost constant; no ground-state recovery is observed on this time scale. The third process (265 ps, panel **c**) will later be assigned to electronic transition back to the ground state. The final spectrum (not shown) can be attributed to the hot ground state.

The most acidic solution in our study has pH ≈ -1. In this case the ground-state distribution is dominated by the N(1)-protonated form RFH^+, as seen again from **Fig. 2a.** Transient fluorescence spectra at pH -0.97 are shown in **Fig. 6**. Now the spectral evolution is equivalent to that at pH -0.20, but the second step is 10 times faster, $\tau_2 = 4.4$ ps. Corresponding transient absorption spectra are shown in **Fig. 7**. Because $(RFH^+)^*$ is the majority species even when pumping at 442 nm ($\varepsilon_{RFH+}[RFH^+]/\varepsilon_{RF}[RF] \approx 1.8$), the general appearance differs qualitatively from that of **Fig. 5**. Ground-state absorption around 400 nm is seen as the only bleached band, which recovers with $\tau_2 = 24.2$ ps. Even though, the minority species RF should also contribute to the transient spectra but is buried under the RFH^+ signal. Looking for similarities with the fluorescence decay of the neutral species in **Fig. 4**, we find a weak rise of ΔOD in a broad range between 490–630 nm with $\tau_1 = 4.5$ ps.

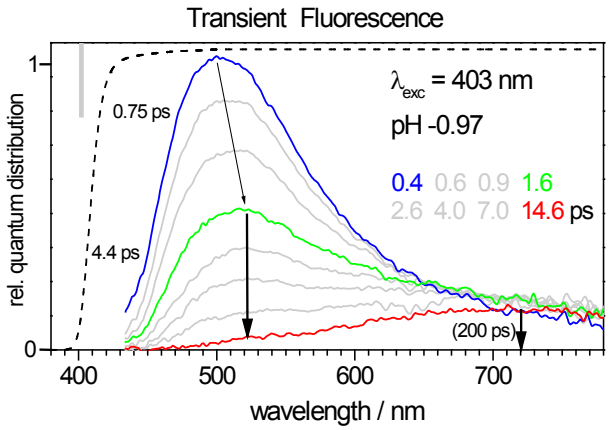

Fig. 6 Broadband transient fluorescence spectra in sulfuric acid at pH -0.97, as in **Fig. 4a.** Time constants from global analysis are associated with characteristic stages of the evolution.

For all intermediate pH values, the evolution of the riboflavin fluorescence spectrum was measured in the same way. The corresponding decay curves are shown in the SI.

3. DISCUSSION

ESPT to flavins in aqueous solution has been studied mostly via fluorescence quenching, that is, drop of quantum yield or shortening of lifetime, as function of pH.[10, 22] Also by transient absorption, the decay of stimulated emission was found to speed up when going from pH 3 to 1.5.[24] Optical transitions of RF* in water at pH 7 (SE and ESA bands) were reported quantitatively from this laboratory.[18] These observations are now combined for an assignment in the transient absorption spectra at pH 0 (**Fig. 5**): the 47 ps process (panel **b**) represents the ESPT reaction RF*→RF*H$^+$. Note that only the protonation *process* is identified here, but no description was made so far of the reaction product. However its $S_n \leftarrow S_1$ absorption spectrum must, in essence, be given by the spectrum marked red, which therefore

constitutes the first direct observation of the elusive product. The bleached $S_2 \leftarrow S_0$ and $S_1 \leftarrow S_0$ bands of RF are easily recognized in the spectra, showing that neutral riboflavin was excited predominantly in our experiment.

In the fluorescence evolution at pH -0.20 (**Fig. 4**) the process with similar time constant ($\tau_2 = 65.1$ ps, see also the SI) is equally attributed to ESPT of RF^*. Consistent with this assignment, the relevant fluorescence spectrum (green line in the upper panel) resembles the SE spectrum, which is seen to disappear in **Fig. 5b**, but the assignment is not unproblematic because optical pumping at 403 nm mainly excites RFH^+, which is required to be completely nonfluorescent for a conclusive analysis of our data.

The question is what happens to RFH^+ when it is excited? Remember that this compound was already protonated at N(1) in the electronic ground state S_0 and then promoted to S_1. With stationary methods, we and others[22] did not find any fluorescence component which might be attributed to this excited species (see also the SI). A more sensitive view, however, is provided by transient absorption, **Fig. 7**. At pH -0.97 the ground state is mostly protonated, and the induced spectra are dominated by the corresponding bleach around 390 nm even when optical pumping is tuned to the far-red edge of the absorption band. The bleach decays with ~24 ps time constant simultaneous with the broad absorption 440–650 nm. No band for stimulated emission resembling the (mirrored) RFH^+ absorption band is found. We speculate that upon excitation, elongation of the N(1)-H bond promotes internal conversion to the electronic ground state. The process is unresolved and therefore occurs before 40 fs (the time resolution of our experiment). The broad transient absorption would reflect a

distribution of distances, probably coupled to vibrational excitation of selected modes, and intramolecular vibrational redistribution and cooling set the time scale for ground-state recovery.

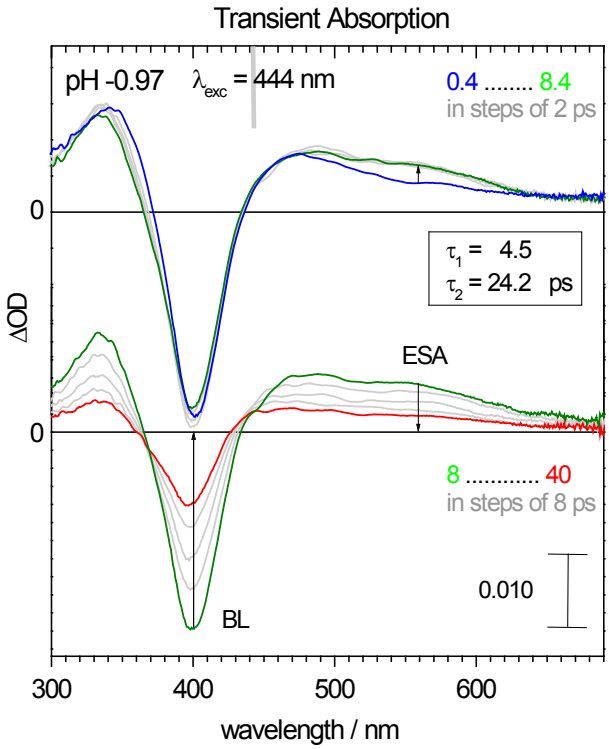

Fig. 7 Transient absorption spectra in sulfuric acid as in **Fig. 5a**, but at pH -0.97 where the excitation of RFH^+ dominates.

In addition an early rise of $\Delta OD(\lambda)$ is observed weakly across the range 470-630 nm (upper panel). This spectral feature and its decay time are identical (within experimental errors) with the stimulated-emission band RF* $\rightarrow$ RF of neutral riboflavin. The latter is also present and excited in the solution, albeit with much lower concentration. In summary, we conclude that emission from coexcited RFH^+ is not present. The fluorescence experiments are therefore considered to monitor only the neutral form of riboflavin and its reaction products.

Let us return to the time evolution of the fluorescence spectra that forms the center of this work. In an acidic environment the evolution (**Figs. 4a, 6**) is seen to have three stages: (1) ultrafast red shift and relaxation into a quasistationary RF* emission band, (2) conversion into weak emission at 660 nm, and (3) decay. Using exponential time functions in a global analysis we obtain the three time constants previously given and the decay-associated spectra. Next, assume a sequence of states $\mathrm{FC} \xrightarrow{\tau 1} \mathrm{S} \xrightarrow{\tau 2} \mathrm{X} \xrightarrow{\tau 3} 0$ to describe the evolution. Species-associated spectra $f_i(\lambda)$ are shown in **Fig. 4c.** FC represents the Franck-Condon state, and the others are "virtual" states, which, in smooth transition, empirically represent the observations. Comparison between different acidities shows that only (2) depends on pH. We tentatively assign (1) to solvation of the excited state by the aqueous medium. Process (2) was already attributed to ESPT. At pH 7 it is absent and the population of S decays slowly to zero. As a new observation we obtain the emission spectrum $f_X(\lambda)$ of the reaction product X, as measured by fluorescence upconversion. Note that both $f_S(\lambda)$ and $f_X(\lambda)$ were measured with the same short time window, and the areas under the curves are therefore related like the respective radiative rates k_i^{rad}. Thus we estimate $k_X^{rad} \approx 0.6\, k_S^{rad}$. From the stationary spectra (**Fig. 3a**, one finds for the fluorescence quantum yields $\Phi_X \approx 0.026\, \Phi_S$. For the lifetime it follows that $\tau_X = \Phi_X / k_X^{rad} = 0.026\, \Phi_S / 0.6\, k_S^{rad} = (0.026/0.6)\, \tau_S \approx 200\,\mathrm{ps}$, consistent with the observations in **Fig. 5c**.

The chemical structure of the emitting product was left entirely open until now. In principle, protonation in the excited state at N(1) is conceivable, but two arguments can be fielded against this idea. First, the same species would be generated

(i) by reaction in the excited state and (ii) by excitation of RFH^+ from the ground state. It is hard to see why the former should be fluorescent whereas the latter is totally nonfluorescent. The second argument concerns the Stokes shift of fluorescence. The absorption spectrum of RFH^+ has its peak at 394 nm while the emission X is observed at 660 nm. The resulting Stokes shift, of more than 10000 cm^{-1}, is not even realized upon intramolecular proton transfer reactions in the excited state. Altogether, it is unlikely that RF* is protonated at N(1).

Protonation at N(5) is supported by comparison with 3-methyl lumiflavin. [29] This compound may be considered as a model for neutral RF. Its emission in acetonitrile peaks at 500 nm, similar to the neutral RF fluorescence in water, an observation that underscores the equivalence of the two chromophores. Carrying the analogy further, we expect that N(5) ethylation of 3-methyl lumiflavin mimics the hypothetical N(5) protonation of RF. The emission of the ethylated model structure occurs in a well-defined band, which is reproduced in **Fig. 3a** by a red line. Indeed, shape and position are practically the same as for our band X. By analogy, the latter may safely be assigned to electronically excited riboflavin, which has been protonated at N(5). (Note in the triplet state protonation is likely at N(5) also[32]).

The ESPT rate constant $k_2 = 1/\tau_2$ is discussed at last. **Fig. 8** shows its dependence on active proton concentration $[H^+]$ (defined in the Experimental Section) for the seven H_2SO_4/water mixtures. The first four data points are described by the Stern-Volmer equation $k_2 = \tau_0^{-1} + k_2^{(1)}[H^+]$. Using $\tau_0 = 4.7\,ns$ for the electronic lifetime of RF* in the absence of protonation reactions, we find the pseudo-first order rate constant $k_2^{(1)} = (1.45 \pm 0.17) \cdot 10^{10}\ s^{-1}\ M^{-1}$ from linear regress (black solid line).

This value is somewhat below but still consistent with the rate constants due to proton diffusion, as reported in the literature: (4, 3.1 and 1.8) x 10^{10} s^{-1} M^{-1}.[22, 25, 33] Note that we vary the proton activity over a much wider range compared to these works, and thus a more detailed view becomes possible. When the activity is increased beyond 5 M the protonation rate k_2 seems to follow a different straight line (gray, with slope $k_2^{(1)} = 3.65\ \ 10^{10}\ \ s^{-1}\ \ M^{-1}$) above the one for proton diffusion. We speculate that diffusion is no longer rate limiting at these high acidities, and the activated protonation rate is observed directly. The turnover at $[H^+] \approx 5$ M also makes sense: here the average distance between protons has contracted to 8.4 Å, similar to the diameter of the excited flavin chromophore (8 Å).[34]

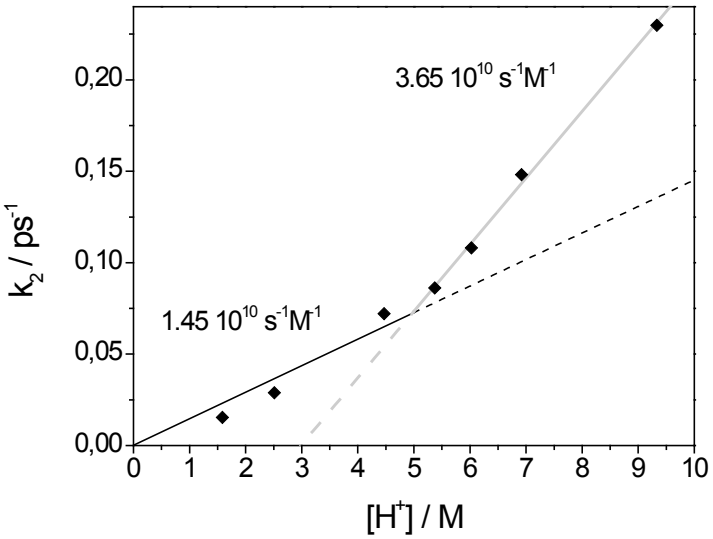

Fig. 8 Protonation rate constants k_2 of RF* depending on proton activity $[H^+]$.

4. CONCLUSIONS

ESPT from aqueous acidic solution to neutral riboflavin was monitored by stationary and femtosecond optical spectroscopies. The process was examined in the pH range from -1 to +2, where a mixture of species exists in the ground state.

(1) Excitation of the N(1) protonated form is followed by internal conversion in < 40 fs. The role of the N(1)-H bond in the deactivation should be examined with quantum-computational methods.

(2) Fluorescence spectroscopies are sensitive to the neutral form exclusively, even if it is the minority species.

(3) Time-resolved fluorescence spectra show three stages of relaxation. Solvation has ~0.9 ps time constant. Protonation with rate constant k_2 leads to an excited form that fluoresces in a well-defined band at 660 nm. This form has a lifetime of ~250 ps.

(4) By comparison with an N(5)-alkylated model flavin, the red-emitting form can be assigned to riboflavin which has been protonated at N(5).[29]

(5) The dependence of k_2 on proton concentration provides two bimolecular rate constants (1.45 and 3.65) x 10^{10} s^{-1} M^{-1}. The former represents bimolecular diffusion while the second represents the $[H^+]$-dependent rate process of a proton to overcome a reaction barrier.

5. EXPERIMENTAL SECTION

Sample preparation. Deionized water was used throughout. Proton activity pH > 0 was measured with a calibrated glass electrode. For sulfuric acid solutions at pH ≤ 0 the distribution of protic species in equilibrium was estimated from the weight fraction of sulfuric acid.[35] The cluster $[HSO_4]^-[H_3O^+]$ is expected to be too stable to act as proton deliverer, hence the concentration of all other protic species is summed and the negative decadic logarithm is denoted by pH (see SI).[36] Riboflavin (>99%, ALDRICH) and H_2SO_4 (>99%, J.T.BAKER) were used as received.

Transient fluorescence spectra were measured by broadband upconversion with 80-180 fs time resolution (fwhm of apparatus function) depending on the nonlinear crystal used.[37, 38] The cell, made of polyetheretherketon (PEEK), had 0.4 mm internal path length between thin fused-silica windows. Sample exchange was achieved by flowing the solution slowly with a syringe pump (forward-backward action) and, in addition, by applying an oscillation to the cell perpendicular to the optical axis. The absorbance of the neutral species at the pump wavelength was estimated to be < 0.4 in all cases. By comparing with the emission bands from standard dyes, *i.e.* upon photometric correction, we obtain the fluorescence quantum distribution (over wavelengths) of excited flavin as function of time. Transient measurements were performed with parallel and perpendicular arrangement of pump and detection polarizations; the spectra at magic angle were then calculated.

Transient absorption spectra were recorded as described.[39, 40] The same cell was used as for transient fluorescence, and the absorbance at the pump wavelength was adjusted to ca. 0.7. Transient spectra cover a range 300 – 690 nm with a temporal apparatus function of 50-60 fs fwhm. In all time-resolved measurements, care was taken to correct for the wavelength-dependence of time-zero.

ACKNOWLEDGEMENT

Support by the Deutsche Forschungsgemeinschaft, through the collaborative research area 1078 “Protonation dynamics in protein function”, is gratefully acknowledged.

SUPPORTING INFORMATION AVAILABLE

Details of pH determination, support that RFH^+ is non-fluorescent, and ESPT rates for all pH values are given. This information is available free of charge via the Internet at http://pubs.acs.org

REFERENCES

[1] Hatefi, Y. The Mitochondrial Electron Transport and Oxidative Phosphorylation System. *Ann. Rev. Biochem.* **1985**, *54*, 1015-1069.

[2] Yasukochi, Y.; Peterson, J. A.; Masters, B. S. S. NADPH-Cytochrome c (P-450) Reductase. *J. Biol. Chem.* **1979**, *254* (15), 7097-7104.

[3] Ghisla, S.; Massey, V. Mechanisms of flavoprotein-catalyzed reactions. *Eur. J. Biochem.* **1989**, *181*, 1-17.

[4] Ahmed, S. A.; Claiborne, A. The Streptococcal Flavoprotein NADH Oxidase. *JBC* **1989**, *264* (33), 19856-19863.

[5] Cashmore, A. R.; Jarillo, J. A.; Wu, Y. J.; Liu, D. M. Cryptochromes: Blue Light Receptors for Plants and Animals. *Science* **1999**, *284*, 760–765.

[6] Briggs, W. R.; Christie, J. M. Phototropins 1 and 2: versatile plant blue-light receptors. *Trends in Plant Science* **2002**, *7*, 204-210.

[7] Cashmore, A. R. Cryptochromes: Enabling Plants and Animals to Determine Circadian Time. *Cell* **2003**, *114*, 537–543.

[8] Van der Horst, M. A.; Hellingwerf, K. J. Photoreceptor Proteins, "Star Actors of Modern Times". *Acc. Chem. Res.* **2004,** *37*, 13-20.

[9] Bouly, J.-P.; Schleicher, E.; Dionisio-Sese, M.; Vandenbussche, F.; Van der Straeten, D.; Bakrim, N.; Meier, S.; Batschauer, A.; Galland, P.; Bittl, R.; Ahmad, M. Cryptochrome Blue Light Photoreceptors Are Activated through Interconversion of Flavin Redox States. *J. Biol. Chem.* **2007**, *282* (13), 9383–9391.

[10] Heelis, P. F. The Photophysical and Photochemical Properties of Flavins. *Chem. Soc. Rev.* **1982**, *11*, 15-39.

[11] Sikorska, E.; Khmelinskii, I. V.; Worrall, D. R.; Koput, J.; Sikorski, M. Spectroscopy and Photophysics of Iso- and Alloxazines: Experimental and Theoretical Study. *J. Fluoresc.* **2004**, *14*, 57-64.

[12] Sikorska, E.; Khmelinskii, I. V.; Koput, J.; Bourdelande, J. L.; Sikorski, M. Electronic structure of isoalloxazines in their ground and excited states. *J. Mol. Struct.* **2004**, *697*, 137–141.

[13] Sikorska, E.; Khmelinskii, I. V.; Koput, J.; Sikorski, M. Electronic structure of lumiflavin and its analogues in their ground and excited states. *J. Mol. Struct. (Theochem)* **2004**, *676*, 155–160.

[14] Insinska-Rak, M.; Sikorska, E.; Herance, J. R.; Bourdelande, J. L.; Khmelinskii, I. V.; Kubicki, M.; Prukała, W.;.Machado, I. F; Komasa, A.; Ferreira, L. F. V.; Sikorski, M. Spectroscopy and photophysics of flavin-related compounds: 3-benzyl-lumiflavin. *Photochem. Photobiol. Sci.* **2005**, *4*, 463-468.

[15] Sikorska, E.; Herance, J. R.; Bourdelande, J. L.; Khmelinskii, I. V.; Williams, S. L.; Worrall, D. R.; Nowacka, G.; Komasa, A.; Sikorski, M. Spectroscopy and photophysics of flavin-related compounds: 3-ethyl-lumiflavin. *J. Photochem. Photobiol. A* **2005**, *170*, 267–272.

[16] Petushkov, V. N.; van Stokkum, I. H. M.; Gobets, B.; van Mourik, F.; Lee, J.; van Grondelle, R.; Visser, A. J. W. G. Ultrafast Fluorescence Relaxation Spectroscopy of 6,7-Dimethyl-(8-ribityl)-lumiazine and Riboflavin, Free and Bound to Antenna Proteins from Bioluminescent Bacteria. *J. Phys. Chem. B* **2003,** *107*, 10934-10939.

[17] Wolf, M. M. N.; Schumann, C.; Gross, R.; Domratcheva, T.; Diller, R. Ultrafast Infrared Spectroscopy of Riboflavin: Dynamics, Electronic Structure, and Vibrational Mode Analysis. *J. Phys. Chem. B* **2008,** *112*, 13424–13432.

[18] Weigel, A.; Dobryakov, A. L.; Veiga, M.; Lustres, J. L. P. Photoinduced Processes in Riboflavin: Superposition of $\pi\pi^*$-$n\pi^*$ States by Vibronic Coupling, Transfer of Vibrational Coherence, and Population Dynamics under Solvent Control. *J. Phys. Chem. A* **2008**, *112*, 12054–12065.

[19] Weigel, A.; Dobryakov, A. L.; Klaumünzer, B.; Sajadi, M.; Saalfrank, P.; Ernsting, N. P. Femtosecond Stimulated Raman Spectroscopy of Flavin after Optical Excitation. *J. Phys. Chem. B* **2011**, *115* (13), 3656–3680.

[20] Zheng, Y.-J.; Ornstein, R. L. A Theoretical Study of the Structure of Flavin in Different Oxidation and Protonation States. *J. Am. Chem. Soc.* **1996**, *118*, 9402-9408.

[21] van den Berg, P. A. W.; Feenstra, K. A.; Mark, A. E.; Berendsen, H. J. C.; Visser, A. J. W. G. Dynamic Conformations of Flavin Adenine Dinucleotide: Simulated Molecular Dynamics of the Flavin Cofactor Related to the Time-Resolved Fluorescence Characteristics. *J. Phys. Chem. B* **2002**, *106*, 8858-8869.

[22] Drössler, P.; Holzer, W.; Penzkofer, A.; Hegemann, P. pH dependence of the absorption and emission behaviour of riboflavin in aqueous solution. *Chem. Phys.* **2002**, *282*, 429-439.

[23] Nishimoto, K.; Watanabe, Y.; Yagi, K. Hydrogen bonding of Flavoprotein. *Biochim Biophys Acta* **1978**, *526*, 34-41.

[24] Li, G.; Glusac, K. D. Light-Triggered Proton and Electron Transfer in Flavin Cofactors. *J. Phys. Chem. A* **2008**, *112,* 4573–4583.

[25] Sengupta, A.; Khade, R. V.; Hazra, P. pH dependent dynamic behaviour of FMN and FAD in femtosecond to nanosecond time scale. *J. Photochem. Photobiol. A* **2011**, 221, 105–112.

[26] Song, P.S. On the Basicity of the Excited State of Flavins. *J. Photochem. Photobiol.* **1968**, *7*, 311-313.

[27] Sikorska, E.; Khmelinskii, I.; Komasa, A.; Koput, J.; Ferreira, L. F.V.; Herance, J. R.; Bourdelande, J. L.; Williams, S. L.; Worrall, D. R.; Insinska-Rak, M.; Sikorski, M. Spectroscopy and photophysics of flavin related compounds: Riboflavin and iso-(6,7)-riboflavin. *Chem. Phys.* **2005**, *314*, 239–247.

[28] Salzmann, S.; Marian, C.M. Effects of protonation on the excitation energies of lumiflavin. *Chem. Phys. Lett.* **2008**, *463*, 400-404.

[29] Sichula, V.; Kucheryavy, P.; Khatmullin, R.; Hu, Y.; Mirzakulova, E.; Vyas, S.; Manzer, S. F.; Hada, C. M.; Glusac, K. D. Electronic Properties of N(5)-Ethyl Flavinium Ion. *J. Phys. Chem. A* **2010**, *114*, 12138-12147.

[30] Michaelis, L.; Schubert, M. P.; Smythe, C. V. Potentiometric Study of the Flavins. *J. Biol. Chem.* **1936**, *116*, 587-607.

[31] Schulmann, S. G. pH Dependence of Fluorescence of Riboflavin and Related Isoalloxazine Derivatives. *J. Pharm. Sci.* **1971**, *60*, 628-631.

[32] Kowalczyk, R. M.; Schleicher, E.; Bittl, R.; Weber, S. The Photoinduced Triplet of Flavins and Its Protonation States. *J. Am. Chem. Soc.* **2004**, *126*, 11393-11399.

[33] Tyagi, A.; Penzkofer, A. Absorption and Emission Spectroscopic Characterization of Lumichrome in Aqueous Solutions. *Photochem. Photobiol.* **2011**, *87*, 524–533.

[34] Climent, T.; Gonzalez-Luque, R.; Merchan, M.; Serrano-Andres, L. Theoretical Insight into the Spectroscopy and Photochemistry of Isoalloxazine, the Flavin Core Ring. *J. Phys. Chem. A* **2006**, *110*, 13584-13590.

[35] Librovich, N. B.; Maiorov, V. D. Ionic-Molecular Composition of Aqueous Sulfuric Acid Solutions. *Ser. Khim.* **1977**, *3*, 684-687.

[36] Kusaka, I.; Wang, Z.-G.; Seinfeld, J. H. Binary nucleation of sulfuric acid-water: Monte Carlo simulation. *J. Chem. Phys.* **1998**, *108* (16), 6829-6848.

[37] Zhao, L.; Perez Lustres, J. L.; Farztdinov, V.; Ernsting, N. P. Femtosecond fluorescence spectroscopy by upconversion with tilted gate pulses. *PCCP* **2005**, *7*, 1716–1725.

[38] Zhang, X-X.; Würth, C.; Zhao, L.; Resch-Genger, U.; Ernsting, N. P. Femtosecond broadband fluorescence upconversion spectroscopy: Improved setup and photometric correction. *Rev. Sci. Instrum.* **2011**, *82*, 063108.

[39] Kovalenko, S. A.; Dobryakov, A. L.; Ruthmann, J.; Ernsting, N. P. Femtosecond spectroscopy of condensed phases with chirped supercontinuum probing. *Phys. Rev. A* **1999**, *59*, 2369-2384.

[40] Dobryakov, A.; Kovalenko, S. A.; Weigel, A.; Pérez-Lustres, J. L.; Lange, J. Femtosecond pump/supercontinuum-probe spectroscopy: Optimized setup and signal analysis for single-shot spectral referencing. *Rev. Sci. Instrum.* **2010**, *81*, 113106.

β-Carotene revisited by Transient Absorption and Stimulated Raman Spectroscopy

Martin Quick, Marc-André Kasper, Celin Richter, Rainer Mahrwald, Alexander L. Dobryakov, Sergey A. Kovalenko, Nikolaus P. Ernsting**

Department of Chemistry, Humboldt-Universität zu Berlin,
Brook-Taylor-Str. 2, D-12489 Berlin, Germany

Abstract

β-Carotene in *n*-hexane was examined by femtosecond transient absorption and stimulated Raman spectroscopy. Electronic change is separated from vibrational relaxation with the help of band integrals. Overlaid on the decay of S_1 excited-state absorption, a picosecond process is found which is absent when the C_9-methyl group is replaced by ethyl or isopropyl. It is attributed to reorganization on the S_1 potential energy surface, involving dihedral angles between C_6 and C_9. In Raman studies, electronic states S_2 or S_1 were selected through resonance conditions. We observe a broad vibrational band at 1770 cm^{-1} in S_2 already. With 200 fs it decays and transforms into the well-known S_1 Raman line for an asymmetric C=C stretching mode. Low-frequency activity (<800 cm^{-1}) in S_2 and S_1 is also seen. A dependence of solvent lines on solute dynamics implies intermolecular coupling between β-carotene and nearby *n*-hexane molecules.

[1] Reprinted ("Adapted" or "in part") with permission from Quick, M.; Kasper, M.-A.; Richter, C.; Mahrwald, R.; Dobryakov, A.L.; Kovalenko, S.A.; Ernsting, N.P. Beta-Carotene Revisited by Transient Absorption and Stimulated Raman Spectroscopy. *Chem. Phys. Chem.*, **2015**, *16*, 3824-3835.

1. Introduction

In a natural environment carotenoids have three important functions: (1) harvesting of blue-green excitation light, (2) photo protection from oxygen via triplet quenching and (3) dissipation of excess energy [1]. Parallel to research in vivo, carotenoids in solution have been studied intensely. Due to the C_{2h} symmetry of the polyene chain, the first bright state at 490 nm (**Fig. 1**) is S_2 ($1B_u^+$). The observation of a dark S_1 ($2A_g^-$) state in long polyenes was first reported by Hudson and Kohler [2] and treated theoretically by Schulten and Karplus [3]. A corresponding $S_y \leftarrow S_1$ transition in β-carotene was probed with ps-transient absorption and found to decay with ~9 ps [4]. The energy of S_1 was estimated at $\nu_1 \approx 14000\ cm^{-1}$ above S_0 ($1A_g^-$) [5,6] and confirmed experimentally, when the S_2-S_1 transition energy ($\nu_2 - \nu_1$) was subtracted from ν_2 [7]. While the lifetime of S_1 does not depend on the environment [8,9], the S_2 ($1B_u^+$) state is highly polarizable and thus, influenced by the solvent [9,10].

A broad excited-state absorption band $S_x \leftarrow S_2$ was recorded in the near infrared (NIR) which decays with ~200 fs [11,12]. Transient absorption and Kerr-gate fluorescence spectroscopy showed that the S_2 lifetime of carotenoids does not follow the energy-gap law. It has been suggested that an intermediate state of $1B_u^-$ symmetry, in between the established S_1 and S_2 states, may assist the internal conversion (IC) process [13,14].

Another dark state, S*, has been proposed to explain a weak shoulder in the blue wing of the $S_y \leftarrow S_1$ excited-state absorption band. Controversies and consistent results about this observation are summarized in ref. **15**. Assignment to an excited electronic state, nearly iso-energetic with S_1, was cast into kinetic schemes termed homogeneous and inhomogeneous [16]. The former starts in S_0 from where population is pumped into S_2. Decay to S_1 and S* proceeds with different rates so that a varying population ratio S_1/S* is created. The inhomogeneous model assumes two ground-state conformers S_0 and S_0* which are pumped into the corresponding S_2 and S_2* states. Conversions to S_1 and S_1* (which is identified with empirical S*) proceed independently. Upon lowering the temperature the blue shoulder of the $S_y \leftarrow S_1$ band is decreased, an observation which is best explained with the inhomogeneous model [17]. More recently, assignment of S* to the hot electronic ground state was concluded from a comparison with hot stationary spectra [18].

Raman measurements on β-carotene in solution have been performed since the 1980s [19-21]. While intense ground-state lines dominate in the range $800 - 1600\ cm^{-1}$, practically no Raman activity has been seen in the low-frequency region. Lines belonging to S_1 were recorded by several groups, with attention focused on an upshifted symmetric C=C-stretching mode >1700 cm^{-1} [7,20-26]. Coupling of S_1/S_0 through this mode causes its upshift by more than 200 cm^{-1} in S_1, compared to the asymmetric mode in S_1 [26-29]. The coupling should be zero between states of B_u^+ and A_g^- symmetry (S_2 and S_1), but the high polarizability of S_2 may promote a breakdown of symmetry [25,30]. As a consequence, a solvent-dependent S_2–S_1 energy gap of β-carotene and S_2 lifetime is observed [10,31,32]. The characterization of the Raman spectrum from the short-lived S_2-state is challenging since vibrational bands are

broad (80 – 100 cm^{-1}) and their distinction from electronic background is difficult. Corresponding results from the literature are still at variance [7,30,33,34].

In this work we re-examine β-carotene in solution with broadband transient absorption and stimulated Raman spectroscopy. The precision and accuracy of our measurements allows us to recognize and quantify hitherto unresolved aspects of the spectral evolution of β-carotene. Derivatives where a methyl group has been replaced by ethyl or isopropyl are studied for comparison.

2. Results

Stationary absorption spectra of β-carotene and asymmetrically substituted C_{19}-methyl- and $C_{19,19}$-dimethyl- β-carotene (referred to as et- and iPr-β-carotene) are shown in **Fig. 1.** As mentioned earlier, the first bright state is S_2 ($1B_u^+$) because of the C_{2h} symmetry of the polyene chain. For β-carotene itself the $S_2 \leftarrow S_0$ band is vibrationally well-pronounced, while some loss of structure is incurred when the methyl-group at C_9 is replaced by larger alkyl-rests. Note that a blue-shift in the absorption spectra of et- and iPr-β-carotene (relative to the parent compound) has been removed for the illustration in **Fig. 1**, by making the minima and maxima of the 2nd derivatives coincide. Materials and methods are described in the supporting information (SI).

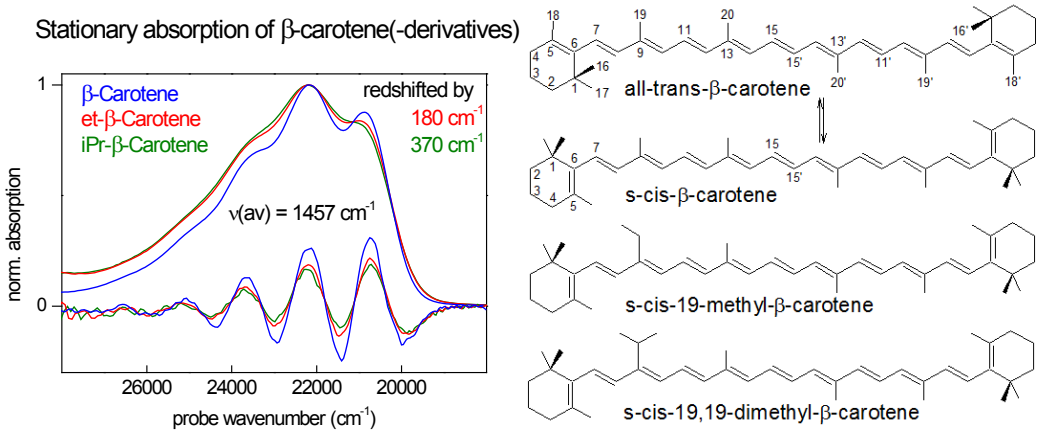

Figure 1: Chemical structures of β-carotene, C_{19}-methyl- and $C_{19,19}$-dimethyl-β-carotene (abbreviated et- and iPr-β-carotene, respectively) and stationary optical absorption spectra in *n*-hexane. Loss of vibronic structure upon substitution is also seen as amplitude drop in the 2nd derivative below. The s-cis conformer of β-carotene is calculated to be 8.8 kJ mol^{-1} more stable than the all-*trans* conformer [58].

2.1 Transient Absorption Spectroscopy

For β-carotene in *n*-hexane, transient absorption (TA) spectra are shown in the left panels of **Fig. 2**. Actinic excitation is performed with 40 fs pulses at 498 nm and spectra are recorded between 270 and 1050 nm. This broad spectral window was in fact constructed from two sub-windows ranging from 270 – 690 nm and 650 – 1050 nm. The effect of

orientational diffusion was eliminated by recording the transient absorption $\Delta A(t,\lambda)$ at magic angle between pump- and probe polarizations. Bands that appear with positive sign correspond to excited state absorption (ESA) and negative bands to bleach (BL) and stimulated emission. Optical excitation creates population in the Franck-Condon region of S_2 from where relaxation starts. The $S_x \leftarrow S_2$ ESA band appears around 990 nm [7,11,12] within the instrument response time and decays fast (τ_1 = 200 fs, **Fig. 2a**) as population reaches S_1 via internal conversion. ESA due to the $S_y \leftarrow S_1$ transition develops around 556 nm and rises further while shifting to shorter wavelengths (τ_2 = 360 fs, **b**) [12,18,35-37]. The $S_y \leftarrow S_1$ ESA band decays simultaneously with the bleach as the ground-state recovers (τ_3=6.9 ps, **c**) [4,12,18,22]. A residual at latest times, with spectral structure between 400 and 530 nm, corresponds to hot ground-state and indicates cooling in S_0 (τ_4 = 13.6 ps) [6,18]. All τ_i values given here and below refer to our global fit which is described in the remainder of this section.

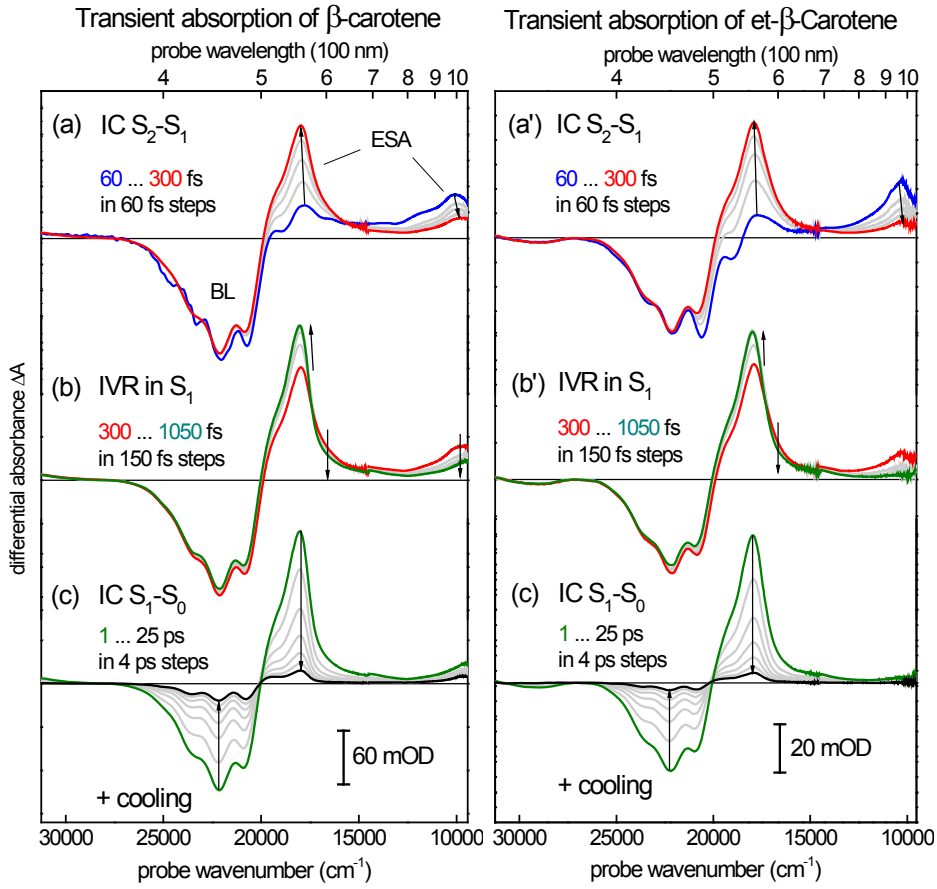

Figure 2: Transient absorption spectra of β-carotene (*left panels*) and et-β-carotene (*right*) in *n*-hexane following 498 nm and 490 nm actinic excitation, respectively. Both carotenes have similar spectral and temporal characteristics. IC – internal conversion, IVR – intramolecular vibrational redistribution.

The kinetic evaluation of the TA data is performed globally with four exponential time-functions together with one stretched-exponential time-function. Leaving out any one of these functions results in a fit which deviates systematically, and significantly, from the measured data (we come back to this point later). Decay-associated spectra (DAS) are also obtained from the global fit. A DAS_i reflects the spectral change that proceeds exponentially

with the respective time-constant τ_l (**Fig. 3**, left panels). The decay of the $S_x \leftarrow S_2$ band and the simultaneous rise of S_1 ESA are characterized by the positive and negative bands around 990 and 556 nm, respectively (panel **a**). A blue-shift of the $S_y \leftarrow S_1$ ESA band in the spectrum appears as a dispersive band-shape in the corresponding DAS, with the negative and positive lobe on the high- and low-energy side (**b**). Internal conversion to the electronic ground-state is indicated by the decay of the positive ESA and negative bleach bands (**c**). Cooling in S_0 causes a withdrawal of red-edge absorption and recovery of vibronic structure (**d**). A fraction of S_1 population converts to S_0 on the same slow time scale, as can be seen by the characteristic ESA peak at 554 nm.

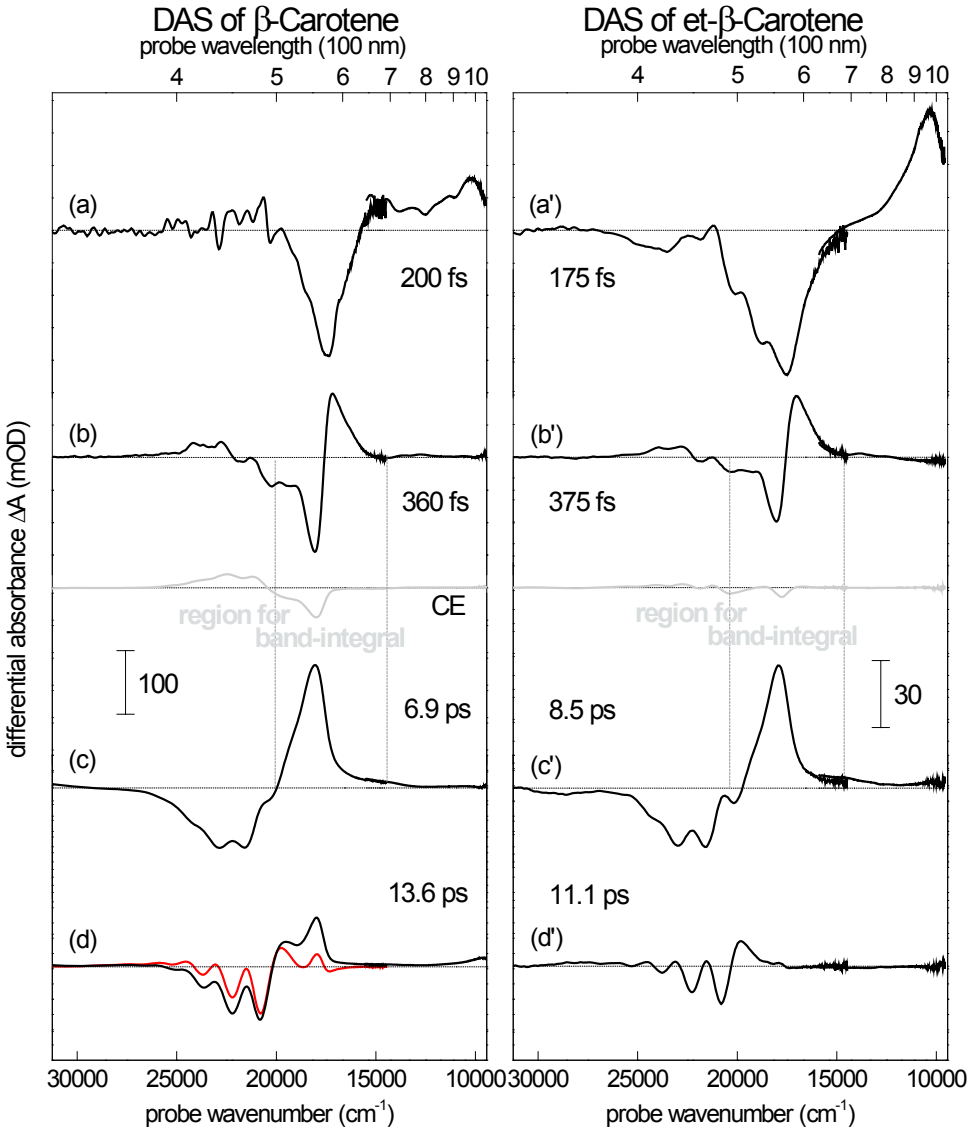

Figure 3: Decay associated spectra (DAS, black lines) representing transient absorption changes following actinic excitation. (**a,a´**) – IC from S_2 to hot S_1 ; (**b,b´**) – vibrational redistribution in S_1; (**c,c´**) – decay of S_1 ESA and Bleach recovery; (**d,d´**) – ground-state cooling (see text). In addition the DAS of the compressed exponential (CE) is shown as a grey line. Its negative region (500 – 600 nm) accounts for a small rise of the ESA band with correlation time 2-3 ps. A positive region (400 – 500 nm) is interpreted as correspondingly-delayed ground-state recovery. For et-β-carotene the non-exponential contribution almost vanishes. Band integrals BI(λ_1,λ_2) over measured TA data are formed over the range indicated, providing the S_1 population traces for **Fig. 4.**

For et-β-carotene in *n*-hexane, transient absorption spectra are generally shown in the right panels, starting with **Fig. 2**. The actinic pump is set to 490 nm because the stationary absorption spectrum is blue-shifted relative to β-carotene. Spectral characteristics are basically the same as for the parent compound, but with slightly different time constants. Transient absorption of iPr-β-carotene in *n*-hexane is performed with $\lambda_{exc.}$ = 490 as well; spectra are shown in **Fig. S2**.

Let us return to parent β-carotene. We find that kinetic traces in the bleach and $S_y \leftarrow S_1$ ESA region all possess an oddly stretched hump, reminiscent of an oscillation, which occurs well within the first 10 ps. To quantify the impression, a band-integral is calculated for the entire $S_y \leftarrow S_1$ band and shown as gray thick line in **Fig. 4a**. The band integral is defined as

$$BI(t;\lambda_1,\lambda_2) = \int_{\lambda_1}^{\lambda_2} \Delta A(t,\lambda)\lambda^{-1} d\lambda \qquad \text{(eq. 1)}$$

The range (λ_1,λ_2)=(496,690) nm is indicated in **Fig. 3b,c**. Formation of the band integral over this range removes the influence of the spectral shift, *i.e.* of the 360 fs component which is characterized in **Fig. 3b**. As a result, the BI trace should reflect the kinetic population scheme $S_2 \rightarrow S_1 \rightarrow S_0$ with 200 fs and 6.9 ps time constants exclusively. A corresponding fit with two exponential time-functions (plus offset) is shown as thin black line in **Fig. 4a**. However, the residuals after subtraction from the experimental band integral deviate systematically from zero, indicating another component to population transfer before ~10 ps. Typical kinetic traces (as mentioned above) for bleach and $S_y \leftarrow S_1$ ESA can be assessed in **Fig. S1**. Note that a hump is also visible in the TA traces of Lenzer *et. al.* (their Fig. 7) [18] and of Xia and coworkers (their Fig. 7, lower panel) [38].

Attempts to describe this feature globally with two additional, independent, exponential time-functions (resulting for the whole time range in a total of six functions!) failed in the sense that no well-defined global minimum could be found for the fit-procedure. Some constraint is necessary in order to make physical sense of our observations. Instead we treat the new feature non-exponentially and use a stretched exponential as model-function:

$$\Delta A \sim C(t) = e^{-(t/\tau^*)^\beta} \qquad \text{(eq. 2)}$$

For the range $0 < \beta < 1$ the parameter τ^* is interpreted as a characteristic relaxation time of a distribution over specific rate processes [39]. For $1 \le \beta \le 2$ one tunes between a single exponential and a Gaussian function, respectively; in this range the function of eq. 2 is often referred to as "compressed exponential" (CE). It can be described by a continuous distribution of Gaussians [40]; examples are given in refs. **41-43**. In most cases the appearance of CE decay is attributed to the relaxation of inner stress, caused by a glassy or jammed

nature of the dynamics [41]. In a global fit all four exponential time parameters adjust close to the literature values for the well-established processes. In addition $\beta = 2$ and $\tau* = 3 – 4$ ps captures the non-exponential part best. Alternatively the latter can be described as relaxation of a critically damped Brownian oscillator:

$$\Delta A \sim C(t) = e^{-\frac{\gamma}{2}t}\left(1 + \frac{\gamma}{2}t\right)$$

(eq. 3)

with optimal parameter γ=1.2 ps^{-1}. The effective relaxation time $\int_0^\infty Cdt$ is approx. 2.4 – 3.0 ps.

The adequacy of the added term is demonstrated in **Fig. 4b.** The experimental curve for the band integral (from the panel above) is reproduced as a thick gray line. Remember that this curve was obtained directly from the data ΔA(t,λ). Alternatively we may first subtract the fitted contribution, due to eq. 2, from the data for all ΔA(t,λ), *i.e.* we perform a global correction. When the band integral is then calculated from the corrected data, the thick pink line in **Fig. 4b** is obtained. As before, a fit with two exponential time-functions is shown as a thin black line. Now the residuals after subtraction from the recalculated band integral are essentially zero. — It is instructive to consider the DAS of the CE which is shown as grey line between **Fig. 3b** and **c**. A negative region (496 – 690 nm) reflects small growth of the $S_y \leftarrow S_1$ band on the ps time scale. This process is clearly seen against the slower (6.9 ps) decay from internal conversion $S_1 \rightarrow S_0$ (**Fig. 4b**). Because of the timescale it must be attributed to reorganization on the potential energy surface (PES) of S_1.

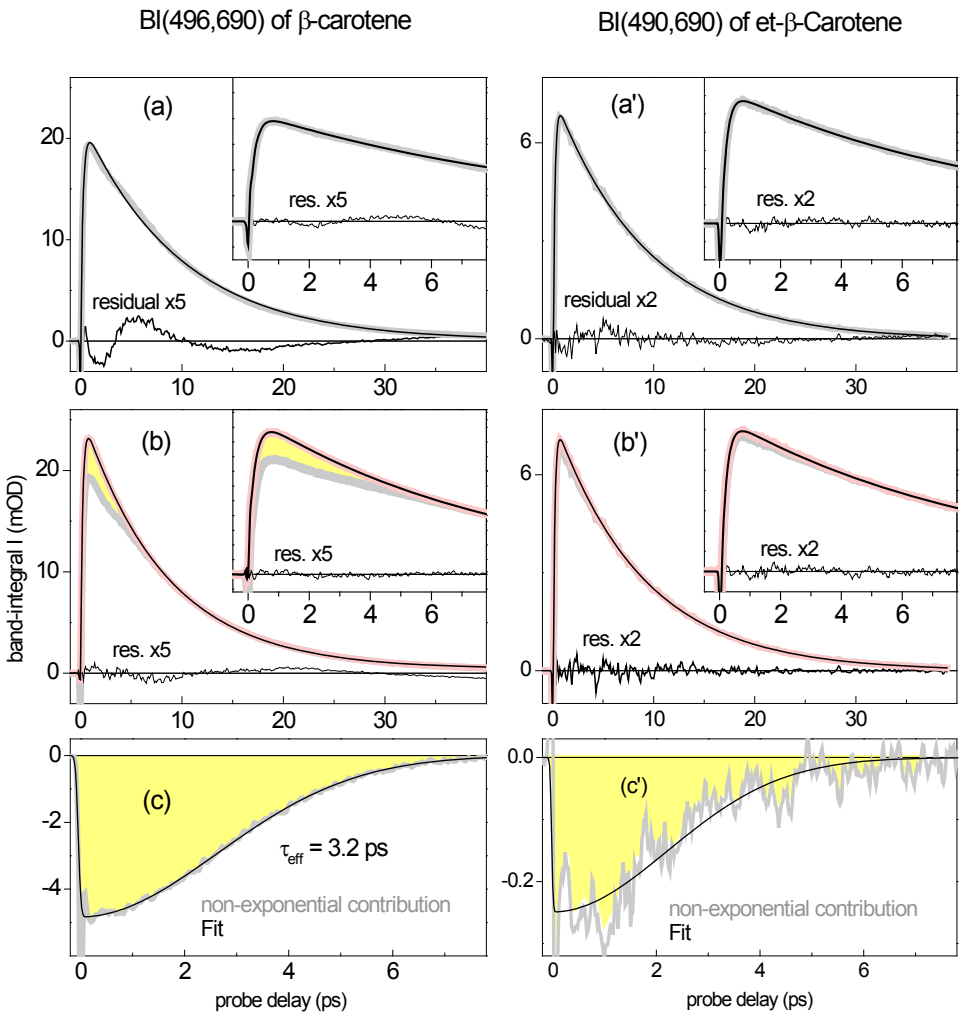

Figure 4: Population in S_1 is monitored by the $S_y \leftarrow S_1$ band-integral (BI, thick grey lines, eq. 1). (**a,a´**) – When a relaxation-scheme $S_2 \rightarrow S_1 \rightarrow S_0$ is assumed, the BI should be well described with two exponential time-functions plus offset (thin black lines). However a residual to the fit fluctuates systematically. (**b,b´**) – In a global analysis of transient spectra, a stretched exponential contribution is assumed in addition, and the corresponding spectral evolution is then removed. Thus modified, the resulting TA spectra give a band-integral (rosé lines) which now has the expected bi-exponential character. (**c,c´**) - One stretched exponential with parameters $\tau = 3 - 4$ ps and $\beta = 2$ describes band-integral over the isolated non-exponential contribution. Note that it represents ~20 % of the population amplitude in β-carotene, while only 3.5 % are found for et-β-carotene.

Finally for this section we turn to the slowest process (τ_4 = 13.6 ps) observed with β-carotene: cooling in S_0 which is characterized by the DAS in **Fig. 3d**. It was already mentioned that internal conversion $S_1 \rightarrow S_0$ partly occurs on this time scale as well, as evidenced by the characteristic ESA band in this spectrum.[a,b] The corresponding contribution is readily removed by subtracting a scaled version of the spectrum above, panel **c**. Now a well-structured progression of vibronic lines emerges (red line), similar to what is observed with et-β-carotene (**Fig. 3d´**). This connection strengthens the conclusion that internal conversion $S_1 \rightarrow S_0$ involves two relaxation processes with β-carotene (77% 6.9 ps and 23% 13.6 ps) but only one with et-β-carotene.

2.2 Femtosecond Stimulated Raman Spectroscopy

FSR spectroscopy is performed with β-carotene (in *n*-hexane) only. Actinic pumping is tuned to 490 nm and three Raman excitation wavelengths λ_R are used. Resonance conditions for transient measurements are shown in **Fig. 5**. λ_R =776 nm is resonant with the $S_x \leftarrow S_2$ transition and spectra are recorded at the *anti*-Stokes side. With 573 nm, resonance is obtained with the red edge of the $S_y \leftarrow S_1$ band. Intermediate 621 nm is pre-resonant with both transitions. In the last two cases, spectra are recorded at the Stokes side. To obtain ground-state spectra the actinic pump is blocked.

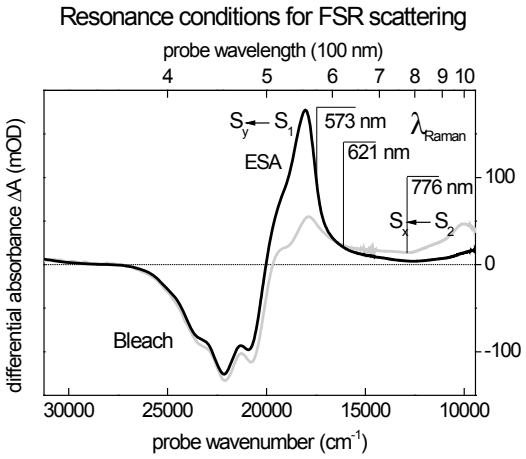

Figure 5: Resonance conditions for the three Raman pump wavelengths λ_R used in transient FSR measurements. An early (100 fs, light grey) and late TA spectrum (1 ps, black) show the positions of the $S_x \leftarrow S_2$ and $S_y \leftarrow S_1$ bands. Pre-resonant conditions apply for λ_R = 621 nm. The actinic pump was set to 490 nm in all FSR experiments with β-carotene, *i.e.* tuned to the 0-0-transition of the $S_2 \leftarrow S_0$ band.

Ground-state Raman spectrum from pre-resonance (λ_R = 540 nm).

Fig. 6 shows the FSR spectrum recorded pre-resonantly with λ_R = 540 nm. Solvent signal has been subtracted, and the instrument band-width is ~30 cm^{-1} (fwhm). At the Stokes side one observes Raman gain throughout, shown here as induced absorbance ΔA<0 (like stimulated emission). The assignment of Raman features follows ref. [44]. The spectrum is dominated by two lines, at 1155 and 1520 cm^{-1}, due to C-C- and C=C stretching modes in the backbone of β-carotene. A medium-sized line at 1005 cm^{-1} indicates a methyl rocking mode. Weaker C-H stretching and rocking modes in the backbone are seen as Raman bands at 1272, 1351 and 1392 cm^{-1}. A line at 1448 cm^{-1} represents asymmetric methyl deformations. A weak shoulder at 1192 cm^{-1} is attributed to a C-C stretching mode located at C_8 and C_9. The weak Raman line at 1600 cm^{-1} is caused by C=C stretching between C_7 and C_8. The assignment of the weak band at 874 cm^{-1} is uncertain but may originate from C-C stretching modes of the β-rings. Raman activity in the low frequency region is very small; from critical

analysis we conclude weak lines at 234, 299, 429, 519 and 600 cm^{-1}. Observed and calculated S_0 Raman lines are listed in **Table S1**.

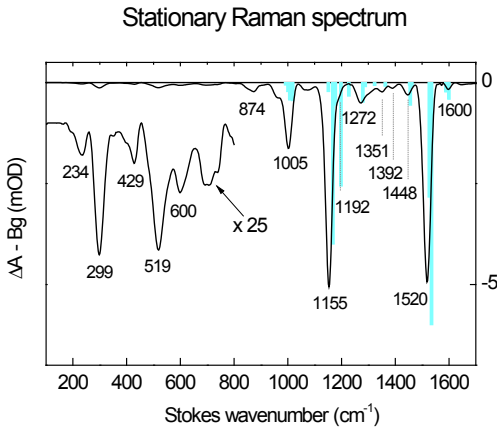

Figure 6: Ground-state FSR spectrum of β-carotene in *n*-hexane, from excitation at λ_R=540 nm and recorded on the Stokes side (black). Calculated Raman lines in the fully relaxed geometry are shown as vertical bars [44].

Excited-state Raman spectra on resonance with $S_x \leftarrow S_2$ *(λ_R = 776 nm)*

are shown in **Fig. 7**, left panels. Actinic photo-excitation with 490 nm pumps population into S_2 initially, and detection favors modes in S_2. Because spectra are recorded at the *anti*-Stokes side, vibrational bands are expected to have positive sign (Raman loss, *cf.* SI). But in order to see Raman-induced lines or line-shapes belonging to excited states in the recorded $\Delta A(t,\lambda)$, several layers of other signal must be stripped away first. (i) The stationary ground-state signal is removed by subtracting a representative spectrum, obtained by averaging over some range t<0. As in all transient measurements, then, bleached bands appear for t>0 (negative lines in this case). (ii) The recovering bleach pattern is removed, appropriate for every t>0, by a procedure which is detailed in the SI. Lastly (iii) note that optical pumping by the ps Raman pulse causes TA changes (population or "sequential" signal [45]) which show up as a time-variable background (BG) to the Raman lines. This background must be recognized and removed. Altogether the pure excited-state Raman signal should ideally be obtained in **Fig. 7**.

At early delay times (for example, blue line in **Fig. 7a**) we observe rich vibrational structure, partly of positive and negative sign. In the low frequency region (<800 cm^{-1}) three broad bands (fwhm ~ 80 cm^{-1}) with positive sign are recorded around 200, 400 and 570 cm^{-1}. They decay with ~200 fs time constant (**Fig. 8a**) and are assigned to S_2. Dispersive-shaped signals in the region 800 – 1600 cm^{-1} disappear on the same time-scale [24]. Most of their central frequencies coincide with stationary β-Carotene lines, pointing out ground-state resonances which are seen from S_2. All dispersive signals that remain belong to *n*-hexane, as will be discussed separately. After fast decay of dispersive bands, positive lines from S_1 become visible at 1013, 1160, 1196, 1246, 1282, 1380 and 1531 cm^{-1} (~30 cm^{-1}, red line in **Fig. 7a**). In the high-frequency region (yellow box >1600 cm^{-1}) another band appears at

earliest time, broadly (~100 cm^{-1}) around 1770 cm^{-1} and with slightly dispersive shape. After conversion to S_1 it turns fully positive and shifts up to 1790 cm^{-1} with τ = 340 fs (**Fig. 8b**) while narrowing (**Fig. 8c**) and rising on the same time scale (**Fig. 7b**). The observed behavior agrees with results for vibrational redistribution from TA measurements**,** and a comparison with previous studies allows the identification of the 1770 cm^{-1} band as belonging to the symmetric C=C stretching mode in S_1 [12,22,23]. The whole spectrum decays with ~9 ps (**Fig. 7c**); small positive residuals at 1145 and 1510 cm^{-1} denote the hot ground state [23,24].

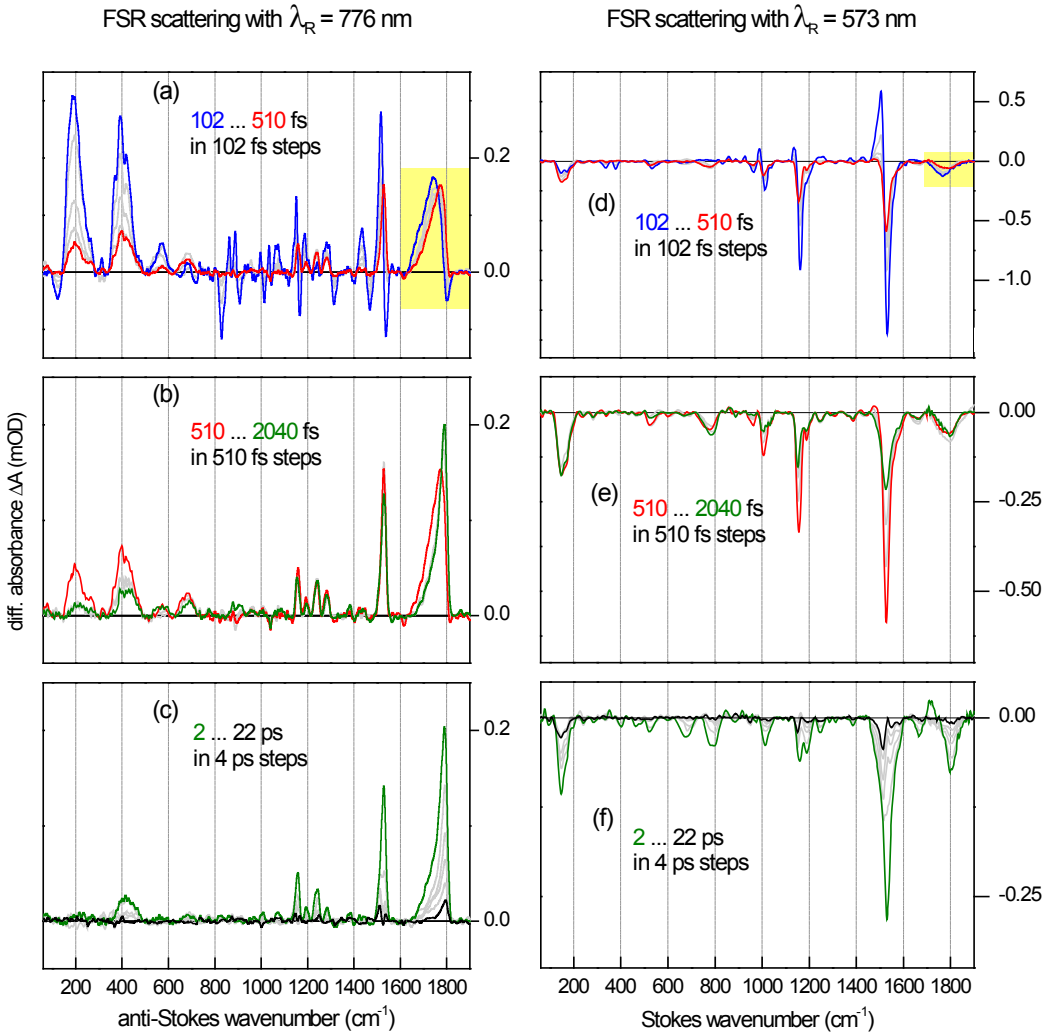

Figure 7: FSR spectra due to excited β-carotene in *n*-hexane. Ground-state signal has been removed; for details see section 2.3. Yellow boxes mark the region of the symmetric C=C stretching mode.

Excited-state Raman spectra on resonance with $S_y \leftarrow S_1$ *(*λ_R *= 573 nm)*

are shown in **Fig. 7**, right panels. In this case detection favors modes in S_1. FSR spectra are recorded on the Stokes side where excited-state Raman signals appear with negative sign (Raman gain). The same procedure for subtracting ground-state signal and treating bleach recovery is applied.

Early spectra are dominated by the aforementioned ground-state resonances seen from S_2, in the region between 800 and 1600 cm^{-1} (dispersive features, blue line in **Fig. 7d**). They change shape and amplitude with $\tau \sim 200$ fs as population reaches S_1 and negative Raman bands are formed at 1013, 1160, 1191, 1246, 1380 and 1531 cm^{-1} (red line). Their average width (fwhm) is ~40 cm^{-1}. A broad Raman band (70 cm^{-1}) in S_2 is detected around 1770 cm^{-1} having negative sign (yellow box). It decays with ~200 fs time-constant and transforms into a band at 1787 cm^{-1}, which is assigned to the symmetric C=C-stretch mode in S_1. As before, subsequent vibrational relaxation is seen as up-shift to 1800 cm^{-1} and narrowing (to 46 cm^{-1}) accompanied by some rise. The low frequency region is dominated by a single Raman band located at 146 cm^{-1} (fwhm = 46 cm^{-1}). Until now this mode in S_1 has been observed only with vibrational techniques in the time domain [46-48]. Strong fluctuations of the population background in our spectra complicate an accurate assessment of this band at early time. But still, a qualitative comparison between 100 and 500 fs suggests that this signal appears after IC to S_1. Loss of intensity is seen for Raman lines between 800 – 1600 cm^{-1} proceeding with 1.3 ps time-constant (**Fig. 7e**). Less obvious is a bi-exponential decay for the low frequency band with 0.7 and ~15 ps (**Fig. 8d**). Two further Raman bands at 675 and 789 cm^{-1} (~30 - 40 μOD) can be attributed to S_1 with certainty because they are not overlaid by bleach. An overview of S_1- and S_2 Raman bands is given in **Tables S2** and **S3**. Decay to the electronic ground state proceeds with $\tau \sim 9$ ps (**Fig. 8e,f**) and small remaining negative signals at 1150 and 1512 cm^{-1} indicate the hot ground state (**Fig. 7f**).

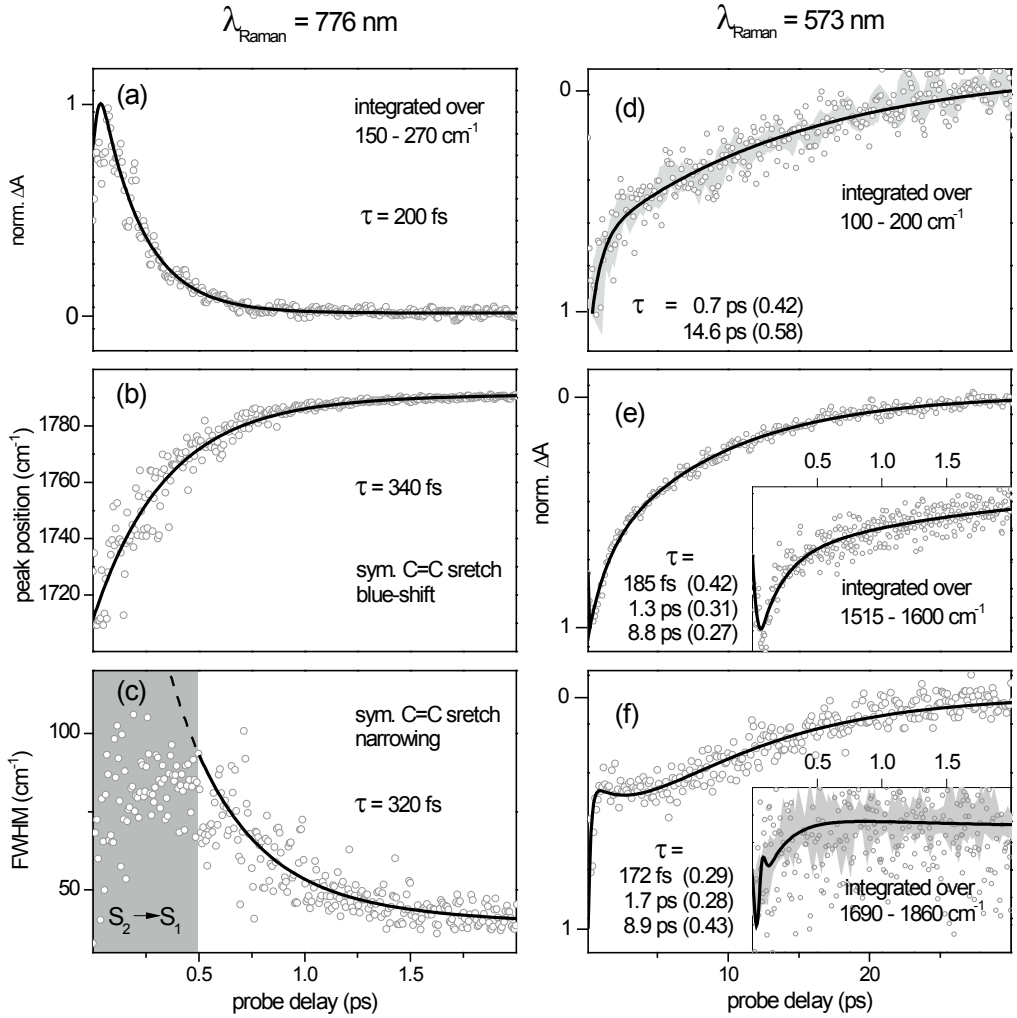

Figure 8: Kinetic traces of FSR signals from photo-excited β-carotene. (**a**) The low-frequency Raman band decays with the lifetime of S_2 (~200 fs). (**b**) The symmetric C=C stretching band shifts and (**c**) narrows with ~330 fs (the width becomes defined only in S_1, *i.e.* for t≥0.5 ps). (**d**) Low frequency activity in S_1 drops with 0.7 ps and then decays with 14.6 ps. (**e**) The integral 1515-1600 cm^{-1} captures two kinds of signal in parts, the negative wing of the band due to coherence in S_0 (seen from S_2) and most of the underlying S_1 band. The S_0 coherence vanishes with the S_2 population (~200 fs) and signal from S_1 becomes visible. Intensity loss of the S_1 band proceeds with 1.3 ps initially and is followed by ~9 ps decay. (**f**) The symmetric C=C stretching band already exists broadly in S_2 and decays with ~200 fs, revealing the same mode more narrowly in S_1. A subsequent rise (τ = 1.7 ps, possibly insignificant) of this mode is followed by 9 ps decay

Excited state Raman spectra pre-resonant with $S_\gamma \leftarrow S_1$ (λ_R = 621 nm).

Now resonance enhancement of excited-state β-carotene modes is minimized and correspondingly, the visibility of solvent signals is increased. Their line-shape depends on whether β-carotene is populated in S_2 or in S_1. For an illustration we process the FSR data differently for both states. In general the actinic pump, Raman pump, and probe are focused onto the same spot in the sample-cell. Difference spectra ΔA are generated by two subsequent shots with the Raman-pump on and off, respectively. The ground-state contribution is removed from ΔA(t) by subtracting a representative spectrum from negative

delays, *i.e.* when the actinic pulse arrives well after the coinciding Raman pump and –probe ($\Delta A(<0)$).

Only in case of populated S_2 the modified spectra $\Delta A(t)-\Delta A(<0)$ are further corrected for ground-state bleach (see above) and electronic background (BG) . The result is shown in **Fig. 9a**. Here the blue line shows a transient spectrum which originates from population in mainly in S_2, due to its early time tag of 200 fs. Ground-state resonances in β-carotene and solvent signals appear with dispersive line-shape and dominate the spectrum below 1600 cm^{-1}. The assignment of specific dispersive signals to *n*-hexane follows from a comparison with the corresponding stationary spectrum. For example the position of the 380 cm^{-1} line from pure *n*-hexane coincides with the center of a transient dispersive signal. Such coincidences are also observed for the solvent lines between 800 and 900 cm^{-1}. All dispersive features vanish within 0.5 ps as population reaches S_1.

In case of populated S_1 we demonstrate the presence of positive solvent lines with the help of **Fig. 9b,** for which $\Delta A(t)-\Delta A(t<0)$ has been corrected solely for BG. This means that ground-state bleach due to actinic pumping at t=0 is visible in the transient spectrum shown (at 2 ps, green line). While some of the positive signals reflect bleached ground state bands of β-carotene (orange line), others mirror the bands of pure *n*-hexane (light orange line). Note that these *n*-hexane bands, recorded for t>0, decay simultaneously with the bleach of β-carotene bands. We will come back to this strange observation at the end of our work.

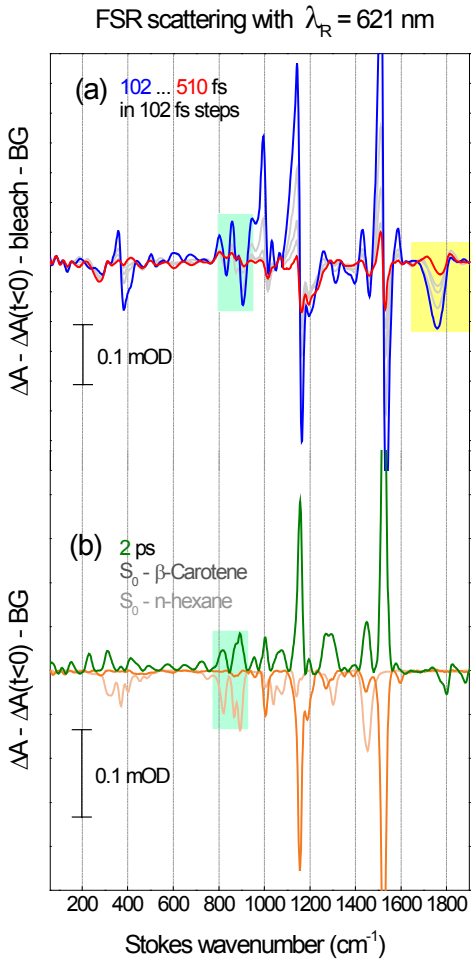

Figure 9: Intermolecular coupling between β-carotene and *n*-hexane is observed with transient FSR measurements. (**a**) Dispersive solvent signals (in green box) vanish with the $S_2 \rightarrow S_1$ internal conversion. The yellow box marks the region of the symmetric C=C stretching mode. (**b**) After subtraction of a spectrum recorded at negative delays, positive solvent bands (Raman loss; olive line in the green box) appear for t > 0.

3. Discussion

3.1 Excited state dynamics of β-carotene in *n*-hexane

S_2 bands are observed < 800 cm^{-1}.

When population is placed initially into S_2 and then scattering is performed along $S_x \leftarrow S_2$, three broad Raman signals immediately appear at 200, 400 and 570 cm^{-1} (**Fig. 7a**). To corroborate that these signals belong to the Franck-Condon region in S_2, we start instead from the electronic ground state and use resonance Raman scattering along $S_2 \leftarrow S_0$. Looking for vibronic resonances in S_2 (on top of the purely vibrational ones in S_0) we find broad signals at 200, 400 and 600 cm^{-1}. Their amplitudes are estimated from the data to be 3-10x that of the vibrational signal underneath. For experimental details and analysis the reader is referred to our previous work. [49]

We attribute the discrepancy between signal amplitudes to a major alteration of the S_2 energy landscape, accessible within the electronic coherence-time (~10 fs) following Raman excitation $S_2 \leftarrow S_0$. As a consequence, different transition dipoles μ and displacements Δ may apply for vibronic and vibrational resonances. Such alteration could be explained by the intermediate state $1B_u^-$. Its location is predicted (in the fully relaxed ground-state geometry) above the $2A_g^-$ state [50,51] and even slightly higher than the S_2 ($1B_u^+$) state [52,53]. If β-carotene in the S_2 state can relax within the electronic coherence time, the two may effectively cross and thereby modify the vibronic resonance. The latter could be intensified by an increase of mode displacements, even though the transition dipole of $1B_u^- \leftarrow 1A_g^-$ is calculated to be smaller than that of $S_2 \leftarrow S_0$ [53].

No S_2 bands are observed in the region 800 – 1600 cm^{-1}.

In the region 800-1600 cm^{-1} we do not observe signal that can be attributed to Raman activity in the S_2 state, contrary to previous reports [7,30,33,34]. Mathies and coworkers described broad S_2 bands centered at 1100, 1300, and 1650 cm^{-1} that decay with the electronic lifetime of S_2,[33] but we cannot reproduce their result. The difficulty lies in the population background BG that rises on a ps time scale and must be estimated accurately, so that its subtraction reveals the coherent signal. However, no matter how accurate or inaccurate the ps background is determined from the data, removing it will always leave signal that carries the 200 fs time signature of the $S_2 \rightarrow S_1$ internal conversion process. That condition is not sufficient for the recognition of vibrational structure.

Takaya et. al. measured transient FSR spectra of β-carotene in cyclohexane with λ_R = 1190 nm (actinic excitation at 480 nm) [7]. At the Stokes side three broad gain bands are observed at 1050, 1240, 1580 cm^{-1} at t = 0 (their **Fig. 2b**). They are partly superimposed by broad coherent signal from water vapor. Three carotene modes are also identified at the *anti*-Stokes side, having dispersive shape with central frequencies at 1030, 1250 and 1560 cm^{-1} (their **Fig. 3**). Because observations from the Stokes- and anti-Stokes side coincide, it is concluded that these three bands are Raman signals from S_2. Their choice of λ_R improves on our ~800 nm for several reasons (better resonance, reduced two-photon excitation, smaller ground-state contribution) and therefore, the sensitivity may be higher in that work.

Sakamoto recorded one broad Raman band around 1550 cm^{-1} (probably consistent with 1580 cm^{-1} from Takaya) with ps time-resolved Raman measurements with λ_R = 1064 nm [30,34].

Symmetric C=C-stretch at 1770 cm^{-1} is also observed in S_2, in addition to S_1.

A symmetric C=C stretching mode plays a central role in β-carotene spectroscopy. In previous work, Raman intensity due to this mode was seen to be rising on the 200 fs time scale as the S_1 state becomes populated. Recently Takaya *et al* (in the experiments which were specified directly above) reported a weak band around 1776 cm^{-1} at time zero already, which shifts to 1792 cm^{-1} while rising. The authors assign this band to the symmetric C=C stretching mode in S_1 also – even during the initial stage when almost all population is in S_2. They argue that the NIR Raman pump has 5-x larger absorbance for S_2 compared to S_1, so that probing of S_2 modes is favored. Interestingly, no corresponding signal is seen in their anti-Stokes spectra. Stokes spectra are also recorded with 403 nm actinic excitation: the band now appears around 1741 cm^{-1} at t = 0. Similar observations have been reported with λ_R=560 nm. [24]

At 100 fs we observe one broad band (fwhm ~ 70 cm^{-1}) at 1770 cm^{-1} for all Raman excitations (**Figs. 7a,d** and **9a**: blue lines in yellow boxes). For λ_R=573 and 621 nm this band shows an initial decay with the lifetime of S_2 (~200 fs – but remember our caveat before) which transforms it into a band around 1790 cm^{-1} (fwhm ~ 40 cm^{-1}). From comparison with previous results we conclude that the latter belongs to the symmetric C=C stretching-mode in S_1 [12,22,33]. The same mode appears as Raman loss in case of λ_R = 776 nm (**Fig. 7a**: red line in yellow box); it evolves from an early broad loss band which has a slightly dispersive shape.

No initial decay of some broad Raman band > 1600 cm^{-1} was previously reported. Instead the rise of the symmetric C=C stretching mode in S_1 has been characterized as being either mono- or bi-exponential [22,24]. Subsequent vibrational redistribution in S_1 is seen (by us and others) as up-shift (340 fs) and narrowing (320 fs) of this signal (a simultaneous rise simply reflects the fact that the oscillator strength is conserved). Excess IC-energy from S_2 is distributed to anharmonically coupled normal modes via the central C=C stretch mode [22,54]. A considerable contribution from low-frequency modes is expected to promote this process [36]. The large up-shift (by ~270 cm^{-1}) of the symmetric C=C mode in S_1, compared to the corresponding asymmetric mode in S_1 (1531 cm^{-1}), is explained by vibronic coupling S_1/S_0 through this symmetric mode [28,29]. Experimental evidence for this coupling was observed as weak over-damped oscillation (ν = 96 cm^{-1}) in the band-integral (380 – 480 nm) from TA [55].

Non-exponential ground-state recovery is seen with TA and – indirectly – with FSR scattering.

For the S_1 state, in the region below 800 cm^{-1} only one band is seen by us, at 146 cm^{-1}. This band has been observed in the time-domain before [46-48]. S_1-signals between 800 and 1600 cm^{-1} are seen with the resonant Raman excitation at 573 nm; the most intense ones are located at 1013, 1160 and 1531 cm^{-1} (see **Table S2**). The entire spectrum decays with

~9 ps, but before, the three intense lines show an initial decay with ~1.3 ps (**Fig. 7e**). No such intensity-loss is recorded for the isolated bands, *i.e.* those that are not overlaid by ground-state bleached lines, either in the low- (146 cm^{-1}) or the high-frequency region (~1800 cm^{-1}). Let us discuss the reason for this difference.

Evolution on a similar time-scale is primarily seen as a non-exponential contribution in the TA-spectra. The corresponding DAS (grey line between **Fig. 3b** and **c**) has a negative part (500 – 650 nm) which describes a small rise of intensity across the entire $S_y \leftarrow S_1$ ESA band, counteracting the 6.9 ps decay to S_0. But also in the bleach region the deviation from mono-exponentiality is felt, as can be seen from a positive part (<500 nm) of the DAS and also directly in a time trace at 450 nm (**Fig. S1c**). We conclude that the non-exponential TA contribution reflects some reorganization on the larger S_1 PES, with the consequence of also a non-exponential repopulation of S_0.

Back to the FSR spectrum, it is that latter recovery process which causes some early peculiarities where the intense S_0 Raman bands are located. Note that bleach recovering mono-exponentially with 9 ps has been subtracted for **Fig. 7**. In this case we find that the reconstructed S_1-signal at 1531 cm^{-1} broadens from 25 cm^{-1} at 0.5 ps to 35 cm^{-1} at 2 ps, whereas from cooling one would expect narrowing. But in reality less bleach should have been subtracted during the first ps, as was explained above. In short, then, the early decay of Raman intensity for the 1013, 1160 and 1531 cm^{-1} lines in **Fig. 7e** is an artifact. The analysis strengthens our earlier conclusion that ground-state recovery is slightly delayed on the ps time scale. The early pseudo-decay is hardly visible in the transient spectra with λ_R = 776 nm. The reason is that the NIR Raman excitation is far from resonance with the S_2-S_0 transition and the contribution of bleach is generally weak.

The entire FSR spectrum decays with ~9 ps (**Fig. 7f**) similar to TA. IC is mostly mediated by the C=C stretching-modes [26,36,56,57]. After IC these modes spread the energy over normal modes in S_0 via IVR and cooling [23,57]. The primary acceptors (C=C and C-C) relax faster than the secondary acceptor modes (C-CH_3 and C-H). Raman lines from the hot-ground state are recorded at 1512 and 1150 cm^{-1} which is in accordance with previous observations [7,23,24].

3.2 Spectral changes upon backbone-substitution

The major alteration in the optical absorption of β-carotene **(Fig. 1)** already occurs when the single methyl group at C_9 is replaced by an ethyl group; no significant change is observed upon further modification to iso-propyl. The loss of structure indicates that vibrational modes in S_2 are dressed differently or even disturbed by breaking the C_{2h} symmetry; the blue-shift indicates some shortening of the polyenic chain.

Excited state transitions $S_x \leftarrow S_2$ and $S_y \leftarrow S_1$ are hardly affected for the substituted carotenes as the respective ESA bands are shifted by only a few nanometers compared to β-carotene. The time-constants for the relaxation processes are also mostly identical for the three compounds. The main difference is that the amplitude of the non-exponential contribution is much smaller for the substituted carotenes than for β-carotene. Reasons for this difference must be found in the increased bulkiness at C_9 for the derivatives.

The chemical structures of β-carotene and et-β-carotene are shown in the right panel of **Fig. 1**. Two main conformations can be adopted by β-carotene: all-*trans* and s-*cis* [58,59]. In the former structure the methyl group at C_5 points to the same direction as the methyl group at C_9 and all double-bonds are arranged in a linear manner. For the s-*cis*-conformer, instead the two methyl-groups at C_1 are on the same side as the methyl-group at C_9; the terminal double bonds between C_5 (C_5') and C_6 (C_6') are now orthogonal to the linear polyene chain. The two conformers can be transformed into each other by a joint 180° rotation along the C_6-C_7 and C_6'-C_7' bonds. Loss of conjugation is energetically compensated by less ring torsion, so that at room temperature mostly s-cis is populated (>97%). Recent theoretical work revealed two energetically close-lying rotamers of s-cis itself, labelled AS1 (70%) and S (not to be confused with electronic states S_0 etc) [60]. Their interconversion involves rotation of the first β-ring around the C_6-C_7 bond, but in the electronic ground state they are separated by a ~9 kJ mol^{-1} (700 cm^{-1}) barrier. We speculate that in S_1 the rotational barrier is small enough to be overcome. The original population distribution from S_0 (mostly AS1) could change in S_1 favoring the rotamer S which we suppose have larger oscillator-strength for the $S_y \leftarrow S_1$ transition. This is then seen as rise of intensity for the dominant ESA band. With our substituted carotenes this process should be reduced, since the bulky substituent increases the energy-barrier for rotation. The population ratio from S_0 is therefore kept throughout the relaxation process and no change in intensity is observed.

Let us go back to unsubstituted β-carotene. The observed non-exponentiality of integrated S_1 ESA intensity, together with delayed ground-state recovery on the same time scale, is thus seen as an indication of conformer dynamics in the S_1 state. We speculate that this observation is causally connected with the appearance of a much slower component to S_1 population decay (13.6 ps, see the characteristic ESA peak in **Fig. 3d**). Possibly we see here the internal conversion $S_1 \rightarrow S_0$ of the conformer which becomes populated in S_1. The hypothesis is illustrated in **Fig. 10**.

One may ask, why was the complex decay of the S_1 ESA band of β-carotene not recognized earlier? Recent reports of lifetimes are collected in **Table 1**. It is striking that the variance of reported $S_1 \rightarrow S_0$ conversion times is larger than the noted precision, suggesting systematic errors because different types of fit were used. Our correlation time of 9.1 ps (for the CE + 6.9 ps processes shown in **Fig. 3**) is within the range of reported lifetimes. It is the use of the band integral which makes our finer distinction possible.

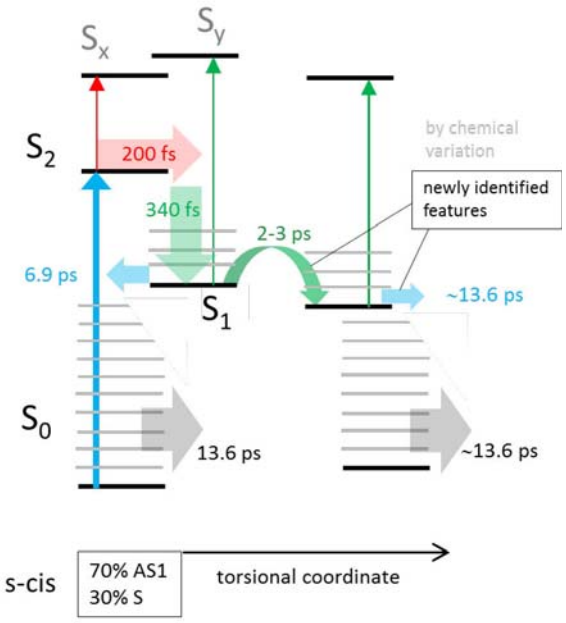

Figure 10: Relaxation scheme for β–carotene based on the work of Lukes *et al* [60]. In the electronic ground state the dominant s-cis form has a sub-distribution of AS1/S conformers. Excitation into S_2 is followed by the well-known relaxation cascade shown at left. Interconversion between the conformers in S_1 is seen to proceed with 2-3 ps correlation time. Ground-state recovery of the second conformer has similar time-constant as cooling in S_0.

Table 1 Decay times for β-carotene in aliphatic solvents

year, first author	type of fit	solvent	T (K)	$S_2 \rightarrow S_1$ (fs)	S_1 IVR (fs)	$S_1 \rightarrow S_0$ (ps)	cool (ps)	
2002 Billsten[36]	3 traces	n-hexane	293	140 - 260	650	9	-	(a)
2002 Weerd[35]	global	n-hexane	298	140±30	400±100	9.1±0.5	-	(b)
2009 Kosumi[14]	1 trace	cyclohexane	298	140±30	-	8.5±0.2	-	(c)
2009 Ostroumov[53]	global	n-hexane	-	~150	~160	~8.3	-	(d)
2010 Lenzer[18]	global	n-hexane	298	160	630	8.7	11.9	-
2013 Takaya[7]	Gaussian analysis	cyclohexane	298	190±20	-	9.2±0.4	-	(e)

(a) no S_0 cooling was seen in bleach-region (484 nm) ; (b) fit was performed for $\lambda > 490$ nm;
(c) parameters given for kinetic fit at isosbestic point of $S_y \leftarrow S_1$ ESA; (d) only the first 2 ps were shown ; (e) in the NIR region.

3.3 Molecular near-field effect?

Remember that we monitor the transmitted probe intensity and register changes ΔA upon switching the Raman pump on and off. Since bulk solvent (*n*-hexane) is present independent of the actinic pumping process, corresponding Raman gain bands are observed at all times during a transient FSR measurement. One may therefore determine the solvent spectrum for delays t<0 first, and then subtract it from the measured spectra at delays t>0. In this way the pure β-carotene spectra should be obtained as function of delay time. For example using λ_R=503 nm at the red flank of the β-carotene $S_2 \leftarrow S_0$ absorption, we find at t<0 that solvent lines below 1000 cm^{-1} are well separated from solute bands and have amplitudes ~10% compared to the strong β-carotene band at 1520 cm^{-1}.

But when the corresponding subtraction is subsequently made for t>0, we always see that the recorded *n*-hexane gain bands are overcompensated and a positive (i.e. Raman loss) solvent contribution is suggested for the transient β-carotene spectra. If the overcompensation were to be avoided, a scaling factor s≈0.90 must be applied to the solvent contribution before subtraction when t>0, whereas s=1.00 when t<0. The imbalance is reproduced consistently and is therefore significant; it implies that the β-carotene solute and nearby *n*-hexane solvent molecules are electronically coupled, similar to what has been observed using hyper-Raman scattering by Hamaguchi and coworkers [61,62].

The question is which optical process in β-carotene is responsible, upon actinic excitation, for the observed change of solvent Raman activity nearby? Is the solvent environment "normal" (i.e. uncoupled) for t<0 and then becomes coupled by excitation of the solute (*case a*)? Or alternatively, is the solvent´s Raman spectrum enhanced when β-carotene offers its full $S_2 \leftarrow S_0$ oscillator strength, which is then reduced by ground-state bleaching of β-carotene at t=0 (*case b*)?

A clue is provided by the FSR spectra in the time-range 100 - 500 fs and at 2 ps which are shown in **Fig. 9a** and **b**, respectively. They were prepared from the recorded data by

subtracting spectra from negative delays and the electronic background. The early FSR spectra were further corrected, at t>0, by the diminished S_0 spectrum of β-carotene due to missing ground-state population (bleach) as described earlier. A similar treatment is necessary for the *n*-hexane lines, in principle, since they show up as positive Raman-loss once S_1 is populated (green box **Fig. 9b**). We are tempted to accept such bleach-like correction with a time-dependent scaling factor s(t) as an empirical correction for some unknown artifact of the measurement. However the empirical correction of the early spectra is insufficient in principle because a residual spectrum always remains in the solvent region below 1000 cm^{-1} and also above, having dispersive character (**Fig. 9a**). It is not possible to correct the entire induced FSR spectrum with just one solvent spectrum; clearly part of the solvent signal reflects the electronic relaxation $S_2 \rightarrow S_1$ of the β-carotene solute. Irrespective of the true value of s, it follows that *case a* is involved for S_2 at least.

Conclusion

Stimulated Raman and transient absorption spectra from states S_2, S_1 and S_0 of β-carotene in *n*-hexane are obtained and discussed. A single methyl/ethyl replacement at the polyene backbone of β-carotene allows to differentiate relaxation processes after optical excitation.

- The earliest features belong to S_2. Broad vibrational bands are seen in the low-frequency region. Dispersive signals in the range 800 – 1600 cm^{-1} denote ground-state coherences. An early band around 1770 cm^{-1} is seen having either broad (Stokes of λ_R = 573, 621 nm) or slightly dispersive (anti-Stokes of λ_R = 776 nm) line-shape. Upon IC $S_2 \rightarrow S_1$ (200 fs) it turns into the band for symmetric C=C-stretching in S_1.
- Already during vibrational redistribution in S_1, a small non-exponential rise of ESA oscillator strength is noted (2-3 ps). The effect disappears when the C_9-methyl group is replaced by ethyl. It is attributed to conformational change in S_1 involving the dihedral angles C6 and C9.
- Internal conversion back to S_0 is seen simultaneously as ground-state recovery and as decay of ESA signal, with 6.9 ps (~77%) and 13.6 ps (~23%) time constants. The two processes are attributed to the two torsional S_1 conformers mentioned above. The latter process is overlaid by cooling, as the vibronic progression of the original absorption spectrum is re-emerges. All S_1 Raman lines disappear with ~9 ps, *i.e.* the average of the aforementioned IC times.
- A near-field-effect on solvent molecules is implied by solvent Raman signal which follows the dynamics of electronically excited β-carotene.

Acknowledgement

We are grateful to the Deutsche Forschungsgemeinschaft for support (ER 154/10-2) and T. Lenzer and K. Oum for critical readings of the manuscript. M.Q. acknowledges funding (in part) by ERC grant No. 259432.

Supporting Information

Experimental, shape and sign of Raman bands, on assignments and conformations, synthesis.

References

[1] R.J.Cogdell, H.A.Frank, *Biochim. Biophys. Acta* **1987**, *895*, 63-79.

[2] B.S. Hudson, B.E. Kohler, *Chem. Phys. Lett.* **1972**, *14*(3), 299-304.

[3] K. Schulten, M. Karplus, *Chem. Phys. Lett.* **1972**, *14*(3), 305-309.

[4] M.R. Wasielewski, L.D. Kispert, *Chem. Phys. Lett.* **1986**, *128*(3), 238-243.

[5] P.O. Andersson, T. Gillbro, A.E. Asato, R.S.H. Liu, *J. Lum.* **1992**, *51*, 11-20.

[6] P.O. Andersson, S.M. Bachilo, R-L. Chen, T. Gillbro, *J. Phys. Chem.* **1995**, *99*, 16199-16209.

[7] T. Takaya, K. Iwata, *J. Phys. Chem. A* **2014**, *118*, 4071-4078.

[8] S.L. Bondarev, S.M. Bachilo, S.S. Dvornikov, S.A. Tikhomirov, *J. Photochem. Photobiol. A* **1989**, *46*, 315-322.

[9] S.L. Bondarev, V.N. Knyukshto, *Chem. Phys. Lett.* **1994**, *225*, 346-50.

[10] A.P. Shreve, J.K. Trautman, T.G. Owens, A.C. Albrecht, , *Chem. Phys. Lett.* **1991**, *178*(1), 89-96.

[11] J-P. Zhang, L.H. Skibsted, R. Fujii, Y. Koyama, , *Photochem. Photobiol.* **2001**, *73*(3), 219-222.

[12] M. Yoshizawa, H. Aoki, H. Hashimoto, *Phys. Rev. B* **2001**, *63*, 180301.

[13] D. Kosumi, K. Yanagi, R. Fujii, H. Hashimoto, M. Yoshizawa, *Chem Phys. Lett.* **2006**, 42*5*, 66-70.

[14] D. Kosumi, M. Fujiwara, R. Fujii, R.J. Cogdell, H. Hashimoto, M. Yoshizawa, *J. Chem. Phys.* **2009**, *130*, 214506.

[15] T. Polivka, V. Sundström, *Chem. Phys. Lett.* **2009**, *477*, 1-11.

[16] E. Papagiannakis, I. H. M. van Stokkum, M. Vengris, R. J. Cogdell, R. van Grondelle, D. S. Larsen, *J. Phys. Chem. B* **2006**, *110*, 5727-5736.

[17] J. Hauer, M. Maiuri, D. Viola, V. Lukes, S. Henry, A. M. Carey, R. J. Cogdell, G. Cerullo, D. Polli, *J. Phys. Chem. A* **2013**, *117*, 6303-6310.

[18] T. Lenzer, F. Ehlers, M. Scholz, R. Oswald, K. Oum, *PCCP* **2010**, *12*, 8832-8839.

[19] S. Saito, I. Harada, M. Tasumi, C. H. Eugster "Resonance Raman Spectra of all-*trans* and 15,15'-*cis*-β,β-Carotene." *Chem. Lett.* **1980**, 1045-1048.

[20] H. Hashimoto, Y. Koyama, *Chem. Phys. Lett.* **1989**, *154*(4), 321-325.

[21] H. Hashimoto, Y. Koyama, *Chem. Phys. Lett.* **1989**, *163* (2,3), 251-256.

[22] D.W. McCamant, J.E. Kim, R.A. Mathies, *J. Phys. Chem. A* **2003**, *107*, 8208-8214.

[23] D.W. McCamant, J.E. Kim, R.A. Mathies, *J. Phys. Chem. A* **2002**, *106*, 6030-6038.

[24] S. Shim, R.A. Mathies, *J. Phys. Chem. B* **2008**, *112*, 4826-4832.

[25] T. Noguchi, H. Hayashi, M. Tasumi, G.H. Atkinson, *J. Phys. Chem.* **1991**, *95*, 3167-3172.

[26] H. Nagae, M. Kuki, J.-P. Zhang, T. Sashima, Y. Mukai, Y. Koyama, *J. Phys. Chem.* **2000**, *104*, 4155-4166.

[27] H. Hashimoto, Y. Koyama, Y. Hirata, N. Mataga, *J. Phys. Chem.* **1991**, *95*, 3072-3076.

[28] G. Orlandi, F. Zerbetto, *Chem. Phys.* **1986**, *108*, 187-195.

[29] F. Zerbetto, M.Z. Zgierski, G. Orlandi, G. Marconi, *J. Chem. Phys.* **1987**, *87*, 2505-2512.

[30] A. Sakamoto, S. Matsuno, M. Tasumi, *J. Mol. Struct.* **2010**, *976*, 310-313.

[31] H. Kandori, H. Sasabe, M. Mimuro, *JACS* **1994**, *116*, 2671-2672.

[32] A.N. Macpherson, T. Gillbro, *J. Phys. Chem. A* **1998**, *102*, 5049-5058.

[33] P. Kukura, D.W. McCamant, R.A. Mathies, *J. Phys. Chem. A* **2004**, *108*, 5921-5925.

[34] A. Sakamoto, S. Matsuno, M. Tasumi, *J. Raman. Spectrosc.* **2006**, *37*, 429-435.

[35] F.L. Weerd, I.H.M. van Stokkum, R. van Grondelle, *Chem. Phys. Lett.* **2002**, *354*, 38-43.

[36] H.H. Billsten, D. Zigmantas, V. Sundström, T. Polivka, *Chem. Phys. Lett.* **2002**, *355*, 465-470.

[37] G. Cerullo, G. Lanzani, M. Zavelani-Rossi, S. De Silvestri, *Phys. Rev. B* **2001**, *63*, 241104.

[38] S. Vdovic, Y. Wang, B. Li, M. Qiu, X. Wang, Q. Guo, A. Xia, *PCCP* **2013**, *15*, 20026-20036.

[39] D. C. Johnston, *Phys. Rev. B* **2006**, *74*, 184430.

[40] E. W.Hansen, X. Gong, Q. Chen, *Macromol. Chem. Physic.* **2013**, *214*, 844-852.

[41] J. Gabriel, T. Blochowicz, B. Stühn, *J. Chem. Phys.* **2015**, *142*, 104902.

[42] A. Adanlete Adjanoh, J. Vogel, M. Ayadi, K. Abdelmoula, *J. Magn. Magn. Mater.* **2011**, *323*, 504-508.

[43] P. Hamm, J. Helbing, J. Bredenbeck, *Chem. Phys.* **2006**, *323*, 54-65.

[44] N. Tschirner, M. Schenderlein, K. Brose, E. Schlodder, M.A. Mroginski, C. Thomsen, P. Hildebrandt, *PCCP* **2009**, *11*, 11471-11478.

[45] A.L. Dobryakov, S.A. Kovalenko, N.P. Ernsting, *J. Chem. Phys.* **2005**, *123*, 044502.

[46] J.P. Kraack, A. Wand, T. Buckup, M. Motzkus, S. Ruhman, *PCCP* **2013**, *15*, 14487-14501.

[47] M. Liebel, P. Kukura, *J. Phys. Chem. Lett.* **2013**, *4*, 1358-1364.

[48] M. Liebel, C. Schnedemann, P. Kukura, *Phys. Rev. Lett.* **2014**, *112*, 198302.

[49] M. Quick, A.L. Dobryakov, S.A. Kovalenko, N.P. Ernsting, *J. Phys. Chem. Lett.* **2015**, *6*, 1216-1220.

[50] J.H. Starcke, M. Wormit, J. Schirmer, A. Dreuw, *Chem. Phys.* **2006**, *329*, 39-49.

[51] D. Ghosh, J. Hachmann, T. Yanai, G.K.-L. Chan, *J. Chem. Phys.* **2008**, *128*, 144117.

[52] M. Kleinschmitt, C.M. Marian, M. Waletzke, S. Grimme, *J. Chem. Phys.* **2009**, *130*, 044708.

[53] E. Ostroumov, M.G. Müller, C.M. Marian, M. Kleinschmidt, A.R. Holzwarth, *Phys. Rev. Lett.* **2009**, *103*, 108302.

[54] H. Okamoto, K. Yoshihara, *Chem. Phys. Lett.* **1991**, *177* (6), 568-572.

[55] J.L. Perez Lustres, A.L. Dobryakov, A. Holzwarth, M. Veiga, *Angew. Chem. Int. Ed.* **2007**, *46*, 3758-3758.

[56] M. R. Wasielewski, D. G. Johnson, E. G. Bradford, L. D. Kispert, *J. Chem. Phys.* **1989**, *91*, 6691-6697.

[57] T. Siebert, R. Maksimenka, A. Materny, V. Engel, W. Kiefer, M. Schmitt, *J. Raman. Spectrosc.* **2002**, *33*, 844-854.

[58] S. Schlücker, A. Szeghalmi, M. Schmitt, J. Popp, W. Kiefer, *J. Ram. Spectrosc.* **2003**, *34*, 413-419.

[59] W-L. Liu, Z-G. Wang, Z-R. Zheng, A-H. Li, W-H. Su, *J. Phys. Chem.* **2008**, *112*, 10580-10585.

[60] V. Lukes, N. Christensson, F. Milota, H. Kauffmann, J. Hauer, *Chem. Phys. Lett.* **2011**, *506*, 122-127.

[61] R. Shimada, H. Hamaguchi, *J. Chem. Phys.* **2011**, *134*, 034516.

[62] R. Shimada, H. Hamaguchi. *J. Chem. Phys.* **2014**, *140*, 204506.

[a] In principle the 556 nm ESA peak in **Fig. 3d** could be an artifact of the global fit procedure. However we rule out this possibility because the characteristic times for the two DAS in **Fig. 3c** and **d** are sufficiently separated. This conclusion was tested with simulated $\Delta A(t,\lambda)$ data (=sum over the DAS with corresponding exponential time functions) with various levels of noise added.

[b] Very weak ESA >1000 nm is also found in the DAS for 13.6 ps. It is attributed to the $S_2 \leftarrow S_1$ transition. A temporal distinction between the two forms of S_1 β-carotene (i.e. into 6.9 and 13.6 ps components) is not possible due to the weakness of our corresponding signal.

Resonance Femtosecond-Stimulated Raman Spectroscopy Without Actinic Excitation Shows Low-Frequency Vibrational Activity in the S_2 State of All-Trans β-Carotene

*Martin Quick, Alexander L. Dobryakov, Sergey A. Kovalenko, and Nikolaus P. Ernsting**

Department of Chemistry, Humboldt-Universität zu Berlin,

Brook-Taylor-Str. 2, D-12489 Berlin, Germany

ABSTRACT: Raman scattering with stimulating femtosecond probe pulses (FSR) was used to observe vibrational activity of all-trans β-carotene in n-hexane. The short-lived excited electronic state S_2 was accessed in two ways: (i) by transient FSR after an actinic pulse to populate the S_2 state, exploiting resonance from an $S_x \leftarrow S_2$ transition, (ii) by FSR without actinic excitation, using $S_2 \leftrightarrow S_0$ resonance exclusively and narrowband Raman / broadband fs probe pulses only. The two approaches have nonlinear optical susceptibilities $\chi^{(5)}$ and $\chi^{(3)}$, respectively. Both methods show low-frequency bands of the S_2 state at 200, 400, and ~600 cm^{-1}, which are reported for the first time. With (ii) the intensities of low-frequency vibrational resonances in S_2 are larger compared to S_0, implying strong anharmonicities/mode

[1] Reprinted ("Adapted" or "in part") with permission from Quick, M.; Dobryakov, A.L.; Kovalenko, S.A.; Ernsting, N.P. Resonance Femtosecond-Stimulated Raman Spectroscopy without Actinic Excitation Showing Low-Frequency Vibrational Activity in the S_2State of All-Trans beta-Carotene. *J. Phys. Chem. Lett*, **2015**, *6*, 1216-1220.

mixing in the excited state. In principle, for short-lived electronic states the $\chi^{(3)}$ method should allow the best characterization of low-frequency modes.

KEYWORDS Femtosecond Stimulated Raman Scattering, FSRS, Vertical Excitation, Electronic Background, Anharmonicities, Mode Mixing.

Vibrations in the primary excited state $S_2(1B_u^+)$ of *all-trans*-β-carotene are hard to determine owing to the ~160 fs electronic lifetime. Rapid internal conversion to the dark state $S_1(2A_g^-)$, some 6000 cm^{-1} below, proceeds through a cascade of levels whose electronic character is still under debate. For a summary of carotenoid photophysics and open questions (as of 2009) the reader is referred to ref. 1. The early vibronic dynamics must be studied in order to understand the molecular mechanisms of light-harvesting and protection by carotenoids in various biological systems. Here we report vibrational resonances in the Franck-Condon state directly upon $S_2 \leftarrow S_0$ absorption of a photon. Low frequency bands at 200, 400 and ~600 cm^{-1} are observed in S_2 even though their activity should be weak, according to preresonant results for S_0[2,3].

First attempts to characterize excited-state relaxation processes in β-carotene by femtosecond vibrational techniques were made in the early 2000s. Electronic excited-state absorption (ESA) $S_x \leftarrow S_2$ was first observed by Yoshizawa *et al* [4] as a broad near-infrared band around 1000 nm, **Fig. 1**. The authors proceeded to record transient fs-stimulated Raman (FSR) spectra of the excited state, hoping to exploit resonance for spectrally narrow excitation at 794 nm. The optical scheme in **Fig. 2a** can be considered a tandem $\chi^{(2)} \times \chi^{(3)}$ process ($\chi^{(5)}$ for brevity). At high frequencies a Raman gain band at 1770 cm^{-1} was observed at 0.2 ps. Its subsequent narrowing and up-shift (0.6 ps time constant) was attributed to a vibrational cascade in S_1[4,5]. Vibrational bands of S_2 have since been reported by three groups[6-8]. All observations were made in the frequency domain above 1000 cm^{-1}, by Raman scattering with $S_x \leftarrow S_2$ for resonance, but results are at variance with each other. Measurements entirely in the time domain, on the other hand, have been limited to the S_1 state[9]. The limitation points to a general problem of techniques that apply a sequence of "actinic" pump, Raman pump, and probe pulses which must be well separated in time. When

the time window after actinic excitation is very short (as with β-carotene in the S_2 state) the pulses are likely to overlap in time and cascades of higher order will spoil the desired signal. For this reason the free induction decay of S_2 signal could only be evaluated after 200 fs[9].To unlock the early time window one must reduce the order of the interaction to $\chi^{(3)}$ while maintaining access to vibrational information. For example Kukura and coworkers[10] used a pump-probe arrangement for broadband transient absorption. The authors created S_2 at the Franck-Condon (FC) geometry by impulsive excitation and then saw rich vibrational coherence in S_1 which must have survived internal conversion. Modes of S_2 were not reported.

Stimulated resonance Raman spectroscopy without actinic excitation, hence without variable time delay and performed as a $\chi^{(3)}$ experiment entirely in the frequency domain, is proposed here for an alternative view of vibrational structure in the excited state. In the current case, narrow (ps) Raman pump and broadband (fs) probe pulses are both tuned to the $S_2 \leftarrow S_0$ electronic transition, **Fig. 2c**. Vertically upward interaction with the respective fields, for example on the ket and bra side, jointly launches a vibrational wavepacket in S_2 at the Franck-Condon geometry. It modulates the electronic coherence which is generated by a further Raman interaction (downward on the ket side). When the transmitted probe pulse is dispersed in a spectrograph, weak absorption (loss) or emission (gain) lines are seen in the spectrum of the transmitted pulse, corresponding to the vibrational activity.

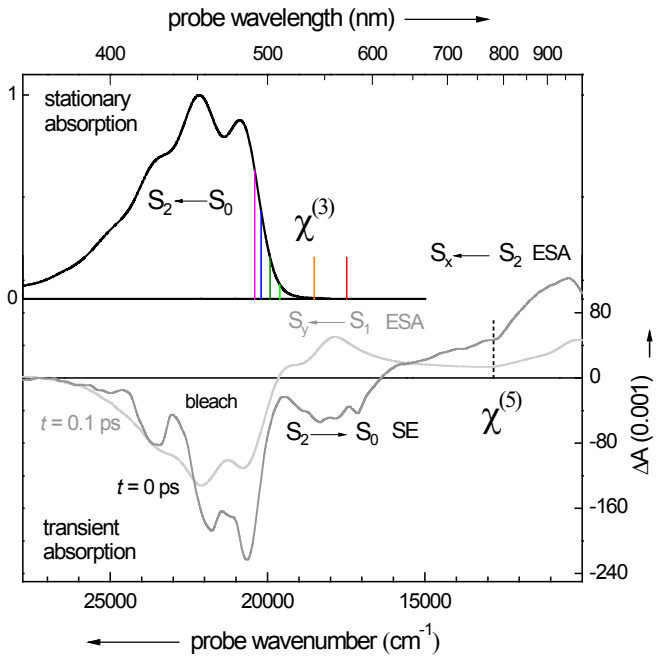

Figure 1. Resonance conditions of β-carotene in *n*-hexane. *Transient* ($\chi^{(5)}$) *femtosecond-stimulated Raman* (FSR) scattering: following actinic excitation at 490 nm, resonance with $S_x \leftarrow S_2$ excited-state absorption (ESA) was exploited at λ_R =780 nm. *Vertical* ($\chi^{(3)}$) FSR scattering: for every Raman wavelength λ_R a 2000 cm^{-1} Stokes window was probed. Induced absorption/gain ΔA in a window involves transitions $S_2 \leftarrow S_0$ and mainly $S_2 \rightarrow S_0$ (stimulated emission, SE).

Note that excited-state vibrational resonances in $\chi^{(3)}(\omega_1,\omega_2,\omega_3)$ are well known, in principle, since the early days of nonlinear molecular spectroscopy[11-13]. What is new here is the technical use of broadband probe pulses with femtosecond duration. This type of experiment with condensed-phase samples has already been demonstrated for the nπ* state of azobenzene[14,15]. For the S_2 state of β-carotene it has the advantage, compared to measurements in the time domain, that the full time window (on the order of $\tau \approx 160$ fs) is available for the inherent Fourier-transformation of the induced polarization $P^{(3)}(t)$.

Considering a vibrational mode at low frequency which is apodized by the electronic S_2 population decay, a well-formed lineshape is expected for $\nu \geq 150$ cm^{-1}.

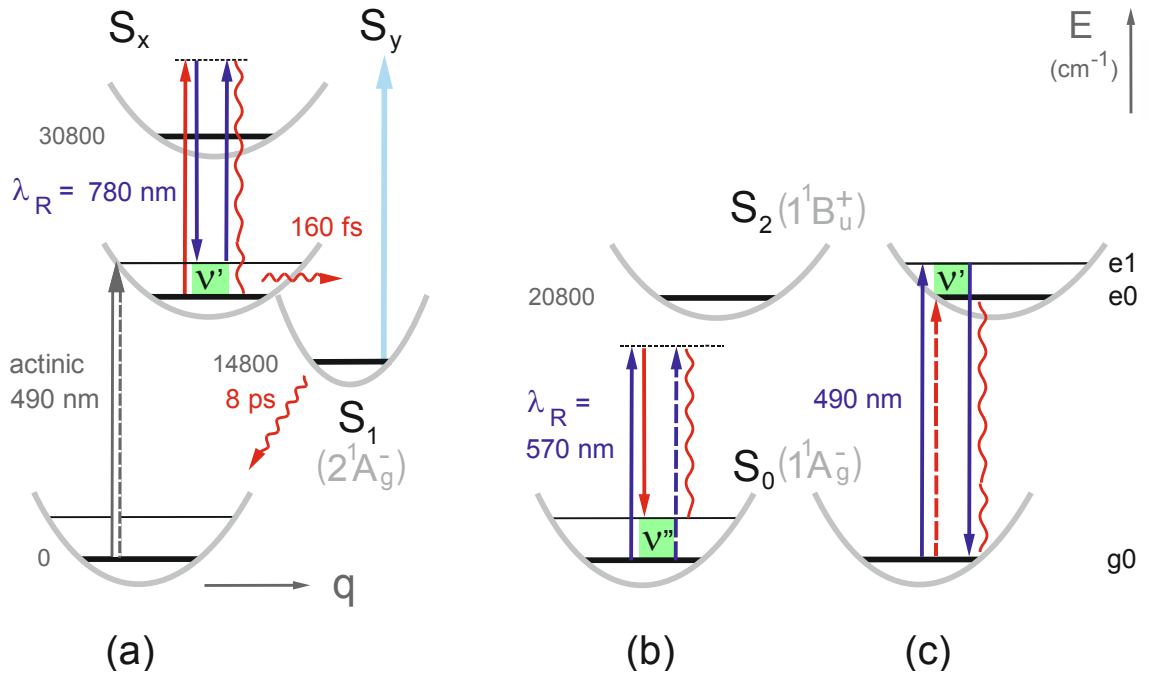

Figure 2. Vibrational coherence (green) is created by interaction with a narrowband Raman (blue) and fs probe field (red) and read out via two subsequent transitions. (**a**) *Transient* FSR scattering after actinic pumping. In this case the anti-Stokes region was probed as a function of delay time. *Vertical* FSR without actinic pump: (**b**) pre-resonant, (**c**) the excited-state contribution which is studied in this work. Shown are potential energy and level schemes for Raman-active coordinate q.

The key advantage is that resonance involves only transitions S_2–S_0 which can be predicted by quantum-chemical calculations. Comparison with observed Raman intensities may then provide information on the electronic structure of the excited state. Altogether, vibrational resonances in the excited state become accessible to photometry. In contrast,

transient FSR measurements with β-carotene have all involved an excited-state absorption $S_x \leftarrow S_2$ for resonance, rendering a quantitative treatment practically impossible.

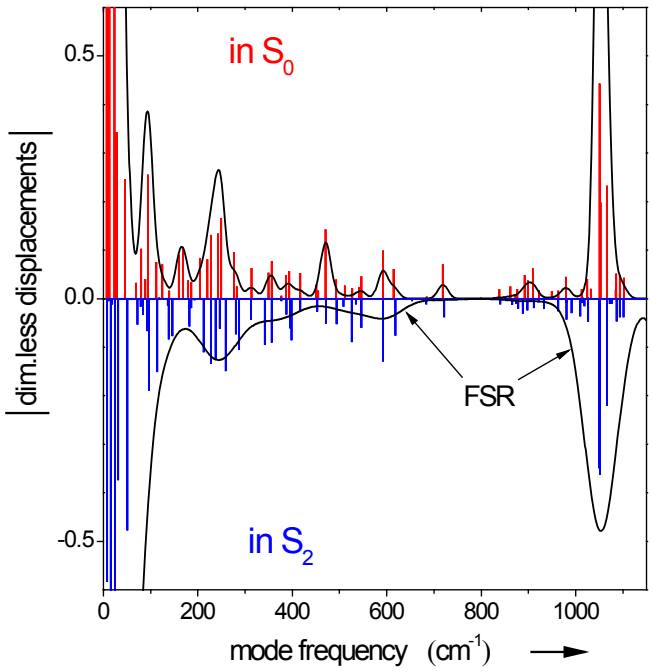

Figure 3. Displacement *vs* mode frequency (stick spectra, from (TD-)CAM-B3LYP/6-31G* calculations[21]; see SI) for an impression of spectral density up to the first intense band near 1000 cm^{-1}. A corresponding estimate of the vertical FSR spectrum is also shown. Thus in S_2, two or three relatively weak bands are expected between 150-700 cm^{-1}.

In this Letter we concentrate on the low-frequency range in the S_2 state. Modes in this range (**Fig. 3**) are important since they reflect large-amplitude, global motion of the polyene chain and thus depend on the environment. Frequencies measured by *transient* ($\chi^{(5)}$) and *vertical* ($\chi^{(3)}$) FSR agree, underlining the potential of the latter method. With vertical FSR, the intensities of vibrational resonances in S_2 are larger compared to S_0, implying strong anharmonicities/mode mixing in the excited state.

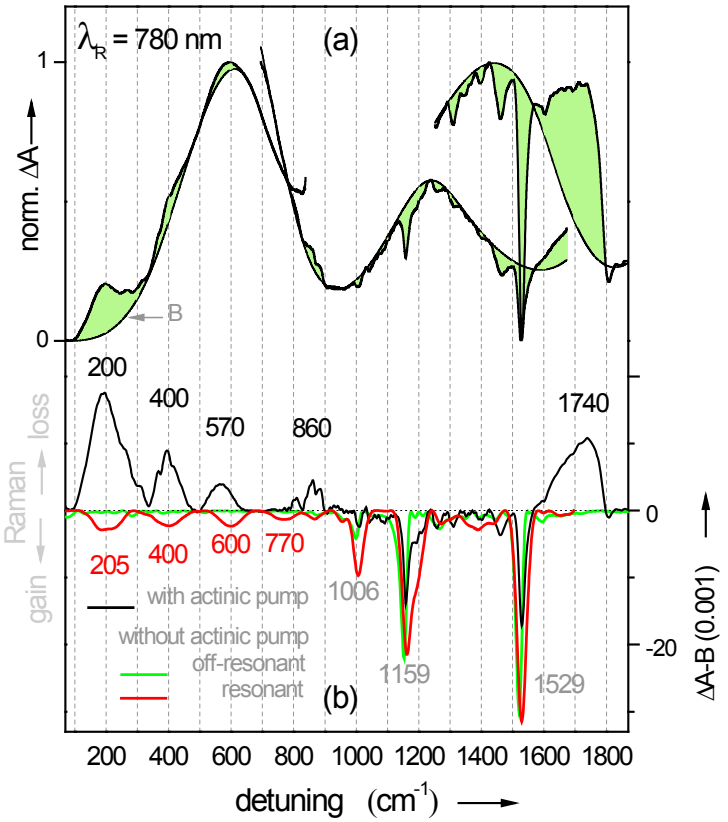

Figure 4. **(a)** Transient FSR spectrum (black lines: average over delays 180 – 250 fs and after subtraction of a spectrum for t<0) showing S_2 Raman activity and ground-state bleach with positive and negative sign, respectively. For its construction the anti-Stokes side was covered by three overlapping probe sub-windows. The contribution of resonances from S_1 is expected to be small because the Raman pump (λ_R =780 nm) is off-resonant with the $S_y \leftarrow S_1$ transition. Background (B) is due to population changes induced by the Raman pump, including two-photon excitation[22]. **(b)** A preview of vertical FSR spectra from **Fig. 5** (colored lines, recorded with λ_R =490 nm on the Stokes side) for comparison. Broad low-frequency modes from S_2 and resonance enhanced ground state Raman lines both have negative sign.

Results from transient FSR scattering after actinic excitation are shown in **Fig. 4** as black lines (ignore the colored lines for the moment). Optical pumping into S_2 was performed at 490 nm, and Raman excitation at 780 nm was resonant with the $S_x \leftarrow S_2$ transition. After a time delay, fs probe pulses were applied at the anti-Stokes side, stimulating the inverse Raman process[4,8]. In the upper panel ΔA is drawn against detuning ν. Here $\Delta A(\nu)$ is the difference between probe absorbance with the Raman pump pulse on or off, respectively. As the probe is tuned to several center frequencies, a set of spectral fragments is obtained. In the current, transient case the signal at negative delay has been subtracted. Simulations of vibrational resonances predict positive signal (Raman loss) for our conditions, as is detailed in the SI. Based on this expectation the resonances are identified by inspection, and a background B is constructed with splines. For every fragment the maximum of $\Delta A(\nu)$ is set to 1 and the minimum to 0 for the figure; therefore the amplitude of a vibrational line may differ between the fragments shown in the upper part. After background subtraction, then, a corresponding set of pure Raman spectra is obtained. By comparing intensities of lines in the overlap region between fragments, it is possible to construct a contiguous Raman spectrum from 50 to 1850 cm^{-1}. The result for a time average over 180-250 fs is is shown in the lower part as a solid black line. Five broad transient bands are detected at 200, 400, 570, 860 and 1740 cm^{-1}. Sharp negative lines between 900 and 1600 cm^{-1} correspond to bleach of S_0 bands and residuals from solvent signal.

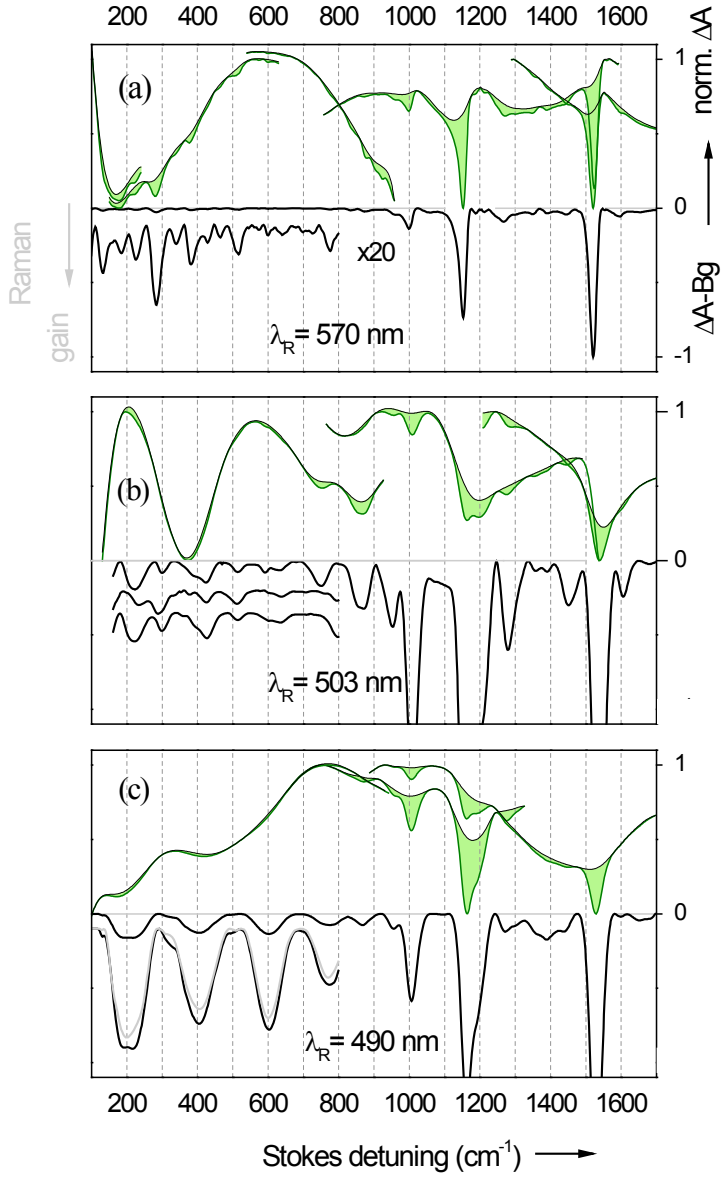

Figure 5. Vertical FSR spectra recorded – without actinic pumping – on the Stokes side of the Raman pulse. **(a)** Pre-resonant spectrum of S_0. **(b)** At the foot of the absorption band. Results from measurements with three different probe shapes are shown. **(c)** On resonance vibrational coherence in S_2 is also created. Corresponding Raman bands emerge in the low-frequency region, superimposed by resonance-enhanced Raman lines from S_0. The successive application of different filter functions discovers pure S_0 resonances (see **Fig. 6**) that sit on top of broad S_2 bands (the latter are shown as grey lines, see SI).

Results from vertical FSR spectra, *i.e.* without actinic excitation, are shown in **Fig. 5**. Of all pump wavelengths three examples are given: (**a**) pre-resonant with λ_R =570 nm, (**b**) starting on resonance with λ_R =503 nm and (**c**) on resonance with λ_R =490 nm. As before the probe was tuned to several positions, this time on the Stokes side. Let us treat the resonant case first. Here a broad induced absorption background, ranging over ~100 mOD, is caused by the Raman pump. By design the Raman pulse has been pumping the sample along $S_2 \leftarrow S_0$ for half of its ps duration by the time the fs probe arrives (for an improvement see ref. 16). On top of this background sharp negative (gain) lines are seen between 900 and 1600 cm^{-1}, which are also found when the Raman pump is non-resonant. In that case only diagram **Fig. 2b** should be operative and the narrow lines must be attributed to S_0; the prominent ones are located at 1006, 1159 and 1529 cm^{-1}. Inspection of all overlapping spectral fragments suggest that the Raman features in the low frequency region (<900 cm^{-1}) appear as negative bands, in agreement with simulations.

We separate Raman signal from background by the degree of curvature (for attempts to measure the background see refs. 17,18). The method applies when Raman gain (or loss) is expected exclusively. By purposely underestimating the Raman amplitude we ensure that it is not contaminated with electronic background. Each spectral fragment $S \equiv \Delta A(\nu)$ is smoothed with a filter function which is broader than the Raman signal, resulting in $\bar{S}(\nu)$. Raman gain is then approximated by all $R(\nu) = S(\nu) - \bar{S}(\nu)$ which are < 0, and by zero otherwise. A corresponding background is constructed as $B(\nu) = S(\nu) - R(\nu)$, whereby holes in $S(\nu)$ become partially filled. The procedure is repeated by substituting this $B(\nu)$ for $S(\nu)$, and so on, until convergence. Thus three broad (~90 cm^{-1} fwhm, compatible with ~70 cm^{-1} for lifetime broadening) gain bands are found at 200, 400, ~600 for all resonant excitations, as shown for example in **Fig. 5c**, in addition to the above-mentioned strong S_0

lines. More structure emerges in the low-frequency range when the filter function is narrowed. In **Fig. 5c** a separation of bands into narrow and broad components is indicated. As one moves gradually out of resonance, the narrow features become better visible. For λ_R=503 nm (**Fig. 5b**) we show results from three measurements for an impression of reproducibility. This is an important issue in FSR spectroscopy since very weak lines, in the range of 10-100 μOD, must be measured reliably on a background of about 100 mOD. In addition the diverse probe pulses may have very different spectral shapes. The only way that reliability can be demonstrated is by reproduction, as shown here. – The filter width for S_0 lines has been adjusted with the help of pre-resonant spectra.

In discussion, note first that resonant $\chi^{(3)}$ and transient $\chi^{(5)}$ Raman spectra show good agreement of band positions in the low-frequency part (lower panel in **Fig. 4**). Thus strong evidence exists that our $\chi^{(3)}$ signals reflect Raman bands in S_2.

With transient FSR we do not observe S_2 activity between 900 and 1600 cm^{-1}. Our result differs from a report by Mathies and coworkers[6] who performed transient FSR with similar Raman excitation, λ_R = 793 nm (see SI). Broad features were seen at 1100 and 1300 cm^{-1} (among others) and assigned to S_2 because of their kinetic signature. It should be mentioned that in our transient spectra all denoted S_2 bands are recognized directly, *i.e.* already before background subtraction. In this sense the upper panel of **Fig. 4** demonstrates the absence of such S_2 activity in our measurements with λ_R = 780 nm.

However when the Raman pump was tuned to the near-infrared fully into resonance with the $S_x \leftarrow S_2$ transition, Takaya & Iwata[8] indeed observed S_2 activity between 900 and 1600 cm^{-1} recently. These authors recorded transient stimulated Raman spectra, using λ_R=1190 nm, on the Stokes-side. Their choice of λ_R improves on ~800 nm for several

reasons (better resonance, reduced two-photon excitation, smaller ground-state contribution) and therefore the sensitivity is higher than ours. Within time resolution they saw 1050 cm^{-1} (CH_3 rock), 1240 cm^{-1} (C-C), and 1580 cm^{-1} (C=C) bands which were assigned to S_2 accordingly. A weak band at 1776 cm^{-1} is consistent with in-phase C=C stretching first in S_2, then in S_1. On the anti-Stokes side dispersive shapes were found at these positions, in agreement with expectations under the pertinent conditions. Unfortunately the low-frequency range was not studied. The group of Sakamoto[7] monitored spontaneous Raman instead and observed one weak band at 1550 cm^{-1} (160 cm^{-1} wide), which strongly resembles the 1580 cm^{-1} C=C stretching mode observed by Takaya & Iwata.

An important finding of the present work is obtained when the Raman intensity of low-frequency modes is compared in S_0 and in S_2, as measured (without actinic excitation) using the S_2–S_0 transition exclusively. Ground-state Raman lines < 900 cm^{-1} are shown enlarged in **Fig. 6** as λ_R is tuned into resonance. Relatively sharp S_0 lines at 230, 300, 430, 520 and 600 cm^{-1} appear for all λ_R and are therefore considered certain. We note here that low-frequency Raman activity of β-carotene has received little attention in the past. Inagaki *et al* [2] wrote that "no Raman line has been detected … in the region between 0 and 500 cm^{-1}". Siebert *et al* [3] showed a RR spectrum with very small lines at 300, around 430, at 520 and near 600 cm^{-1}, which is enlarged in our figure. Turning to S_2, the integrated intensity of its low-frequency bands (**Fig. 5c**) is consistently larger by a factor 3-10, compared to the S_0 bands from the same Raman excitation (**Fig. 6**). On resonance with an electronic two-level system, however, one expects about the same intensity.[19] The discrepancy may be due partly to uncertainties when bands are extracted from recorded spectra. But let us consider the consequences if the intensity difference is confirmed experimentally: it implies (see SI) that a nuclear wavepacket in S_2 is detected better than a wavepacket in S_0. Since no other electronic transition provides oscillator strength at our Raman frequencies, some FC factor

must favor detection in S_2. Inspection of a pertinent ladder diagram, **Fig. 2c**, shows that only the final interaction with the Raman pump field can make the difference. Its FC factor must have increased on the 10-100 fs time scale (compared to the initial situation in S_2) and therefore the effective mode displacement has increased substantially. This in turn implies strong anharmonicities and mixing of low-frequency modes in S_2. Our conclusion is in agreement with recent observations[20] on resonance excitation profiles (REP) and quantum-chemical predictions for modes > 900 cm^{-1} in β-carotene.[21]

In summary, low-frequency modes from S_2 were observed at 200, 400, ~600 cm^{-1} in β-carotene for the first time. They are seen as broad resonances in transient FSR spectra at earliest times. As an alternative, especially for short-lived (~200 fs) excited electronic states, vertical FSR provides access to vibrational modes in the FC state.

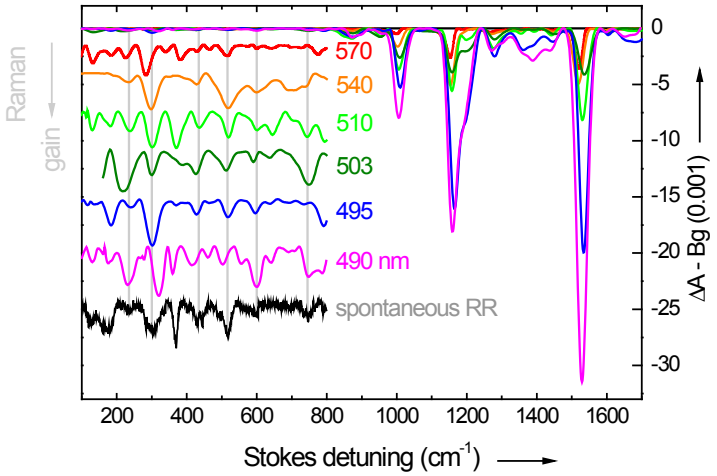

Figure 6. Ground-state signal in vertical FSR spectra. Shown is the structure which remains when broad features are removed from the spectra in the upper panels of **Fig. 4** (see text). By tuning the Raman pump into resonance with the $S_2 \leftarrow S_0$ transition, a general increase of intensities is observed. Peak positions at 230,

300, 430, 520 and 600 cm^{-1} are reproduced (structure shown magnified by a factor 18 or 28 on or off resonance, respectively). The spontaneous Raman spectrum in the low frequency region (black) was obtained from Siebert *et.al* [3].

ASSOCIATED CONTENT

Supporting Information.

Experimental and computational details and further spectroscopic data. This material is available free of charge via the Internet at http://pubs.acs.org.

AUTHOR INFORMATION

Corresponding Author

*Email: nernst@chemie.hu-berlin.de

*Voice/Fax: +49-30-2093 5551/3

ACKNOWLEDGMENT

We thank S. Banerjee, D. Kröner and P. Saalfrank (U Potsdam) for the quantum-chemical calculations, furthermore T. Siebert and W. Kiefer (U Würzburg) for a stationary RR spectrum and critical reading of the manuscript. M.Q. acknowledges partial support through ERC grant No. 259432. This work was supported by the Deutsche Forschungsgemeinschaft (ER 154/10-3).

REFERENCES

(1) Polivka, T.; Sundström, V. Dark Excited States of Carotenoids: Consensus and Controversy. *Chem*. *Phys*. *Lett*. **2009**, *477*, 1-11.

(2) Inagaki, F.; Tasumi, M.; Miyazawa, T. Vibrational Analysis of Polyene Chains: Assignment of the Resonance Raman Lines of Poly(Acetylene) and β-Carotene. *J*. *Raman*. *Spectrosc*. **1975**, *3*, 335-343.

(3) Siebert, T.; Maksimenka, R.; Materny, A.; Engel, V.; Kiefer, W.; Schmitt, M. The Role of Specific Normal Modes during Non-Born-Oppenheimer Dynamics: the S_1-S_0 Internal Conversion of β-Carotene Interrogated on a Femtosecond Time-Scale with Coherent Anti-Stokes Raman Scattering. *J*. *Raman*. *Spectrosc*. **2002**, *33*, 844-854.

(4) Yoshizawa, M.; Aoki, H.; Hashimoto, H. Vibrational Relaxation of the $2A_g^-$ Excited State in all-*trans*-β-carotene Obtained by Femtosecond Time-Resolved Raman Spectroscopy. *Phys*. *Rev*. *B* **2001**, *63*, 180301.

(5) McCamant, D. W.; Kukura, P.; Mathies, R. A. Femtosecond Time-Resolved Stimulated Raman Spectroscopy: Application to the Ultrafast Internal Conversion in β-Carotene. *J*. *Phys*. *Chem*. *A*. **2003**, *107*, 8208-8214.

(6) Kukura, P.; McCamant, D. W.; Mathies, R. A. Femtosecond Time-Resolved Stimulated Raman Spectroscopy of the S_2 ($1B_u^+$) Excited State of β-Carotene. *J*. *Phys*. *Chem*. *A* **2004**, *108*, 5921-5925.

(7) Sakamoto, A.; Matsuno, S.; Tasumi, M. Picosecond Near-Infrared Excited Transient Raman Spectra of β-Carotene in the Excited S_2 State: Solvent Effects

on the In-Phase C=C Stretching Band and Vibronic Coupling. *J. Mol. Struct.* **2010**, *976*, 310-313.

(8) Takaya, T.; Iwata, K. Relaxation Mechanism of β-Carotene from S_2 ($1B_u^+$) State to S_1 ($2A_g^-$) State: Femtosecond Time-Resolved Near-IR Absorption and Stimulated Resonance Raman Studies in 900-1550 nm Region. *J. Phys. Chem.* A **2014**, *118*, 4071-4078.

(9) Kraack, J. P.; Wand, A.; Buckup, T.; Motzkus, M.; Ruhman, S. Mapping Multidimensional Excited State Dynamics using Pump-Impulsive-Vibrational-Spectroscopy and Pump-Degenerate-Four-Wave-Mixing. *Phys. Chem. Chem. Phys.* **2013**, *15*, 14487-14501.

(10) Liebel, M.; Schnedermann, C.; Kukura. P. Vibrationally Coherent Crossing and Coupling of Electronic States during Internal Conversion in β-Carotene. *Phys. Rev. Lett.* **2014**, *112*, 198302.

(11) Prior, Y.; Bogdan, A. R.; Dagenais, M.; Bloembergen, N. Pressure-Induced Extra Resonances in Four-Wave Mixing. *Phys. Rev. Lett.* **1981**, *46*, 111-114.

(12) Andrews, J. R.; Hochstrasser, R. M. Thermally Induced Excited-State Coherent Raman Spectra of Solids, *Chem. Phys. Lett.* **1981**, 82, 381-385.

(13) Mukamel, S. Stochastic Theory of Resonance Raman Line Shapes of Polyatomic Molecules in condensed Phases. *J. Chem. Phys.* **1985**, *82*, 5398-5408.

(14) Quick, M.; Dobryakov, A. L.; Gerecke, M.; Richter, C.; Berndt, F.; Ioffe, I. N.; Granovsky, A. A.; Mahrwald, R.; Ernsting, N. P.; Kovalenko, S. A. Photoisomerization Dynamics and Pathways of *trans*- and *cis*-Azobenzene in

Solution from Broadband Femtosecond Spectroscopies and Calculations. *J. Phys. Chem. B*. **2014**, *118*, 8756-8771.

(15) Dobryakov, A. L.; Quick, M.; Ioffe, I. N.; Granovsky, A. A.; Ernsting, N.P. Excited-State Raman Spectroscopy with and without Actinic Excitation: S_1 Raman Spectra of *trans*-Azobenzene. *J. Chem. Phys*. **2014**, *140*, 184310.

(16) Hoffmann, D. P.; Valley, D.; Ellis, S. R.; Creelman. M.; Mathies, R. A. Optimally Shaped Narrowband Picosecond Pulses for Femtosecond Stimulated Raman Spectroscopy. *Optics Express* **2013**, *21*, 21685-21692.

(17) Weigel, A.; Dobryakov, A.; Klaumünzer, B.; Sajadi, M.; Saalfrank, P.; Ernsting, N. P. Femtosecond Stimulated Raman Spectroscopy of Flavin after Optical Excitation. *J. Phys. Chem. B* **2011**, *115*, 3656-3680.

(18) Kloz, M.; van Grondelle, R.; Kennis, J. T. M. Wavelength-Modulated Femtosecond Stimulated Raman Spectroscopy – Approach towards Automatic Data Processing. *Phys. Chem. Chem. Phys.* **2011**, *13*, 18123-18133.

(19) Albrecht, A. C. On the Theory of Raman Intensities. *J. Chem. Phys*. **1961**, *34*, 1476-1484.

(20) Tschirner, N.; Schenderlein, M.; Brose, K.; Schlodder, E.; Mroginski, M. A.; Thomsen, C., Hildebrandt, P.; Resonance Raman Spectra of β-Carotene in Solution and in Photosystems Revisited: an Experimenal and Theoretical Study. *Phys. Chem. Chem. Phys.* **2009**, *11*, 11471-11478.

(21) Banerjee, S.; Kröner, D.; Saalfrank, P. Resonance Raman and Vibronic Absorption Spectra with Duschinsky Rotation from a Time-Dependent Perspective: Application to β-Carotene. *J. Chem. Phys.* **2012**, *137*, 22A534.

(22) Buckup, T.; Weigel, A.; Hauer, J.; Motzkus, M. Ultrafast Multiphoton Transient Absorption of β-Carotene. *Chem. Phys.* **2010**, *373*, 38-44.

5 Comprehensive Discussion - New Results with TA, FLUPS and FSR Spectroscopy

In this section the new findings on riboflavin and β-carotene will be outlined and discussed in context with the determining factors that enabled their detection.

5.1 Riboflavin in aqueous solution

The first publication addresses the pH-dependent behavior of riboflavin in aqueous solution which was studied with absorption- and fluorescence spectroscopies. Here the center of attention lies on the lower pH range, below 3. In previous works it was already reported that oxidized riboflavin (or similar molecules, like FMN) in the electronic ground-state exists in three states of protonation that are called protonated-, neutral- and deprotonated riboflavin. As the pH value drops below 0 the protonated form of riboflavin becomes the dominant form. Here the protonation site is at N(1). Studies that are performed with stationary and transient fluorescence suggest that excited-state proton-transfer (ESPT) from the solvent to the chromophore occurs and that this process is accelerated with increasing acidity of the solvent. From calculations it became generally clear that ESPT takes place on N(5) even though no experimental evidence existed. Until then, transient measurements of the emission were restricted to the detection at single wavelengths, usually where the fluorescence spectrum of neutral riboflavin has its maximum. A weak emission band around 660 nm in the stationary fluorescence spectrum was previously attributed to protonated riboflavin in the electronic ground-state and not considered any further. However, two aspects oppose this assignment: First, the energetic difference between the supposed 0-0-transitions for absorption and emission is too large for a Stokes shift (~ 10000 cm^{-1}). Second, the intensity profile of this emission-band does not follow the pH dependent mole-fraction of the protonated riboflavin in the ground-state. Instead, it appears on the same pH scale as riboflavin becomes protonated via ESPT and disappears in accordance with the decreasing mole fraction of neutral riboflavin around pH 0. This result already suggests that the red emission-band originates from the neutral riboflavin but protonated in the excited state. To confirm this assumption the ESPT must be monitored with broad-band time-resolved fluorescence spectroscopy. So far, no such transient spectra existed for flavins in acidic solution and the reason for that might be the following. Because the relation between the red emission band and ESPT has never been noticed in previous work there was hitherto no necessity to record transient fluorescence spectra over a broad spectral range.

In the first publication the ESPT is monitored in a range from 400 to 800 nm (> 10000 cm^{-1}). The non-linear medium in which the NIR pulse gates the fluorescence light is a BBO-crystal [1]. For a fixed geometry the spectral acceptance for type II phase matching in BBO is narrow, which is why a range of ~10000 cm^{-1} cannot be up-converted efficiently. To circumvent this disadvantage the collection optics in combination with a calcite prism allow the two spectral ends of the fluorescence cone to vary by ~5° relative to the gate beam which is sufficient to

create efficient phase matching in the range 400 – 800 nm. Before that our FLUPS setup was operated with KDP where the up-conversion efficiency is flat for one wavelength over a wide angular span but 10-times smaller. In a first attempt to measure transient fluorescence of riboflavin in sulfuric acid at pH 0 the earlier setup was used. As a result the fluorescence decay of the neutral form around 530 nm was observed (Fig. 2, left) but no rise of emission in the region around 660 nm could be detected. The S/N ratio was quite enough for fluorescence around 530 nm because the solubility of riboflavin is sufficiently high at low pH values. But still, scattering of the second harmonic of the gate pulse and fluorescence light that has not been up-converted disturb the spectral window >600 nm and prevented us from detecting weak signals. The experiment was repeated under similar conditions but with BBO as non-linear medium in the FLUPS setup (Fig. 2, right). Now with the advantage of larger up-conversion efficiency the S/N ratio increases even as the number of averaged spectra stays the same. The influence of scattered light to the spectra is therefore minimized and allows observing the red emission band of the protonated riboflavin via ESPT.

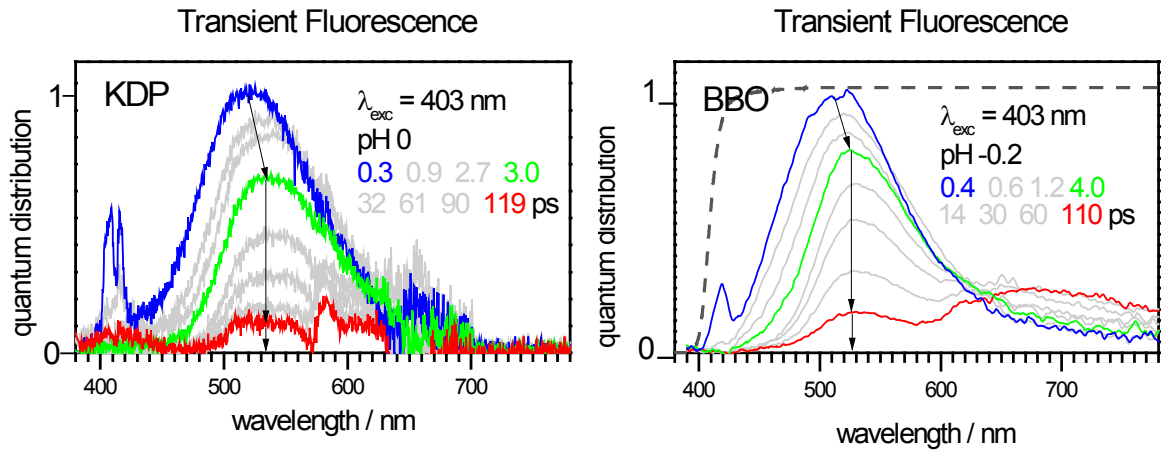

Figure 2: Transient fluorescence spectra of riboflavin in acidic solution (pH ~ 0). The experiment is performed with KDP (left) and BBO (right) as non-linear medium for up-conversion, respectively.

Transient absorption and –broad-band-fluorescence up-conversion spectra are measured for riboflavin in solution at several pH-values, ranging from 0 to -1. At early time a SE-band is seen with negative sign around 570 nm which corresponds to the fluorescence band of neutral riboflavin, seen around 530 nm in the FLUPS spectra. With a time-constant of 47 ps a broad ESA-band develops in the same region and covers the spectral for larger wavelengths completely. In principle, based on this observation in the transient absorption spectra it cannot be concluded that the rise of ESA is accompanied by the decay of SE because both bands overlap. Also there is no evidence for stimulated emission in the region

>600 nm since no negative optical density can be observed. The importance of broad-band transient fluorescence as a complementary method to transient absorption is shown right in this case. The monitored fluorescence decay with 65.1 ps in FLUPS proofs that stimulated emission in transient absorption decays simultaneously as ESA appears. Beside the technical challenge to monitor the fluorescence in the red spectrum, it also illustrates that the absence of band-shape in absorption does not proof its non-existence.

This example addresses two further aspects. The first aspect is the large potential that is inherent in stationary measurements. In previous studies that concern the pH-dependency of riboflavin the red emission-band was either overlooked due to noisy data or misinterpreted. As it was thoroughly characterized via stationary spectroscopy, the next logical step is to measure transient fluorescence via broad-band techniques. If the behavior of this red emission band had been recognized earlier, then more groups would have made attempts to establish FLUPS for broad-band imaging in their laboratories. That connects to the second aspect. Not only is the construction of a setup the result of further examination of a system but also its development and improvement. In our case, when a fixed geometry is used, then KDP was considered as standard among all non-linear media due to its larger spectral acceptance for phase-matching. The insufficient up-conversion efficiency and undesired scattering led to improvements in the FLUPS scheme as outlined above. Alternatively, one might assume that other groups would have reached the same point and similar improvements were considered. After all, riboflavin (and basically all fundamental chromophores) in its importance as a research object provides an excellent motivation to widespread spectroscopic schemes and to accelerate creative improvements for already existing setups.

5.2 β-carotene in hexane

5.2.1 Results from Transient Absorption

β-carotene in hexane is examined with femtosecond transient absorption and stimulated Raman spectroscopy. The new result which is obtained with transient absorption will be discussed first. As outlined in the introduction, β-carotene is a well characterized molecule and has been studied in various disciplines. Results that have been established with TA over the years, such as ESA bands and time-constants, are reproduced here. However the use of four exponential time-functions is apparently not enough to fit the absorption data globally as can be seen in the systematical fluctuations of the residuals (see Fig. 4 in publication 2). Even the visual impression of superimposed time-traces and fits without the residual already suggests the application of at least one further time-function. A stretched exponential time-function is used to describe the initial non-exponential behavior in the spectrum. From the respective DAS it appears that ~20 % of the population reaches the ground-state with some delay. This amount propagates to a different manifold of the PES in S_1 (representing a different conformational isomer) from where relaxation to S_0 occurs. The

remaining 80 % return to the electronic ground-state with $\tau = 6.9$ ps. These fluctuations from the global fit, however, are not mentioned in previous publications even though they appear to be quite significant. Two reasons can be quoted for the discovery of the additional non-exponential kinetics. The first reason is the decreased noise in the time-traces due to the use of a reference spectrograph in addition to the signal spectrograph. The generated super-continuum is split in half whereby 50 % enters the sample cell and the rest is dispersed in the reference spectrograph. Advantageous is that the recorded spectrum on the signal site is corrected for the spectral shape of the probe at each shot. Thereby spectral contamination due to different probe shapes is avoided when a transient absorption spectrum is calculated (pump on – pump off). As a consequence the quality of the spectra and the S/N ratio both increase. The second reason is the aforementioned calculation of the residual from the global analysis which can be used to estimate the quality of the fit. In previous work about β-carotene no such residuals are shown for the fits. Unfortunately, this makes the critical assessment of illustrated data rather difficult because possibly unusual behavior cannot be recognized by others. As a consequence, new research channels that could be opened by that keep being closed.

5.2.2 Results from Femtosecond Stimulated Raman Spectroscopy

Femtosecond stimulated Raman (FSR) spectroscopy is a comparably new spectroscopic technique to probe vibrational modes in the ground- and in the excited state. Nonetheless, β-carotene is one of the most studied chromophores due to its properties as an effective Raman scatterer and its well separated ESA bands. The focus is thereby set on the stretching modes that are mainly located in the polyene-chain which determines the electronic properties of the chromophore. The new findings with FSR spectroscopy are listed below and then discussed successively.

- Low frequency modes in S_2 at 200, 400 and ~600 cm^{-1}
- The symmetric C=C stretching mode in S_1 at 1800 cm^{-1} also exists in S_2 around 1770 cm^{-1}
- Non-exponential behavior in the kinetic of TA is also visible in bleach-bands of ground-state modes
- Solvent lines do not vanish after subtraction of an averaged Raman spectrum from negative delay times

The reason why these broad bands from S_2 in the region <700 cm^{-1} (see publication 2 and 3) have not been observed earlier cannot be explained with certainty. In principle, the number of publications in which these bands could have been reported is limited to those that use NIR pulses for Raman excitation (see refs.2-5). Only in these cases, signal enhancement is provided through electronic resonance with the $S_x \leftarrow S_2$ transition. The illustrated spectra within refer to the region above 900 cm^{-1} although their choice of Raman pump and –probe

enables the monitoring of vibrational bands even below (except for ref. 2,3). Because there is no obvious reason, it can only be speculated that the low-frequency range was simply of no interest since associated modes are rather insignificant compared to the local C=C- and C-C stretching modes having frequencies above. However many groups report on S_2 signals in the region between 900 and 1600 cm^{-1} which are partly at variance with each other. The reason is that broad signals from S_2 (FWHM ~ 100 cm^{-1}) were mistaken for electronic background and vice versa. Because the life-time of S_2 is short (τ ~ 200 fs) much less than the full vibrational dephasing-time (τ ~1 ps) is provided for the inherent Fourier transformation of the induced polarization and the respective signals appear broadened. To be confident with our result the vibrational modes of S_2 were also probed with a complementary method: FSR without preceding actinic pump. In this approach vibrational coherence is created in S_2 while population is still located in the electronic ground-state. It is necessary that the energy of the Raman pump matches the $S_2 \leftarrow S_0$ transition; otherwise the resonance enhancement is too weak to create sufficient polarization within the chromophore. The technical requirements on such an experiment are both a tunable Raman pump and –probe. In various experiments the Raman wavelength assumes values that range from off- to on-resonance with the ground-state absorption. While in the off-resonance case only signals from S_0 show up, Raman bands from modes in S_2 emerge as the pump is tuned into the stationary absorption spectrum (see Fig. 5 in publication 3). A comparison between the results from conventional FSR and Resonance Raman (RR) spectroscopy shows good agreement in the spectral positions for the low-frequency signals and the identification as vibrational bands is ensured (see Fig. 4 in publication 3). Not only us but also other groups that study β-carotene have realized the technical implementation of a tunable Raman pump [6]. However the practical usage of Resonance Raman spectroscopy to probe excited state modes is currently restricted to the frequency range below 1000 cm^{-1}. As the Raman pump and -probe are tuned into the lowest vibronic transition of β-carotene they simultaneously overlap with the stimulated emission band. In principle, to probe high frequency modes the Raman energy must be increased but two aspects prevent from signal acquisition. First, the NOPA stages at which the Raman pump is generated and amplified have finite spectral and angular acceptance conditions so that tunability is feasible only in the range between 470 and 690 nm. For β-carotene the optimal Raman wavelength for generating S_2 signals < 1000 cm^{-1} via RR spectroscopy is found to be ~ 490 nm. However, modes with frequencies above need Raman excitation with a smaller wavelength than 470 nm. Second, even if appropriate Raman excitation was accessible the $S_2 \rightarrow S_0$ transition does no longer contribute to the generation of polarization because the Raman pump is tuned away from the emission band. Instead, resonance with higher transitions from S_2 is required or else insufficient polarization prevent from observing Raman signals.

Nonetheless, the general procedure to further confirm an observation with advanced spectroscopic techniques is similar to the case of riboflavin. There, a detailed analysis with stationary spectroscopies suggests a new finding, the assignment of the emission around

660 nm to ESPT. To confirm this assumption the established FLUPS setup was used in a more advanced constitution; by replacing KDP with BBO while adapting the collection optics. In a similar process the authenticity of low frequency modes in β-carotene is secured. A record of the full spectral window (80 – 2000 cm^{-1}) with FSR spectroscopy shows three broad signals at 200, 400 and ~600 cm^{-1}. To prevent ambiguity in assignment of signals the applicability of this vibrational technique was extended by RR as a complementary method to probe modes in the excited state. The aforementioned potential of RR has probably not been recognized earlier because the low frequency part was for β-carotene of no particular interest. Otherwise the demand for complementary methods to identify uncertain bands would have led to earlier efforts in implementing comparable techniques.

Another broad band is observed around 1770 cm^{-1} and assigned to S_2 due to its kinetic signature. Its assignment as symmetric C=C stretching mode follows a comparison with a similarly upshifted Raman line around 1800 cm^{-1} that has been attributed to the same mode but in S_1. The large upshift compared to the asymmetric C=C stretching mode <1600 cm^{-1} is explained by vibronic coupling between S_1 and S_0 through this mode. A consistent view was established in several previous publications in which β-carotene was studied with vibrational techniques: The signal for the symmetric C=C stretching mode in S_1 appears with τ ~ 200 fs and shifts up to ~ 1800 cm^{-1} while rising within 2 ps. No reports exist about a preceding Raman signal from S_2 even though its attendance is actually conspicuous already in spectra that have not been corrected for the electronic background yet (Fig. 3). Shown are the first 510 fs of evolution in the FSR spectrum in 102 fs steps for λ_{Raman} = 621 (left panel) and 776 nm (right panel).

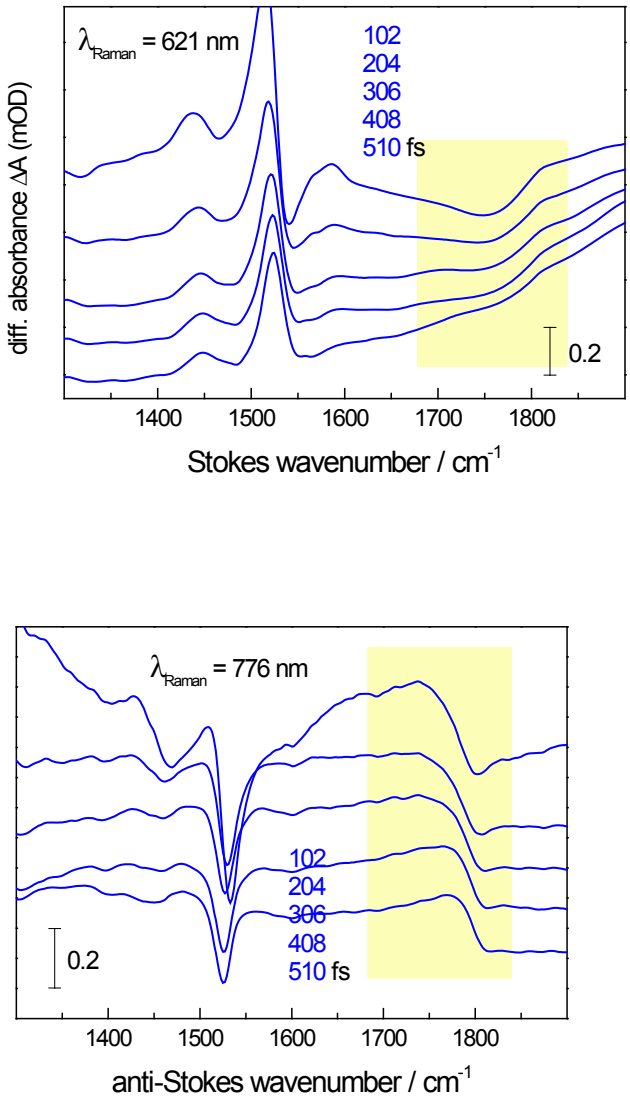

Figure 3: Early transient Raman spectra recorded with 621 and 776 nm Raman excitation. An averaged spectrum from negative delay times was subtracted from the data. The yellow area marks the position of the S_2 band from the symmetric C=C stretching mode.

The FSR spectra that are measured with 776 nm Raman excitation were recorded on the anti-Stokes side. Vibrational signals from the excited state appear with positive sign when plotted against differential absorbance. In principle, with our current setup modes from S_2 are best monitored with this Raman wavelength because resonance enhancement can be exploited from the $S_x \leftarrow S_2$ transition which is located around 990 nm. On the other hand the early broad S_2 band (with negative sign on the Stokes side) is also well observable in the FSR spectra that were recorded with pre-resonant λ_{Raman} = 621 nm. Beside its isolated position in the spectrum the good visibility of this band can be explained by the smooth and temporally unaltered progression of the electronic background within the first 510 fs. The

interactions of the incident Raman pump and –probe with the chromophore result in a coherent (Raman signal) and a sequential (electronic signal) part, respectively that both contribute to the FSR spectra. Because the TA spectrum around 621 nm is weak, flat and does not show significant changes within the first picosecond the sequential contribution does not mask broad bands by a curvy background. Indeed, the spectrum at 102 fs for the resonant case (right panel) does not lead to a conclusive distinction of electronic background and Raman signal. Instead, looking over the same time-delay in the left panel makes a clear identification of the broad S_2 band around 1770 cm^{-1} possible. When the Raman-pump in previous work was in spectral overlap with the fast decaying ESA of the bright $S_x \leftarrow S_2$ transition then the sequential contribution contributes with an equally fast and intense electronic background that impedes the recognition of broad Raman bands.

Another finding is related to the non-exponential kinetics which is found in the time-traces of TA. Since, after excitation, ~20 % of the population returns to the electronic ground-state with delay, the same non-exponential behavior must be observable for bleach signals in the Raman spectrum. To separate bleach that recovers with delay from the amount of bleach that decays exponentially, the latter must be subtracted for all time delays. The respective procedure is illustrated in Fig. 4 for λ_{Raman} = 573 and 776 nm and the following outline refers to both cases (panels a and b). A global fit with just one exponential time-function is carried out from 5 ps onwards; by starting here the residual from the fit no longer deviates systematically from zero. The corresponding DAS (blue line in either panel) contains both, Raman signal from S_1 and from bleach. Because bleach is the result of missing population in S_0, the respective signal pattern can be constructed from the stationary Raman spectrum of the solute, adjusted with a factor to be optimized. The red line shows the scaled stationary solute spectrum having the optimal factor, *i.e.* when the corresponding bleach is no longer recognized directly. After subtraction the green line is obtained; it is shown on the same ordinate scale (with the help of an offset). However this spectrum still contains a vibrational pattern from the solvent (this phenomenon is described in the second publication) which must be removed in the same way, this time by using a scaled stationary spectrum of pure n-hexane (dark grey line on the same vertical scale, also offset). When the solvent signal is removed as well, then the black line is obtained in which Raman bands from S_1 may now be located (arrows). Finally the sum of the two scaled stationary spectra (of β-carotene and *n*-hexane) is multiplied with the original single-exponential time function (τ~9 ps). The resulting matrix, representing our bleach model, is subtracted from the raw recorded FSR data $\Delta A(t,\lambda)$. In **Fig. 4a** we also show the effect of using inappropriate scaling factors for the solute.

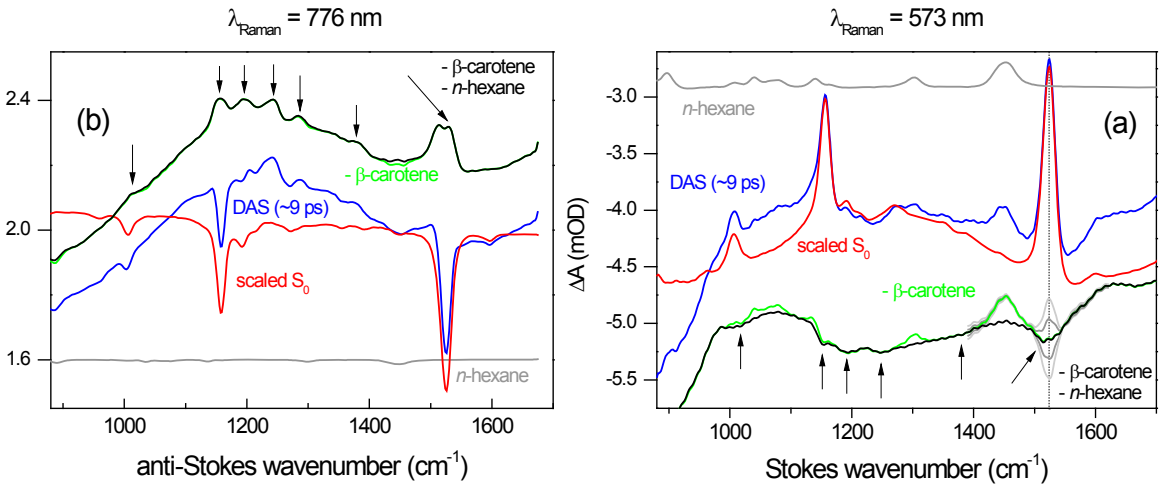

Figure 4: A bleach spectrum is constructed from scaled S_0 spectra, see text above.

A time-varying electronic background BG(t) is subtracted in two steps. In a first step, background is removed on a coarse wavelength scale. For this purpose we start from a fit of $\Delta A(t,\lambda)$ with several exponential time-functions. The DAS are splined, setting a few points by inspection so that the background is roughly described. The resulting spectral interpolation functions are multiplied with the corresponding exponential time functions and are so extended to all t>0. Thus, a matrix representing the coarse background is obtained and subtracted from the bleach-corrected FSR data. In a second step, background remaining on a finer wavelength scale is also removed. The time evolution is viewed and spline points are placed between the Raman bands or –shapes, to be kept for all times. For every time t, then, the interpolated spectral background function is subtracted. **Fig. 5** show some spectra from measurements with $\lambda_R = 573$ nm (colored lines) together with the sum of (coarse and fine) spline function (grey lines).

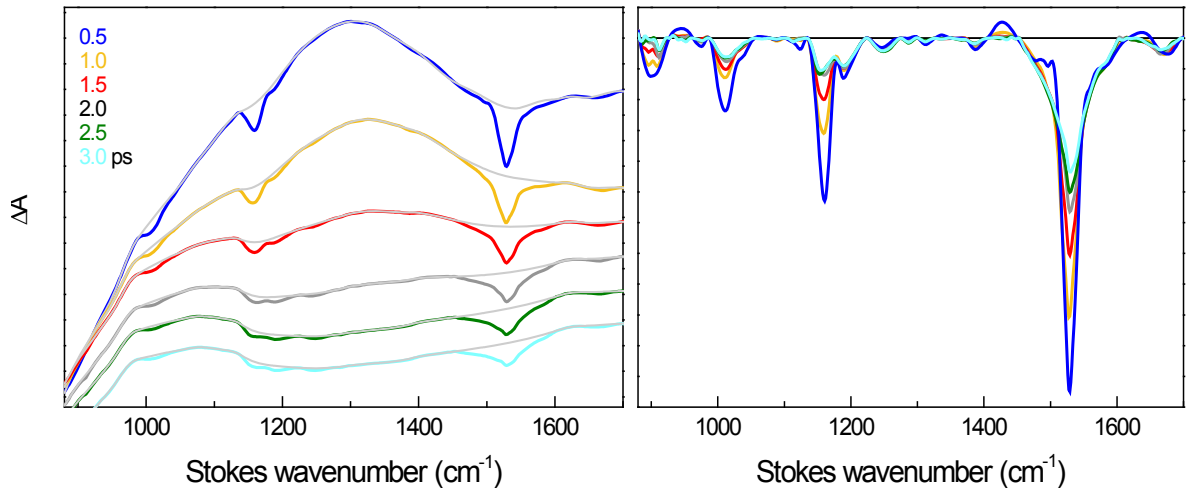

Figure 5: FSR spectra after subtraction of bleach are further corrected by their electronic background (BG, left panel). Spline-functions are used to approximate the BG (gray lines). After subtraction, excited-state Raman spectra are obtained.

As can be seen in **Fig. 5** (right panel) a fast decay proceeds on a 2 – 3 ps time-scale. We conclude that these evolving Raman signals do not originate from S_1 but reflect the non-exponential recovery of ground-state population. This conclusion is best comprehended with the help of the kinetic trace at 1524 cm^{-1} (**Fig. 6)** where the Raman bands from the C=C stretch mode in S_0 (positive bleach) and S_1 (negative) overlap. For this purpose the FSR spectra have been corrected for electronic background only, whereas the bleach is still visible in the figure (in fact it dominates the trace, which is therefore positive throughout). But contrary to expectation from bleach recovery, the amplitude appears to be constant at first, from 0.5 to 3 ps (before 0.5 ps there is evolution due to decay of dispersive signal), and only then the amplitude decays exponentially with ~9 ps (grey line). Clearly this late decay reflects bleach recovery. Subtraction with one exponential time-function is might be expected to leave evolution of signal amplitude from S_1. However, since we must observe here the same bleach behavior as in TA (non-exponential and exponential), it follows that the initial constant amplitude in the FSR trace in **Fig. 6** belongs to the non-exponential part of bleach recovery. This means if only the exponential part is subtracted, then the early part will be over-estimated: it looks like S_1 signal, but it really reflects the spectral evolution of bleach (with negative sign, yellow area) evolving within 1 – 3 ps. This picture is equivalent to **Fig. 4 c** and **c'** in publication 2.

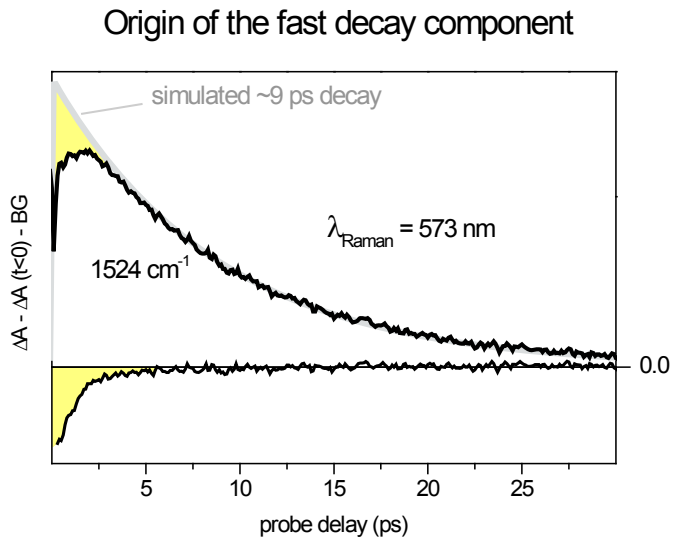

Figure 6: The early decay is shown for the band at 1524 cm^{-1} which (due to its construction) reflects predominantly the lack of population in S_0. The black line represents the band amplitude in the background-corrected spectra; see text.

The observation of non-exponential ground-state recovery is possible due to the subtraction of a time-dependent bleach model matrix from the original data set. Usually the stationary spectra of both, the chromophore and/or solvent are removed from all spectra individually [2,3,6]. In this way no attention is paid to the temporal evolution of bleach, and odd behavior might be overlooked. The point-wise subtraction by hand has one additional disadvantage: because it is very time-consuming only relatively few spectra can be evaluated in this way; typically between 20 and 30. As a consequence the obtained temporal information from only few spectra is less significant and carries a larger error. The construction and application of a bleach model matrix allows the use of the full data set for evaluation; typically several hundred spectra.

Solvent-lines from hexane do not disappear for t>0 when an averaged Raman spectrum from negative delay times is subtracted. They are supposed to be enhanced by β-carotene due to the molecular near-field effect. When an averaged spectrum from negative delay times is subtracted from the data then two kinds of solvent bands can be observed for t>0: the solvent signals appear with dispersive band-shape when population is in S_2 and transform into fully positive or negative lines (depending on whether the spectrum is recorded on the Stokes or anti-Stokes side) after IC to S_1. They are apparent in basically all FSR measurements independent from the Raman excitation. The reasons why these enhanced solvent lines were not recognized earlier can only be speculated. As mentioned above, the ground-state contribution is removed from the spectra one by one without a precedent subtraction of an averaged spectrum from negative delay times [2,3,6]. In doing so, the decreased intensity of the solvent signal upon populated S_1 in β-carotene will not be recognized but simply removed with a scaled stationary spectrum of the solvent (scaling factor < 1). The oversight of the early dispersive solvent signal might be explained with a historical overview about FSR studies of β-carotene in solution. But as a preliminary point it has to be mentioned that the dispersive band-shapes indeed appear to be significant once they are recognized. But nonetheless no one explicitly began to search for this corresponding small effect because no such behavior was expected from the solvent. In the earliest work about FSR spectroscopy on β-carotene Yoshizawa *et al.* used 794 nm Raman excitation [4]. Shown are spectra at -5, 0.2, 0.6 and 2 ps which are normalized to the Raman signal of benzene at 991 cm^{-1} without subtracting the solvent afterwards. Because the molecular near-field effect only acts on few benzene molecules nearby their dispersive contribution to the solvent signal is largely superimposed by the regular Raman signal from the overwhelming rest. The group of McCamant reports on β-carotene in cyclohexane which was measured with a 793 nm Raman-pump [2]. The early spectra up to 400 fs are crossed by a ripple structure due to a pump induced interference artifact. It is therefore impossible to recognize any signature of small dispersive solvent signals. Spectra were recorded under similar conditions by Kukura and coworkers but no strong interference patter show up this time [3]. The main difference, however, is the 30 times smaller concentration (9 µM against 270 µM) of the solution which might be too low to make the molecular near-field effect

visible. Shim *et al.* show transient spectra which were recorded with 560 and 590 nm Raman excitation, respectively [6]. For the former case spectra are shown up to 500 fs but no sign of dispersive signal from cyclohexane are observable. Instead a strong contribution from ground-state coherences, enhanced by the resonant Raman wavelength, superimposes possibly present dispersive band-shapes. The solvent signal around 800 cm^{-1} would have been a more appropriate mode in cyclohexane to observe since it is more intense and isolated, but the low frequency border of the spectrum shown is 900 cm^{-1}. Spectra for λ_{Raman} = 590 nm are shown not for delay times before one picosecond because the focus lays on Raman lines from vibrationally excited ground-state. The discovery of the electronic interaction between chromophore and solvent is basically accounted for the subtraction of negative delay from the complete data set, hereby ranging from 80 to 2000 cm^{-1}. In this way all consequences that the absorption of a photon implies are observable; that applies to the vibrational and electronic level, respectively. The subsequent treatment of these spectra depends on how all the elements within are comprehended. Bleach is easily recognized because it matches the stationary spectrum and it can be removed globally as explained above. Signals that are generated in the excited state of the chromophore should be identified by their sign and band-shape. In β-carotene signals from S_2 and S_1 are either fully positive or negative, depending on whether they are recorded on the Stokes- or anti-Stokes side, respectively. Dispersive signals appear when β-carotene is populated in S_2. Their central frequencies match the spectral positions of ground-state lines which is why the assignment to modes in S_0 is conclusive. All remaining early signals also have dispersive band-shapes but they cannot be attributed to the chromophore. Instead a comparison with the stationary spectrum of the solvent explains their origin. To finally model the electronic background with interpolation-functions requires full knowledge about position and band-shape of all present signals (from the chromophore and solvent). The splining-points have to be set in such a way that the spline is smooth and no signal is disturbed.

6 Zusammenfassung

Die Kombination aus Breit-Band Spektroskopie-Methoden auf hohem Niveau ermöglicht eine umfassende Einsicht in das elektronische System von Molekülen im angeregten Zustand. Hierbei ist transiente Absorptions-Spektroskopie die am weitesten verbreitete Methode. Mit ihr kann beobachtet werden wie sich Population zwischen elektronischen Zuständen bewegt und wann die Rückkehr in den elektronischen Grundzustand erfolgt. Trotz der Unkompliziertheit der Methode und der Übersicht, die sie liefert, wohnen ihr jedoch zwei Nachteile inne: Zum Einen besteht das Spektrum aus drei Beiträgen (Absorption im angeregten Zustand, Stimulierte Emission und Grundzustands-Ausbleichen), die sich gegenseitig überlagern. Ohne eine Trennung der beteiligten Übergänge, kann keine exakte Aussage über die Form und Entwicklung der Banden gemacht werden. Im schlimmsten Fall bleiben Bandenformen komplett unsichtbar. Zum Anderen ist die Breite der beteiligten Banden durch die kurze elektronische Dephasierungs-Zeit bestimmt, wodurch keine Aussagen über die Beteiligung von Vibrationsmoden gemacht werden können. Durch den Einsatz von komplementären Spektroskopie-Methoden können die Ergebnisse aus der transienten Absorptions-Spektroskopie um diese fehlenden Informationen ergänzt werden. Eine davon ist Fluoreszenz-Aufkonversion, mithilfe dessen das Emissionsverhalten eines Moleküls breitbandig beobachtet und unabhängig von anderen Beiträgen charakterisiert werden kann. Von Bedeutung ist hierbei der Einsatz eines BBO-Kristals als nichtlineares Medium, der trotz seiner intrinsischen Einschränkungen für die Aufnahme Breitband-Spektren in einer fixierten Messanordnung genutzt werden kann. Die fehlende spektrale Auflösung liefert die femtosekunden stimulierte Raman-Spektroskopie, mit der Raman-Signale mit bis zu 20 cm^{-1} Breite beobachtet werden können. Durch den lokalen Charakter einiger Moden kann diese Spektroskopie-Methode durchaus ortsaufgelöste Informationen liefern. Die technische Implementierung eines durchstimmbaren Raman-Pulses ermöglicht die gezielte Resonanzverstärkung für Raman-Signale eines elektronischen Zustandes.

Neben der Datenbeschaffung braucht es auch eine angemessene Auswertungs-Prozedur, um bis dato unerkanntes Verhalten im angeregten Zustand sichtbar zu machen. Dabei ist es notwendig, Kriterien zu befolgen, die über die Qualität der erzielten Ergebnisse entscheiden.

Der erste Chromophor ist Riboflavin und wird mittels transienter Absorptions und Breitband Fluoreszenz-Aufkonversion in verschiedenen pH-Lösungen untersucht. Aus stationären Messungen geht hervor, dass eine Fluoreszenzbande um 660 nm nicht direkt aus der Anregung einer der Formen des Riboflavins folgt. Mit transienter Absorption wird zwar der Protonen-Transfer vom Lösungsmittel auf das Riboflavin beobachtet, jedoch ist stimulierte Emission im roten Spektralbereich zu schwach um als negative Bande im Spektrum erkannt zu werden. Mit Hilfe der Fluoreszenz-Aufkonversion beobachtet man nun das Auftauchen dieser Fluoreszenz-Bande mit dem zeitgleichen Verschwinden der Emission von neutralem Riboflavin. Ein Zusammenhang mit dem Protonen-Transfer im angeregten Zustand kann somit hergestellt werden.

β-Karotin in Hexan wird mit transienter Absorption und femtosekunden-stimulierter Raman Spektroskopie gemessen. Die Relaxationsprozesse vom angeregten Zustand S_2 über S_1 bis zum elektronischen Grundzustand kann mit vier Zeitkonstanten (aus der Literatur bekannt) beschrieben werden. Neu ist die zusätzliche Verwendung einer nicht-exponentiellen Zeitfunktion, die die Umverteilung von Population auf ein anderes Konformer in S_1 beschreibt. Diese Umverteilung äußert sich auch in den Raman-Signalen welche vom Grundzustands-Ausbleichen stammen. Neue Raman-Banden aus dem S_2-Zustand werden im niederfrequenten (<800 cm^{-1}) und hochfrequenten Bereich (>1600 cm^{-1}) erkannt und erstere mit Resonanz-Raman-Spektroskopie bestätigt. Die Kombination aus hoher Sensitivität des Detektionssystems und stabilem Weißlicht ermöglicht die Beobachtung von Nah-Feld-Effekten durch den Chromophor auf die umliegenden Hexan-Moleküle.

7 Abstract

The combination of broad-band spectroscopic methods on a high level allows a comprehensive view of the electronic system of excited molecules. Here- transient absorption spectroscopy is the most wide-spread technique. It is possible to observe the migration of excited state population until it returns to the electronic ground-state. Despite the simplicity of this method and the picture that it provides there are two inherent disadvantages: First, the spectrum consists of three contributions (excited-state absorption, stimulated emission and bleach) that are all superimposed. Without sophisticating separation of these bands their exact form and evolution keeps being unclear or – in the worst case – completely hidden. Second, the large widths of the electronic bands in the absorption spectrum arise from short electronic dephasing. A distinction between vibronic transitions is therefore impossible and the involvement of specific modes remains speculative. With the application of complementary spectroscopic methods all the results from transient absorption can be supplemented with this complementary information. One method is fluorescence up-conversion with which the emission of a chromophore can be monitored broad-band and independent from any other contribution. Of importance is the use of a BBO crystal as nonlinear medium that still enables the broad-band imaging in a fixed geometry despite its intrinsic constraints. The lack of spectral resolution is compensated with femtosecond stimulated Raman spectroscopy with Raman signals of ~20 cm^{-1} width. The local character of some modes (C-C and C=C stretching modes) allows the localization of excited-state evolution. The technical implementation of a tunable Raman-pulse enables the enhancement of Raman signals from a specific electronic state.

Besides the acquisition of data, an appropriate evaluation procedure is needed to reveal hitherto unrecognized behavior in the excited state. It is therefore necessary to follow criteria that determine the quality of a result.

The first chromophore to be examined is riboflavin at different pH-values with transient absorption and fluorescence up-conversion. From stationary measurements it follows that an emission band around 660 nm cannot originate from riboflavin directly after photo excitation. Transient absorption indeed monitors the proton transfer from the solvent to the chromophore but no sign of stimulated emission is seen in the red spectral region. With fluorescence up-conversion it is possible to observe the emerging red fluorescence band while simultaneously emission from the neutral form decays. In this sense a connection between excited-state proton transfer and the fluorescence band at 660 nm is made.

β-carotene is examined with transient absorption and stimulated Raman spectroscopy. The relaxation from S_2 to the electronic ground-state can be described with four time-constants (as already known in literature). New is an additional non-exponential time-function that describes the migration of population to a different conformer in S_1. The same non-exponential behavior is seen in the bleach signals from stimulated Raman spectra. New

Raman bands are observed in the low- (<800 cm^{-1}) and high-frequency region (>1600 cm^{-1}) while the former is confirmed with Resonance Raman spectroscopy. The combination of a high sensitive detection system and only weakly fluctuating white-light enables the observation of enhanced solvent lines which suggests the molecular near-field effect from the chromophore to the neighboring hexane molecules.

8 Literature

1 Introduction

[1] P. F. Heelis, The Photophysical and Photochemical Properties of Flavins. Chem. Soc. Rev. 1982, 11, 15−39.

[2] P. Drössler, W. Holzer, A. Penzkofer, P. Hegemann, pH Dependence of the Absorption and Emission Behaviour of Riboflavin in Aqueous Solution. Chem. Phys. 2002, 282, 429−439.

[3] G. Li, K. D. Glusac, Light-Triggered Proton and Electron Transfer in Flavin Cofactors. J. Phys. Chem. A 2008, 112, 4573−4583.

[4] J-P. Zhang, L.H. Skibsted, R. Fujii, Y. Koyama, Transient Absorption from the $1B_u^1$ State of All-trans-β-carotene Newly Identified in the Near-infrared Region. *Photochem. Photobiol.* **2001**, *73*(3), 219-222.

[5] M. Yoshizawa, H. Aoki, H. Hashimoto, Vibrational Relaxation of the $2A_g^-$ Excited State in All-*trans*-β-Carotene Obtained by Femtosecond Time-resolved Raman spectroscopy. *Phys. Rev. B* **2001**, *63*, 180301.

[6] T. Lenzer, F. Ehlers, M. Scholz, R. Oswald, K. Oum, Assignment of Carotene S* State Features to the Vibrationally Hot Ground Electronic State. *PCCP* **2010**, *12*, 8832-8839.

[7] D.W. McCamant, J.E. Kim, R.A. Mathies, Femtosecond Time-Resolved Stimulated Raman Spectroscopy: Application to the Ultrafast Internal Conversion in β-Carotene. *J. Phys. Chem. A* **2003**, *107*, 8208-8214.

[8] S. Shim, R.A. Mathies, Development of a Tunable Femtosecond Stimulated Raman Apparatus and Its Application to β-Carotene. *J. Phys. Chem. B* **2008**, *112*, 4826-4832.

[9] P. Kukura, D.W. McCamant, R.A. Mathies, Femtosecond Time-Resolved Stimulated Raman Spectroscopy of the S_2 ($1B_u^-$) Excited State of β-Carotene. *J. Phys. Chem. A* **2004**, *108*, 5921-5925.

[10] J. Hauer, M. Maiuri, D. Viola, V. Lukes, S. Henry, A. M. Carey, R. J. Cogdell, G. Cerullo, D. Polli, Explaining the Temperature Dependence of Spirilloxanthin's S* Signal by an Inhomogeneous Ground State Model. *J. Phys. Chem. A* **2013**, *117*, 6303-6310.

[11] P. F. Moulton, Spectroscopic and Laser Characteristics of Ti:Al_2O_3. *J. Opt. Soc. Am. B* **1986**, *3*, 125-133.

[12] D. E. Spence, P. N. Kean, W. Sibbet, 60-fsec Pulse Generation from a Self-Mode-Locked Ti:Sapphire Laser. *Opt. Lett.* **1991**, *16*, 42-44.

[13] Y. P. Tong, J. M. Sutherland, P. M. W. French, J. R. Taylor, A. V. Shestakov, B. H. Chai, Self-Starting Kerr-Lens Mode-Locked Femtosecond Cr^{4+}:YAG and Picosecond Pr^{3+}:YLF Solid-State Lasers. *Opt. Lett.* **1996**, *21*, 644-666.

[14] M.R. Wasielewski, L.D. Kispert, Direct Measurement of the Lowest Singlet State Lifetime of all-*trans*-β-Carotene and Related Carotenoids. *Chem. Phys. Lett.* **1986**, *128*(3), 238-243.

[15] A.P. Shreve, J.K. Trautman, T.G. Owens, A.C. Albrecht, Determination of the S_2 Lifetime of β-carotene. *Chem. Phys. Lett.* **1991**, *178*(1), 89-96.

[16] G. Cerullo, G. Lanzani, M. Zavelani-Rossi, S. De Silvestri, Early Events of Energy Relaxation in All-*trans*-β-Carotene Following Sub-10 fs Optical-Pulse Excitation. *Phys. Rev. B* **2001**, *63*, 241104.

[17] W. Wohlleben, T. Buckup, H. Hashimoto, R. J. Cogdell, J. L. Herek, M. Motzkus, Pump- Deplete-Probe Spectroscopy and the Puzzle of Carotenoid Dark States. *J. Phys. Chem. B* **2004**, *108*, 3320-3325.

[18] T. Takaya, K. Iwata, Relaxation Mechanism of β‑Carotene from S_2 ($1B_u^+$) State to S1 ($2A_g^-$) State: Femtosecond Time-Resolved Near-IR Absorption and Stimulated Resonance Raman Studies in 900−1550 nm Region. *J. Phys. Chem. A* **2014**, *118*, 4071-4078.

[19] G. Cerullo, D. Polli, G. Lanzani, S. De Silvestri, H. Hashimoto, R. J. Cogdell, Photosynthetic Light Harvesting by Carotenoids: Detection of an Intermediate Excited State. *Science* **2002**, *298*, 2395-2398.

[20] J.L. Perez Lustres, A.L. Dobryakov, A. Holzwarth, M. Veiga, $S_2 \rightarrow S_1$ Internal Conversion in β-Carotene: Strong Vibronic Coupling from Amplitude Oscillations of Transient Absorption Bands. *Angew. Chem. Int. Ed.* **2007**, *46*, 3758-3758.

[21] G. Lanzani, G. Cerullo, M. Zavelani-Rossi, S. De Sylvestri, Sub-10 fs Time Resolved Study of Excited State Relaxation in *all-trans*-β-carotene. *Synthetic Met.* **2001**, *116*, 1-3.

[22] J.P. Kraack, A. Wand, T. Buckup, M. Motzkus, S. Ruhman, Mapping Multidimensional Excited State Dynamics Using Pump-Impulsive-Vibrational-Spectroscopy and Pump-Degenerate-Four-Wave-Mixing. *PCCP* **2013**, *15*, 14487-14501.

[23] M. Liebel, P. Kukura, Broad-Band Impulsive Vibrational Spectroscopy of Excited Electronic States in the Time Domain. *J. Phys. Chem. Lett.* **2013**, *4*, 1358-1364.

2 Nonlinear Spectroscopy

[1] A. Weigel, *Femtosecond Stimulated Resonance Raman Spectroscopy: Towards Mapping the Primary Steps in Biological Photoreceptors*. (Humboldt University: Dissertation, 2010, 9-26).

[2] S. Mukamel, *Principles of Nonlinear Optical Spectroscopy* (Oxford University: New York, 1995).

[3] A. L. Dobryakov, M. Quick, I. N. Ioffe, A. A. Granovsky, N. P. Ernsting and S. A. Kovalenko, Excited-state Raman Spectroscopy with and without Actinic Excitation: S_1 Raman Spectra of trans-azobenzene, *J. Chem. Phys.* **2014**, *140*, 184310.

[4] S.A. Kovalenko, A.L. Dobryakov, J. Ruthmann, N.P. Ernsting, Femtosecond Spectroscopy of Condensed Phases with Chirped Supercontinuum Probing. *Phys. Rev. A* **1999**, *59***,** 2369.

[5] A.L. Dobryakov, S.A. Kovalenko, N. P. Ernsting, Electronic and Vibrational Coherence Effects in Broadband Transient Absorption Spectroscopy with Chirped Supercontinuum Probing. *J. Chem. Phys.* **119**, 988 (2003).

[6] A.L. Dobryakov, S.A. Kovalenko, N.P. Ernsting, Coherent and Sequential Contributions to Femtosecond Transient Absorption Spectra of a Rhodamine Dye in Solution. *J. Chem. Phys.* **123**, 044502 (2005)

[7] A.L. Dobryakov, N.P. Ernsting, W. Gawelda, C. Bressler, M. Chergui, in: O. Kühn, L. Wöste (Eds) Analysis and Control of Ultrafast Photoinduced Reactions, Springer Series in Chemical Physics, Vol. 87, Springer, Heidelberg, 2007, pp.689.

[8] A.L. Dobryakov, J.L. Perez Lustres, S.A. Kovalenko, N. P. Ernsting, Femtosecond Transient Absorption with Chirped Pump and Supercontinuum Probe: Perturbative Calculation of Transient Spectra with General Lineshape Functions, and Simplifications. *Chem. Phys.* **2008**, *347*, 127-138.

[9] A.L. Dobryakov, N. P. Ernsting, Lineshapes for Resonant Impulsive Stimulated Raman Scattering with Chirped Pump and Supercontinuum Probe Pulses. *J. Chem. Phys.* **129**, 184504 (2008).

[10] A. Weigel, A. Dobryakov, B. Klaumuenzer, M. Sajadi, P. Saalfrank, N.P. Ernsting, Femtosecond Stimulated Raman Spectroscopy of Flavin After Optical Excitation. *J. Phys.Chem. B* **2011**, *115*, 3656.

[11] Y.J. Yan, S. Mukamel, Femtosecond Pump-Probe Spectroscopy of Polyatomic Molecules in Condensed Phases. *Phys. Rev. A* **1990**, *41*, 6485.

[12] S. Mukamel, Femtosecond Optical Spectroscopy: A Direct Look at Elementary Chemical Events. *Annu. Rev. Phys. Chem.* **1990**, *41*, 647-681.

[13] R.F. Loring, Y.J. Yan, S. Mukamel, Time-resolved Fluorescence and Hole-Burning Line Shapes of Solvated Molecules: Longitudinal Dielectric Relaxation and Vibrational Dynamics. *J. Chem. Phys.* **1987**, *87*, 5840.

[14] Y.J. Yan, L.E. Fread, S. Mukamel, Ultrafast Pump-Probe Spectroscopy: Femtosecond Dynamics in Liouville Space. *J. Phys. Chem.* **1989**, *93*, 8149-8126.

[15] O. Stern, M. Volmer, Über die Abklingungszeit der Fluoreszenz. *Physikalische Zeitschrift* **1919**, *20*, 183-188

3 Experimental Section

[1] R. W. Boyd, *Nonlinear Optics – Second Edition* (Academic Press, 2003)

[2] R. Schanz, S. A. Kovalenko, V. Kharlanov, N. P. Ernsting, Broad-band Fluorescence Upconversion for Femtosecond Spectroscopy. *Appl. Phys. Lett.* **2001**, *79*, 566-568.

[3] X.-X. Zhang, C. Würth, L. Zhao, U. Resch-Gengar, N. P. Ernsting, Improved Setup and Photometric Correction. *Rev. Sci. Instrum.***2011**, *82*, 063108.

[4] M. Sajadi, M. Quick, N. P. Ernsting, Femtosecond Broadband Fluorescence Spectroscopy by Down- and Up-conversion in β-barium-borate Crystals. *Appl. Phys. Lett.* **2013**, *103*, 173514.

[5] A. L. Dobryakov, S. A. Kovalenko, A. Weigel, J. L. Pérez-Lustres, J. Lange, A. Müller, N. P. Ernsting, Femtosecond Pump/Supercontinuum-probe Spectroscopy: Optimized Setup and Signal Analysis for Single-shot Spectral Referencing. *Rev. Sci. Instrum.* **2010**, *81*, 113106.

[6] S. A. Kovalenko, A. L. Dobryakov, N. P. Ernsting, An Efficient Setup for Femtosecond Stimulated Raman Spectroscopy. *Rev. Sci. Instrum.* **2011**, *82*, 063102.

[7] F. Raoult, A. C. L. Boscheron, D. Husson, C. Sauteret, A. Modena, V.Malka, F. Dorchies, A. Migus, Efficient Generation of Narrow-Bandwidth Picosecond Pulses by Frequency Doubling of Femtosecond Chirped Pulses. *Opt. Lett*. **1998**, *23*, 1117.

[8] O. E. Martinez, 3000 Times Grating Compressor With Positive Group Velocity Dispersion: Application to Fiber Compensation in 1.3-1.6 µm Region . *IEEE J. Quantum Electron.* **1987**, *23*, 59-64.

[9] O. E. Martinez, Grating and Prism Compressors in the Case of Finite Beam Size. *J. Opt. Soc. Am. B* **1986**, *3*, 929-934.

[10] S. A. Kovalenko, A. L. Dobryakov, J. Ruthmann, N. P. Ernsting, Femtosecond Spectroscopy of Condensed Phases with Chirped Supercontinuum Probing. *Phys. Rev. A* **1999**, *59*, 2369- 2384.

[11] M. Quick, A. L. Dobryakov, S. A. Kovalenko, N. P. Ernsting, Resonance Femtosecond-Stimulated Raman Spectroscopy Without Actinic Excitation Shows Low-Frequency Vibrational Activity in the S_2 State of All-Trans β-Carotene. *J. Phys. Chem. Lett.* **2015**, *6*, 1216-1220.

4 Publications

4.1 M. Quick, A. Weigel, N. P. Ernsting, Fluorescence Following Excited-State Protonation of Riboflavin at N(5), *J. Phys. Chem. B* **2013**, *117*, 5441-5447.

[1] Y. Hatefi, The Mitochondrial Electron Transport and Oxidative Phosphorylation System. *Ann. Rev. Biochem.* **1985**, *54*, 1015-1069.

[2] Y. Yasukochi, J. A. Peterson, B. S. S. Masters, NADPH-Cytochrome c (P-450) Reductase. *J. Biol. Chem.* **1979**, *254* (15), 7097-7104.

[3] S. Ghisla, V. Massey, Mechanisms of Flavoprotein-Catalyzed Reactions. *Eur. J. Biochem.* **1989**, *181*, 1-17.

[4] S. A. Ahmed, A. Claiborne, The Streptococcal Flavoprotein NADH Oxidase. *JBC* **1989**, *264* (33), 19856-19863.

[5] A. R. Cashmore, J. A. Jarillo, Y. J. Wu, D. M. Liu, Cryptochromes: Blue Light Receptors for Plants and Animals. *Science* **1999**, *284*, 760–765.

[6] W. R. Briggs, J. M. Christie, Phototropins 1 and 2: Versatile Plant Blue-Light Receptors. *Trends in Plant Science* **2002**, *7*, 204-210.

[7] A. R. Cashmore, Cryptochromes: Enabling Plants and Animals to Determine Circadian Time. *Cell* **2003**, *114*, 537–543.

[8] M. A. Van der Horst, K. J. Hellingwerf, Photoreceptor Proteins, “Star Actors of Modern Times”. *Acc. Chem. Res.* **2004,** *37*, 13-20.

[9] J.-P. Bouly,; E. Schleicher, M. Dionisio-Sese, F. Vandenbussche, D. Van der Straeten, N. Bakrim, S. Meier, A. Batschauer, P. Galland, R. Bittl, M. Ahmad, Cryptochrome Blue Light Photoreceptors Are Activated through Interconversion of Flavin Redox States. *J. Biol. Chem.* **2007**, *282* (13), 9383–9391.

[10] P. F. Heelis, The Photophysical and Photochemical Properties of Flavins. *Chem. Soc. Rev.* **1982**, *11*, 15-39.

[11] E. Sikorska, I. V. Khmelinskii, D. R. Worrall, J. Koput, M. Sikorski, Spectroscopy and Photophysics of Iso- and Alloxazines: Experimental and Theoretical Study. *J. Fluoresc.* **2004**, *14*, 57-64.

[12] E. Sikorska, I. V. Khmelinskii, J. Koput, J. L. Bourdelande, M. Sikorski, Electronic Structure of Isoalloxazines in their Ground and Excited States. *J. Mol. Struct.* **2004**, *697*, 137–141.

[13] E. Sikorska, I. V. Khmelinskii, J. Koput, M. Sikorski, Electronic Structure of Lumiflavin and its Analogues in their Ground and Excited States. *J. Mol. Struct. (Theochem)* **2004**, *676*, 155–160.

[14] M. Insinska-Rak, E. Sikorska, J. R. Herance, J. L. Bourdelande, I. V. Khmelinskii, M. Kubicki, W. Prukała, I. F. Machado, A. Komasa, L. F. V. Ferreira, M. Sikorski, Spectroscopy and Photophysics of Flavin-Related Compounds: 3-benzyl-lumiflavin. *Photochem. Photobiol. Sci.* **2005**, *4*, 463-468.

[15] E. Sikorska, J. R. Herance, J. L. Bourdelande, I. V. Khmelinskii, S. L. Williams, D. R. Worrall, G. Nowacka, A. Komasa, M. Sikorski, Spectroscopy and Photophysics of Flavin-Related Compounds: 3-ethyl-Lumiflavin. *J. Photochem. Photobiol. A* **2005**, *170*, 267–272.

[16] V. N. Petushkov, I. H. M. van Stokkum, B. Gobets, F. van Mourik, J. Lee, R. van Grondelle, A. J. W. G. Visser, Ultrafast Fluorescence Relaxation Spectroscopy of 6,7-Dimethyl-(8-ribityl)-lumiazine and Riboflavin, Free and Bound to Antenna Proteins from Bioluminescent Bacteria. *J. Phys. Chem. B* **2003,** *107*, 10934-10939.

[17] M. M. N. Wolf, C. Schumann, R. Gross, T. Domratcheva, R. Diller, Ultrafast Infrared Spectroscopy of Riboflavin: Dynamics, Electronic Structure, and Vibrational Mode Analysis. *J. Phys. Chem. B* **2008,** *112*, 13424–13432.

[18] A. Weigel, A. L. Dobryakov, M. Veiga, J. L. P. Lustres, Photoinduced Processes in Riboflavin: Superposition of $\pi\pi^*$-$n\pi^*$ States by Vibronic Coupling, Transfer of Vibrational Coherence, and Population Dynamics under Solvent Control. *J. Phys. Chem. A* **2008**, *112*, 12054–12065.

[19] A. Weigel, A. L. Dobryakov, B. Klaumünzer, M. Sajadi, P. Saalfrank, N. P. Ernsting, Femtosecond Stimulated Raman Spectroscopy of Flavin after Optical Excitation. *J. Phys. Chem. B* **2011**, *115* (13), 3656–3680.

[20] Y.-J. Zheng, R. L. A Ornstein, Theoretical Study of the Structure of Flavin in Different Oxidation and Protonation States. *J. Am. Chem. Soc.* **1996**, *118*, 9402-9408.

[21] P. A. W. den Berg, K. A. Feenstra, A. E. Mark, H. J. C. Berendsen, A. J. W. G. Visser, Dynamic Conformations of Flavin Adenine Dinucleotide: Simulated Molecular Dynamics of the Flavin Cofactor Related to the Time-Resolved Fluorescence Characteristics. *J. Phys. Chem. B* **2002**, *106*, 8858-8869.

[22] P. Drössler, W. Holzer, A. Penzkofer, P. Hegemann, pH Dependence of the Absorption and Emission Behaviour of Riboflavin in Aqueous Solution. *Chem. Phys.* **2002**, *282*, 429-439.

[23] K. Nishimoto, Y. Watanabe, K. Yagi, Hydrogen Bonding of Flavoprotein. *Biochim Biophys Acta* **1978**, *526*, 34-41.

[24] G. Li, K. D. Glusac, Light-Triggered Proton and Electron Transfer in Flavin Cofactors. *J. Phys. Chem. A* **2008**, *112,* 4573–4583.

[25] A. Sengupta, R. V. Khade, P. Hazra, pH Dependent Dynamic Behaviour of FMN and FAD in Femtosecond to Nanosecond Time Scale. *J. Photochem. Photobiol. A* **2011**, 221, 105–112.

[26] P.S. Song, On the Basicity of the Excited State of Flavins. *J. Photochem. Photobiol.* **1968**, *7*, 311-313.

[27] E. Sikorska, I. Khmelinskii, A. Komasa, J. Koput, L. F.V. Ferreira, J. R. Herance, J. L. Bourdelande, S. L. Williams, D. R. Worrall, M. Insinska-Rak, M. Sikorski, Spectroscopy and Photophysics of Flavin Related Compounds: Riboflavin and Iso-(6,7)-Riboflavin. *Chem. Phys.* **2005**, *314*, 239–247.

[28] S. Salzmann, C.M. Marian, Effects of Protonation on the Excitation Energies of Lumiflavin. *Chem. Phys. Lett.* **2008**, *463*, 400-404.

[29] V. Sichula, P. Kucheryavy, R. Khatmullin, Y. Hu, E. Mirzakulova, S. Vyas, S. F. Manzer, C. M. Hada, K. D. Glusac, Electronic Properties of N(5)-Ethyl Flavinium Ion. *J. Phys. Chem. A* **2010**, *114*, 12138-12147.

[30] L. Michaelis, M. P. Schubert, C. V. Smythe, Potentiometric Study of the Flavins. *J. Biol. Chem.* **1936**, *116*, 587-607.

[31] S. G. Schulmann, pH Dependence of Fluorescence of Riboflavin and Related Isoalloxazine Derivatives. *J. Pharm. Sci.* **1971**, *60*, 628-631.

[32] R. M. Kowalczyk, E. Schleicher, R. Bittl, S. Weber, The Photoinduced Triplet of Flavins and Its Protonation States. *J. Am. Chem. Soc.* **2004**, *126*, 11393-11399.

[33] A. Tyagi, A. Penzkofer, Absorption and Emission Spectroscopic Characterization of Lumichrome in Aqueous Solutions. *Photochem. Photobiol.* **2011**, *87*, 524–533.

[34] T. Climent, R. Gonzalez-Luque, M. Merchan, L. Serrano-Andres, Theoretical Insight into the Spectroscopy and Photochemistry of Isoalloxazine, the Flavin Core Ring. *J. Phys. Chem. A* **2006**, *110*, 13584-13590.

[35] N. B. Librovich, V. D. Maiorov, Ionic-Molecular Composition of Aqueous Sulfuric Acid Solutions. *Ser. Khim.* **1977**, *3*, 684-687.

[36] I. Kusaka, Z.-G. Wang, J. H. Seinfeld, Binary Nucleation of Sulfuric Acid-Water: Monte Carlo Simulation. *J. Chem. Phys.* **1998**, *108* (16), 6829-6848.

[37] L. Zhao, J. L. Perez Lustres, V. Farztdinov, N. P. Ernsting, Femtosecond Fluorescence Spectroscopy by Upconversion with Tilted Gate Pulses. *PCCP* **2005**, *7*, 1716–1725.

[38] X-X. Zhang, C. Würth, L. Zhao, U. Resch-Genger, N. P. Ernsting, Femtosecond Broadband Fluorescence Upconversion Spectroscopy: Improved Setup and Photometric Correction. *Rev. Sci. Instrum.* **2011**, *82*, 063108.

[39] S. A. Kovalenko, A. L. Dobryakov, J. Ruthmann, N. P. Ernsting, Femtosecond Spectroscopy of Condensed Phases with Chirped Supercontinuum Probing. *Phys. Rev. A* **1999**, *59*, 2369-2384.

[40] A. Dobryakov, S. A. Kovalenko, A. Weigel, J. L. Pérez-Lustres, J. Lange, Femtosecond Pump/Supercontinuum-Probe Spectroscopy: Optimized Setup and Signal Analysis for Single-Shot Spectral Referencing. *Rev. Sci. Instrum.* **2010**, *81*, 113106.

4.2 Martin Quick, Marc-André Kasper, Celin Richter, Rainer Mahrwald, Alexander L. Dobryakov, Sergey A. Kovalenko, Nikolaus P. Ernsting, β-Carotene revisited by Transient Absorption and Stimulated Raman Spectroscopy. *Chem. Phys. Chem.* 2015,…

[1] R.J.Cogdell, H.A.Frank, How Carotenoids Function in Photosynthetic Bacteria. *Biochim. Biophys. Acta* **1987**, *895*, 63-79.

[2] B.S. Hudson, B.E. Kohler, A Low-Lying Weak Transition in the Polyene α,ω-Diphenyloctatetraene. *Chem. Phys. Lett.* **1972**, *14*(3), 299-304.

[3] K. Schulten, M. Karplus,On the Origin of a Low-Lying Forbidden Transition in Polyenes and Related Molecules. *Chem. Phys. Lett.* **1972**, *14*(3), 305-309.

[4] M.R. Wasielewski, L.D. Kispert, Direct Measurement of the Lowest Excited Singlet State Lifetime of All-*trans*-β-Carotene and Related Carotenoids. *Chem. Phys. Lett.* **1986**, *128*(3), 238-243.

[5] P.O. Andersson, T. Gillbro, A.E. Asato, R.S.H. Liu, Dual Singlet State Emission in a Series of mini-Carotenes. *J. Lum.* **1992**, *51*, 11-20.

[6] P.O. Andersson, S.M. Bachilo, R-L. Chen, T. Gillbro, Solvent and Temperature Effects on Dual Fluorescence in a Series of Carotenoids. Energy Gap Dependence of the Internal Conversion Rate. *J. Phys. Chem.* **1995**, *99*, 16199-16209.

[7] T. Takaya, K. Iwata, Relaxation Mechanism of β‑Carotene from S2 ($1B_u^+$) State to S1 ($2A_g^-$) State: Femtosecond Time-Resolved Near-IR Absorption and Stimulated Resonance Raman Studies in 900−1550 nm Region. *J. Phys. Chem. A* **2014**, *118*, 4071-4078.

[8] S.L. Bondarev, S.M. Bachilo, S.S. Dvornikov, S.A. Tikhomirov, $S_2 \rightarrow S_0$ Fluorescence and Transient $S_n \leftarrow S_1$ Absorption of All-*trans*-β-Carotene in Solid and Liquid Solutions. *J. Photochem. Photobiol. A* **1989**, *46*, 315-322.

[9] S.L. Bondarev, V.N. Knyukshto, Fluorescence from the S_1 (2^1A_g) State of All-*trans*-β-Carotene. *Chem. Phys. Lett.* **1994**, *225*, 346-50.

[10] A.P. Shreve, J.K. Trautman, T.G. Owens, A.C. Albrecht, Determination of the S_2 Lifetime of β-Carotene. *Chem. Phys. Lett.* **1991**, *178*(1), 89-96.

[11] J-P. Zhang, L.H. Skibsted, R. Fujii, Y. Koyama, Transient Absorption from the $1B_u^1$ State of All-*trans*-β-carotene Newly Identified in the Near-infrared Region. *Photochem. Photobiol.* **2001**, *73*(3), 219-222.

[12] M. Yoshizawa, H. Aoki, H. Hashimoto, Vibrational Relaxation of the $2A_g^1$ Excited State in All-*trans*-β-Carotene Obtained by Femtosecond Time-resolved Raman spectroscopy. *Phys. Rev. B* **2001**, *63*, 180301.

[13] D. Kosumi, K. Yanagi, R. Fujii, H. Hashimoto, M. Yoshizawa, Conjugation Length Dependence of Relaxation Kinetics in β-Carotene Homologs Probed by Femtosecond Kerr-Gate Fluorescence Spectroscopy. *Chem Phys. Lett.* **2006**, 425, 66-70.

[14] D. Kosumi, M. Fujiwara, R. Fujii, R.J. Cogdell, H. Hashimoto, M. Yoshizawa, The Dependence of the Ultrafast Relaxation Kinetics of the S_2 and S_1 States in β-Carotene Homologs and Lycopene on Conjugation Length Studied by Femtosecond Timeresolved Absorption and Kerr-Gate Fluorescence Spectroscopies. *J. Chem. Phys.* **2009**, *130*, 214506.

[15] T. Polivka, V. Sundström, Dark Excited states of Carotenoids: Consensus and Controversy. *Chem. Phys. Lett.* **2009**, *477*, 1-11.

[16] E. Papagiannakis, I. H. M. van Stokkum, M. Vengris, R. J. Cogdell, R. van Grondelle, D. S. Larsen, Excited-State Dynamics of Carotenoids in Light-Harvesting Complexes. 1. Exploring the Relationship between the S_1 and S* States. *J. Phys. Chem. B* **2006**, *110*, 5727-5736.

[17] J. Hauer, M. Maiuri, D. Viola, V. Lukes, S. Henry, A. M. Carey, R. J. Cogdell, G. Cerullo, D. Polli, Explaining the Temperature Dependence of Spirilloxanthin's S* Signal by an Inhomogeneous Ground State Model. *J. Phys. Chem. A* **2013**, *117*, 6303-6310.

[18] T. Lenzer, F. Ehlers, M. Scholz, R. Oswald, K. Oum, Assignment of Carotene S* State Features to the Vibrationally Hot Ground Electronic State. *PCCP* **2010**, *12*, 8832-8839.

[19] S. Saito, I. Harada, M. Tasumi, C. H. Eugster, Resonance Raman Spectra of All-*trans* and 15,15'-*cis*-β,β-Carotene. *Chem. Lett.* **1980**, 1045-1048.

[20] H. Hashimoto, Y. Koyama, The C=C Stretching Raman Lines of β-Carotene Isomers in the S_1 State as Detected by Pump-Probe Resonance Raman Spectroscopy. *Chem. Phys. Lett.* **1989**, *154*(4), 321-325.

[21] H. Hashimoto, Y. Koyama, Raman Spectra of All-*trans*-β-Carotene in the S_1 and T_1 States Produced by Direct Photoexcitation. *Chem. Phys. Lett.* **1989**, *163* (2,3), 251-256.

[22] D.W. McCamant, J.E. Kim, R.A. Mathies, Femtosecond Time-Resolved Stimulated Raman Spectroscopy: Application to the Ultrafast Internal Conversion in β-Carotene. *J. Phys. Chem. A* **2003**, *107*, 8208-8214.

[23] D.W. McCamant, J.E. Kim, R.A. Mathies, Vibrational Relaxation in *β*-Carotene Probed by Picosecond Stokes and Anti-Stokes Resonance Raman Spectroscopy. *J. Phys. Chem. A* **2002**, *106*, 6030-6038.

[24] S. Shim, R.A. Mathies, Development of a Tunable Femtosecond Stimulated Raman Apparatus and Its Application to *β*-Carotene. *J. Phys. Chem. B* **2008**, *112*, 4826-4832.

[25] T. Noguchi, H. Hayashi, M. Tasumi, G.H. Atkinson, Solvent Effects on the a_g C=C Stretching Mode in the $2^1A_g^-$ Excited State of β-Carotene and two Derivatives: Picosecond Time-Resolved Resonance Raman Spectroscopy. *J. Phys. Chem.* **1991**, *95*, 3167-3172.

[26] H. Nagae, M. Kuki, J.-P. Zhang, T. Sashima, Y. Mukai, Y. Koyama, Vibronic Coupling through the In-Phase, C=C Stretching Mode Plays a Major Role in the $2A_g^-$ to $1A_g^-$ Internal Conversion of *all-trans-β*-Carotene. *J. Phys. Chem.* **2000**, *104*, 4155-4166.

[27] H. Hashimoto, Y. Koyama, Y. Hirata, N. Mataga, S_1 and T_1 Species of β-Carotene Generated by Direct Photoexcitation from the All-Trans, 9-Cis, and 15-Cis Isomers as Revealed by Picosecond Transient Absorption and Transient Raman Spectroscopies. *J. Phys. Chem.* **1991**, *95*, 3072-3076.

[28] G. Orlandi, F. Zerbetto, .Vibronic Coupling in Polyenes: The Frequency Increase of the Active C=C a_g Stretching Mode in the Absorption Spectra. *Chem. Phys.* **1986**, *108*, 187-195.

[29] F. Zerbetto, M.Z. Zgierski, G. Orlandi, G. Marconi, Vibronic Coupling in Polyenes and their Derivatives. Interpretation of the Absorption and Emission Spectra of a Derivative of Dodecahexaene. *J. Chem. Phys.* **1987**, *87*, 2505-2512.

[30] A. Sakamoto, S. Matsuno, M. Tasumi, Picosecond Near-Infrared Excited Transient Raman Spectra of β-Carotene in the Excited S_2 State: Solvent Effects on the In-phase C=C Stretching Band and Vibronic Coupling. *J. Mol. Struct.* **2010**, *976*, 310-313.

[31] H. Kandori, H. Sasabe, M. Mimuro, Direct Determination of a Lifetime of the S_2 State of β-Carotene by Femtosecond Time-Resolved Fluorescence Spectrsocopy. *JACS* **1994**, *116*, 2671-2672.

[32] A.N. Macpherson, T. Gillbro, Solvent Dependence of the Ultrafast S_2-S_1 Internal Conversion Rate of β-Carotene. *J. Phys. Chem. A* **1998**, *102*, 5049-5058.

[33] P. Kukura, D.W. McCamant, R.A. Mathies, Femtosecond Time-Resolved Stimulated Raman Spectroscopy of the S_2 ($1B_u^+$) Excited State of β-Carotene. *J. Phys. Chem. A* **2004**, *108*, 5921-5925.

[34] A. Sakamoto, S. Matsuno, M. Tasumi, Construction of Picosecond Time-Resolved Raman Spectrometers with Near-Infrared Excitation. *J. Raman. Spectrosc.* **2006**, *37*, 429-435.

[35] F.L. Weerd, I.H.M. van Stokkum, R. van Grondelle, Subpicosecond Dynamics in the Excited State Absorption of All-*trans*-β-Carotene. *Chem. Phys. Lett.* **2002**, *354*, 38-43.

[36] H.H. Billsten, D. Zigmantas, V. Sundström, T. Polivka, Dynamics of Vibrational Relaxation in the S_1 State of Carotenoids having 11 Conjugated C=C Bonds. *Chem. Phys. Lett.* **2002**, *355*, 465-470.

[37] G. Cerullo, G. Lanzani, M. Zavelani-Rossi, S. De Silvestri, Early Events of Energy Relaxation in All-*trans*-β-Carotene Following Sub-10 fs Optical-Pulse Excitation. *Phys. Rev. B* **2001**, *63*, 241104.

[38] S. Vdovic, Y. Wang, B. Li, M. Qiu, X. Wang, Q. Guo, A. Xia, Excited State Dynamics of β-Carotene Studied by Means of Transient Absorption Spectroscopy and Multivariate Curve Resolution Alternating Least-Squares Analysis. *PCCP* **2013**, *15*, 20026-20036.

[39] D. C. Johnston, Stretched Exponential Relaxation Arising from a Continuous Sum of Exponential Decays. *Phys. Rev. B* **2006**, *74*, 184430.

[40] E. W.Hansen, X. Gong, Q. Chen, Compressed Exponential Response Function Arising From a Continuous Distribution of Gaussian Decays – Distribution Characteristics. *Macromol. Chem. Physic.* **2013**, *214*, 844-852.

[41] J. Gabriel, T. Blochowicz, B. Stühn, Compressed Exponential Decays in Correlation Experiments: The Influence of Temperature Gradients and Convection. *J. Chem. Phys.* **2015**, *142*, 104902.

[42] A. Adanlete Adjanoh, J. Vogel, M. Ayadi, K. Abdelmoula, Compressed Exponential Form for Disordered Domain Wall Motion in Ultra-Thin Au/Co/Au Ferromagnetic Films. *J. Magn. Magn. Mater.* **2011**, *323*, 504-508.

[43] P. Hamm, J. Helbing, J. Bredenbeck, Stretched Versus Compressed Exponential Kinetics in α-Helix Folding. *Chem. Phys.* **2006**, *323*, 54-65.

[44] N. Tschirner, M. Schenderlein, K. Brose, E. Schlodder, M.A. Mroginski, C. Thomsen, P. Hildebrandt, Resonance Raman spectra of β-carotene in solution and in Photosystems Revisited: an Experimental and Theoretical Study. *PCCP* **2009**, *11*, 11471-11478.

[45] A.L. Dobryakov, S.A. Kovalenko, N.P. Ernsting, Coherent and Sequential Contributions to Femtosecond Transient Absorption Spectra of a Rhodamine Dye in Solution. *J. Chem. Phys.* **2005**, *123*, 044502.

[46] J.P. Kraack, A. Wand, T. Buckup, M. Motzkus, S. Ruhman, Mapping Multidimensional Excited State Dynamics Using Pump-Impulsive-Vibrational-Spectroscopy and Pump-Degenerate-Four-Wave-Mixing. *PCCP* **2013**, *15*, 14487-14501.

[47] M. Liebel, P. Kukura, Broad-Band Impulsive Vibrational Spectroscopy of Excited Electronic States in the Time Domain. *J. Phys. Chem. Lett.* **2013**, *4*, 1358-1364.

[48] M. Liebel, C. Schnedemann, P. Kukura, Vibrationally Coherent Crossing and Coupling of Electronic States during Internal Conversion in *β*-Carotene. *Phys. Rev. Lett.* **2014**, *112*, 198302.

[49] M. Quick, A.L. Dobryakov, S.A. Kovalenko, N.P. Ernsting, Resonance Femtosecond-Stimulated Raman Spectroscopy without Actinic Excitation Showing Low-Frequency Vibrational Activity in the S_2 State of All-Trans β-Carotene. *J. Phys. Chem. Lett.* **2015**, *6*, 1216-1220.

[50] J.H. Starcke, M. Wormit, J. Schirmer, A. Dreuw, How Much Double Excitation Character do the Lowest Excited States of Linear Polyenes have?. *Chem. Phys.* **2006**, *329*, 39-49.

[51] D. Ghosh, J. Hachmann, T. Yanai, G.K.-L. Chan, Orbital Optimization in the Density Matrix Renormalization Group, with Applications to Polyenes and β-Carotene. *J. Chem. Phys.* **2008**, *128*, 144117.

[52] M. Kleinschmitt, C.M. Marian, M. Waletzke, S. Grimme, Parallel Multireference Configuration Interaction Calculations on mini-β-Carotenes and β-Carotene. *J. Chem. Phys.* **2009**, *130*, 044708.

[53] E. Ostroumov, M.G. Müller, C.M. Marian, M. Kleinschmidt, A.R. Holzwarth, Electronic Coherence Provides a Direct Proof for Energy-Level Crossing in Photoexcited Lutein and β-Carotene. *Phys. Rev. Lett.* **2009**, *103*, 108302.

[54] H. Okamoto, K. Yoshihara, Femtosecond Time-Resolved Coherent Raman Scattering from β-Carotene in Solution. Ultrahigh Frequency (11 THz) Beating Phenomenon and Sub-Picosecond Vibrational Relaxation. *Chem. Phys. Lett.* **1991**, *177* (6), 568-572.

[55] J.L. Perez Lustres, A.L. Dobryakov, A. Holzwarth, M. Veiga, S2→S1 Internal Conversion in β-Carotene: Strong Vibronic Coupling from Amplitude

Oscillations of Transient Absorption Bands. *Angew. Chem. Int. Ed.* **2007**, *46*, 3758-3758.

[56] M. R. Wasielewski, D. G. Johnson, E. G. Bradford, L. D. Kispert, Temperature dependence of the lowest excited singlet-state lifetime of all-*trans*-β-carotene and fully deuterated all-*trans*-β-carotene. *J. Chem. Phys.* **1989**, *91*, 6691-6697.

[57] T. Siebert, R. Maksimenka, A. Materny, V. Engel, W. Kiefer, M. Schmitt, Probing the Kinetics of a Nonadiabatic Transition Initiating Out of Vibrationally Excited as Well as Ground State Modes with Femtosecond Time-Resolved Transient Gratings. *J. Raman. Spectrosc.* **2002**, *33*, 844-854.

[58] S. Schlücker, A. Szeghalmi, M. Schmitt, J. Popp, W. Kiefer, Density Functional and Vibrational Spectroscopic Analysis of β-Carotene. *J. Ram. Spectrosc.* **2003**, *34*, 413-419.

[59] W-L. Liu, Z-G. Wang, Z-R. Zheng, A-H. Li, W-H. Su, Effect of β-Ring Rotation on the Structures and Vibrational Spectra of β-Carotene: Density Functional Theory Analysis . *J. Phys. Chem.* **2008**, *112*, 10580-10585.

[60] V. Lukes, N. Christensson, F. Milota, H. Kauffmann, J. Hauer, Electronic Ground State Conformers of β-Carotene and their Role in Ultrafast Spectroscopy. *Chem. Phys. Lett.* **2011**, *506*, 122-127.

[61] R. Shimada, H. Hamaguchi, Solute–Solvent Intermolecular Vibronic Coupling as Manifested by the Molecular Nearfield Effect in Resonance Hyper-Raman Scattering. *J. Chem. Phys.* **2011**, *134*, 034516.

[62] R. Shimada, H. Hamaguchi, Molecular Near-Field Antenna Effect in Resonance Hyper-Raman Scattering: Intermolecular Vibronic Intensity Borrowing of Solvent from Solute Through Dipole-Dipole and Dipole-Quadrupole Interactions. *J. Chem. Phys.* **2014**, *140*, 204506.

4.3 Martin Quick, Alexander L. Dobryakov, Sergey A. Kovalenko, and Nikolaus P. Ernsting Resonance Femtosecond-Stimulated Raman Spectroscopy without Actinic Excitation Showing Low-Frequency Vibrational Activity in the S2 State of All-Trans β-Carotene, *J. Phys. Chem. Lett.* **2015**, *6*, 1216-1220.

[1] T. Polivka, V. Sundström, Dark Excited States of Carotenoids: Consensus and Controversy. *Chem*. *Phys*. *Lett*. **2009**, *477*, 1-11.

[2] F. Inagaki, M. Tasumi, T. Miyazawa, Vibrational Analysis of Polyene Chains: Assignment of the Resonance Raman Lines of Poly(Acetylene) and β-Carotene. *J*. *Raman*. *Spectrosc*. **1975**, *3*, 335-343.

[3] T. Siebert, R. Maksimenka, A. Materny, V. Engel, W. Kiefer, M. Schmitt, The Role of Specific Normal Modes during Non-Born-Oppenheimer Dynamics: the

S_1-S_0 Internal Conversion of β-Carotene Interrogated on a Femtosecond Time-Scale with Coherent Anti-Stokes Raman Scattering. *J*. *Raman*. *Spectrosc*. **2002**, *33*, 844-854.

[4] M. Yoshizawa, H. Aoki, H. Hashimoto, Vibrational Relaxation of the $2A_g^-$ Excited State in All-*trans*-β-Carotene Obtained by Femtosecond Time-Resolved Raman Spectroscopy. *Phys*. *Rev*. *B* **2001**, *63*, 180301.

[5] D. W. McCamant, P. Kukura, R. A. Mathies, Femtosecond Time-Resolved Stimulated Raman Spectroscopy: Application to the Ultrafast Internal Conversion in β-Carotene. *J*. *Phys*. *Chem*. *A*. **2003**, *107*, 8208-8214.

[6] P. Kukura, D. W. McCamant, R. A. Mathies, Femtosecond Time-Resolved Stimulated Raman Spectroscopy of the S_2 ($1B_u^+$) Excited State of β-Carotene. *J. Phys. Chem. A* **2004**, *108*, 5921-5925.

[7] A. Sakamoto, S. Matsuno, M. Tasumi, Picosecond Near-Infrared Excited Transient Raman Spectra of β-Carotene in the Excited S_2 State: Solvent Effects on the In-Phase C=C Stretching Band and Vibronic Coupling. *J*. *Mol*. *Struct*. **2010**, *976*, 310-313.

[8] T. Takaya, K. Iwata, Relaxation Mechanism of β-Carotene from S_2 ($1B_u^+$) State to S_1 ($2A_g^-$) State: Femtosecond Time-Resolved Near-IR Absorption and Stimulated Resonance Raman Studies in 900-1550 nm Region. *J*. *Phys*. *Chem*. A **2014**, *118*, 4071-4078.

[9] J. P. Kraack, A. Wand, T. Buckup, M. Motzkus, S. Ruhman, Mapping Multidimensional Excited State Dynamics using Pump-Impulsive-Vibrational-Spectroscopy and Pump-Degenerate-Four-Wave-Mixing. *Phys. Chem. Chem. Phys.* **2013**, *15*, 14487-14501.

[10] M. Liebel, C. Schnedermann, P. Kukura. Vibrationally Coherent Crossing and Coupling of Electronic States during Internal Conversion in β-Carotene. *Phys. Rev. Lett.* **2014**, *112*, 198302.

[11] Y. Prior, A. R. Bogdan, M. Dagenais, N. Bloembergen, Pressure-Induced Extra Resonances in Four-Wave Mixing. *Phys. Rev. Lett.* **1981**, *46*, 111-114.

[12] J. R. Andrews, R. M. Hochstrasser, Thermally Induced Excited-State Coherent Raman Spectra of Solids, *Chem. Phys. Lett*. **1981**, 82, 381-385.

[13] S. Mukamel, Stochastic Theory of Resonance Raman Line Shapes of Polyatomic Molecules in Condensed Phases. *J. Chem. Phys*. **1985**, *82*, 5398-5408.

[14] M. Quick, A. L. Dobryakov, M. Gerecke, C. Richter, F. Berndt, I. N. Ioffe, A. A. Granovsky, R. Mahrwald, N. P. Ernsting, S. A. Kovalenko, Photoisomerization Dynamics and Pathways of *trans*- and *cis*-Azobenzene in Solution from Broadband Femtosecond Spectroscopies and Calculations. *J. Phys. Chem. B.* **2014**, *118*, 8756-8771.

[15] A. L. Dobryakov, M. Quick, I. N. Ioffe, A. A. Granovsky, N.P. Ernsting, Excited-State Raman Spectroscopy with and without Actinic Excitation: S_1 Raman Spectra of *trans*-Azobenzene. *J. Chem. Phys.* **2014**, *140*, 184310.

[16] D. P. Hoffmann, D. Valley, S. R. Ellis, M. Creelman, R. A. Mathies, Optimally Shaped Narrowband Picosecond Pulses for Femtosecond Stimulated Raman Spectroscopy. *Optics Express* **2013**, *21*, 21685-21692.

[17] A. Weigel, A. Dobryakov, B. Klaumünzer, M. Sajadi, P. Saalfrank, N. P. Ernsting, Femtosecond Stimulated Raman Spectroscopy of Flavin after Optical Excitation. *J. Phys. Chem. B* **2011**, *115*, 3656-3680.

[18] M. Kloz, R. van Grondelle, J. T. M. Kennis, Wavelength-Modulated Femtosecond Stimulated Raman Spectroscopy – Approach Towards Automatic Data Processing. *Phys. Chem. Chem. Phys.* **2011**, *13*, 18123-18133.

[19] A. C. Albrecht, On the Theory of Raman Intensities. *J. Chem. Phys.* **1961**, *34*, 1476-1484.

[20] N. Tschirner, M. Schenderlein, K. Brose, E. Schlodder, M. A. Mroginski, C. Thomsen, P. Hildebrandt, Resonance Raman Spectra of β-Carotene in Solution and in Photosystems Revisited: an Experimenal and Theoretical Study. *Phys. Chem. Chem. Phys.* **2009**, *11*, 11471-11478.

[21] S. Banerjee, D. Kröner, P. Saalfrank, Resonance Raman and Vibronic Absorption Spectra with Duschinsky Rotation from a Time-Dependent Perspective: Application to β-Carotene. *J. Chem. Phys.* **2012**, *137*, 22A534.

[22] T. Buckup, A. Weigel, J. Hauer, M. Motzkus, Ultrafast Multiphoton Transient Absorption of β-Carotene. *Chem. Phys.* **2010**, *373*, 38-44.

5 Comprehensive Discussion - New Results with TA, FLUPS and FSR Spectroscopy

[1] M. Sajadi, M. Quick, N. P. Ernsting, Femtosecond Broadband Fluorescence Spectroscopy by Down- and Up-conversion in β-barium-borate Crystals. *Appl. Phys. Lett.* **2013**, *103*, 173514.

[2] D.W. McCamant, J.E. Kim, R.A. Mathies, Femtosecond Time-Resolved Stimulated Raman Spectroscopy: Application to the Ultrafast Internal Conversion in β-Carotene. *J. Phys. Chem. A* **2003**, *107*, 8208-8214.

[3] P. Kukura, D.W. McCamant, R.A. Mathies, Femtosecond Time-Resolved Stimulated Raman Spectroscopy of the S_2 ($1B_u^+$) Excited State of *β*-Carotene. *J. Phys. Chem. A* **2004**, *108*, 5921-5925.

[4] M. Yoshizawa, H. Aoki, H. Hashimoto, Vibrational Relaxation of the $2A_g^1$ Excited State in All-*trans*-β-Carotene Obtained by Femtosecond Time-resolved Raman spectroscopy. *Phys. Rev. B* **2001**, *63*, 180301.

[5] T. Takaya, K. Iwata, Relaxation Mechanism of β-Carotene from S_2 ($1B_u^+$) State to S_1 ($2A_g^-$) State: Femtosecond Time-Resolved Near-IR Absorption and Stimulated Resonance Raman Studies in 900-1550 nm Region. *J. Phys. Chem.* A **2014**, *118*, 4071-4078.

[6] S. Shim, R.A. Mathies, Development of a Tunable Femtosecond Stimulated Raman Apparatus and Its Application to *β*-Carotene. *J. Phys. Chem. B* **2008**, *112*, 4826-4832.

Danksagung

Ich möchte an dieser Stelle all denjenigen danken, die mich während meiner Arbeitszeit unterstützt haben.

Insbesondere möchte ich Herrn Professor Nikolaus Ernsting für die Überlassung der Themen und die Betreuung der Doktorarbeit danken.

Mein weiterer Dank gilt den Mitgliedern des Arbeitskreises

Dr. Sergey Kovalenko danke ich für die Einarbeitung und Unterstützung bei den zeitaufgelösten Messungen in der Absorption- und Ramanspektroskopie.
Dr. Alexander Dobryakov danke ich für die Unterstützung bei theoretischen Fragen, sowie die Bereitstellung von Programmen.
Dr. Horst Hennig danke ich für Diskussionen im Themenbereich „Thermodynamik“, die für den Bereich der Lehre von Nutzen waren.
Dr. Alexander Weigel danke ich dafür, den Anstoß für mein Dissertationsthema gegeben zu haben.
Dr. Mohsen Sajadi Hezaveh und Dr. Xinxing Zhang danke ich für die Einarbeitung und Unterstützung bei der Fluoreszenz-Aufkonversion.
Dr. Lars Dehmel danke ich seine Unterstützung im informatischen Bereich und für seine stete Hilfsbereitschaft.
Mario Gerecke danke ich für anregende Diskussionen während der Arbeitszeit und in den Pausen
Celin Richter und Marc Andre Kasper danke ich für die Synthese der substituierten Karotine.
Heiderose Steingräber und Sabrina Dabrowski danke ich für ihre administrative Unterstützung.

Weiterhin danke ich den Mitarbeitern der Feinmechanik-Werkstatt für die präzisen Anfertigungen und den Mitarbeitern der Elektronik-Werkstatt für die Bereitstellung von Magnetspulen.

Für die finanzielle Unterstützung danke ich

dem Sonderforschungsbereich 1078, Proteinfunktion und Protonierungsdynamik
der deutschen Forschungsgemeinschaft ER 154/10-3
dem European Research Council

Bei meinen Eltern und Geschwistern bedanke ich mich für ihre Unterstützung.

Selbstständigkeitserklärung

Hiermit erkläre ich, dass die vorliegende Arbeit selbstständig und nur unter Verwendung der von mir angegebenen Hilfsmittel und Literatur angefertigt habe. Sie ist in keinem früheren Verfahren schon einmal begutachtet worden.

Ich erkläre, dass ich mich weder anderwärts um einen Doktorgrad in dem Promotionsfach beworben habe noch, dass ich einen entsprechenden Doktorgrad besitze.

Ich erkläre, dass ich Kenntnis über die dem angestrebten Verfahren zugrunde liegende Promotionsordnung habe.

Berlin, 14.09.2015 Martin Quick